Title

Search for dark matter in events with missing transverse momentum and a Higgs boson decaying into two photons in pp collisions at s = 13 TeV with the ATLAS detector

Journal

Journal of High Energy Physics, 2021(10)

ISSN

1126-6708

Authors

Aad, G
Abbott, B
Abbott, DC
et al.

Publication Date

2021-10-01

DOI

10.1007/jhep10(2021)013

Peer reviewed

Published for SISSA by Springer

Received: *April 28, 2021*
Accepted: *August 5, 2021*
Published: *October 1, 2021*

Search for dark matter in events with missing transverse momentum and a Higgs boson decaying into two photons in pp collisions at $\sqrt{s} = 13$ TeV with the ATLAS detector

The ATLAS collaboration

E-mail: atlas.publications@cern.ch

Abstract: A search for dark-matter particles in events with large missing transverse momentum and a Higgs boson candidate decaying into two photons is reported. The search uses 139 fb^{-1} of proton-proton collision data collected at $\sqrt{s} = 13$ TeV with the ATLAS detector at the CERN LHC between 2015 and 2018. No significant excess of events over the Standard Model predictions is observed. The results are interpreted by extracting limits on three simplified models that include either vector or pseudoscalar mediators and predict a final state with a pair of dark-matter candidates and a Higgs boson decaying into two photons.

Keywords: Hadron-Hadron scattering (experiments)

ArXiv ePrint: 2104.13240

https://doi.org/10.1007/JHEP10(2021)013

JHEP10(2021)013

Contents

JHEP10(2021)013

1 Introduction

The discovery of a particle exhibiting the expected properties of a Standard Model (SM) Higgs boson in 2012 by the ATLAS [1] and CMS [2] Collaborations has opened up new possibilities in searches for physics beyond the SM (BSM). The precision reached since then in the production cross-section and mass measurements of the observed Higgs boson with the additional data collected by the LHC experiments [3, 4] provides sharp tools to probe the possible existence of new physics.

Astrophysical data [5, 6] support the existence of dark matter (DM) in our universe, while there is yet no evidence of a non-gravitational interaction between DM and SM particles, nor any indication of the microscopic nature of any possible DM particles.

Assuming the weakly interacting nature of DM, DM particles (χ) are expected to escape detection at the LHC. For this reason, searches concentrate on final states with missing transverse momentum ($E_{\mathrm{T}}^{\mathrm{miss}}$) produced in association with detectable particles (X) complementing the undetectable particles' signatures, giving rise to $X+E_{\mathrm{T}}^{\mathrm{miss}}$ final states.

The detectable particle X is usually chosen to be a photon [7], a W or Z boson [8], a jet [9], a single top quark [10], or a pair of top quarks [11], all emitted from a light quark or gluon as initial-state radiation through the usual SM gauge interactions. However, X can

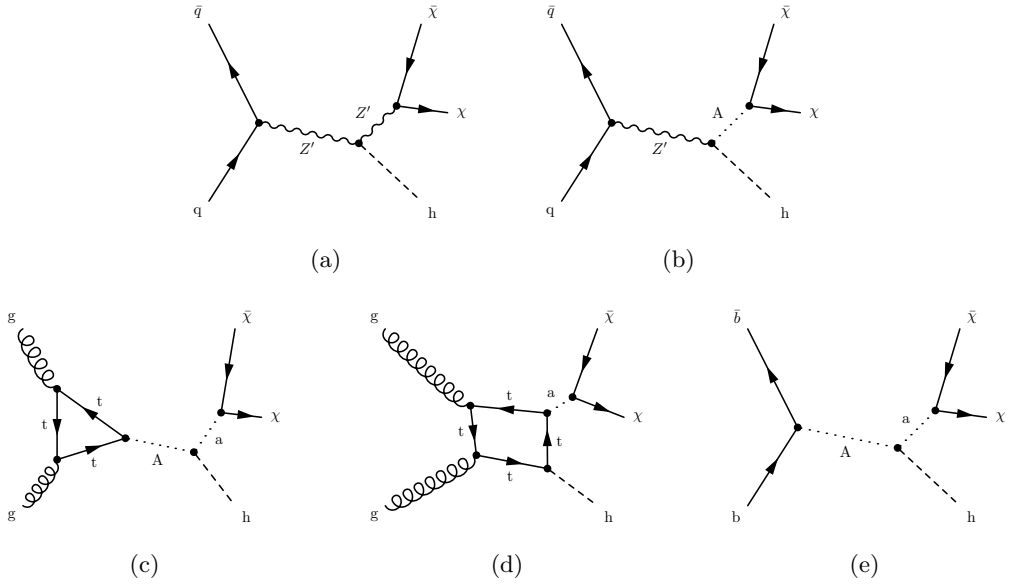

Figure 1. The Feynman diagrams of DM (χ) production in association with the observed Higgs boson (h) arising from three theoretical models considered in this paper: (a) the Z'_B model, (b) the Z'-2HDM model, and (c), (d), and (e) the 2HDM+a model.

also be the neutral Higgs boson (h) observed at the LHC with a mass of about 125 GeV whose radiative production is highly suppressed. In that case, pp collision events with h produced in association with some $E_{\mathrm{T}}^{\mathrm{miss}}$ can be very sensitive probes of the structure of the BSM physics responsible for producing DM [12].

Both the ATLAS and CMS Collaborations have previously searched for such h+$E_{\mathrm{T}}^{\mathrm{miss}}$ final states using 20.3 fb^{-1} of pp collision data at $\sqrt{s} = 8$ TeV [13, 14], and up to 36.1 fb^{-1} of pp collision data at $\sqrt{s} = 13$ TeV [15–21], considering the decay of h into a pair of photons, b-quarks, τ leptons, W bosons, or Z bosons. In principle, the diphoton channel has lower sensitivity than the $b\bar{b}$ channel because the $h \to \gamma\gamma$ branching fraction is smaller than that of $h \to b\bar{b}$ by two orders of magnitude. However, if a possible excess were to be seen in the b-quarks final state, the diphoton channel could offer a way to cross-check this evidence for a sizeable fraction of the new-physics parameter space covered by the $b\bar{b}$ channel [22]. It also provides complementary sensitivity at lower $E_{\mathrm{T}}^{\mathrm{miss}}$ where the $b\bar{b}$ final state is limited by the experimental $E_{\mathrm{T}}^{\mathrm{miss}}$ trigger threshold, since the diphoton channel is triggered using the photon pair, allowing for much lower and better resolved $E_{\mathrm{T}}^{\mathrm{miss}}$ in the event. This paper presents an updated search for DM particles produced in association with the decay of h into a pair of photons using the full LHC Run 2 pp collision dataset collected at $\sqrt{s} = 13$ TeV by ATLAS from 2015 to 2018. This corresponds to an integrated luminosity of 139 fb^{-1}, four times higher than that used in the previous analysis published by the ATLAS Collaboration [18].

Three theoretical benchmark models are considered in this analysis. The leading-order (LO) Feynman diagrams representing the production of h+$E_{\mathrm{T}}^{\mathrm{miss}}$ in these three simplified models [23] are shown in figure 1.

JHEP10(2021)013

In the first model, called Z'_B [12], a massive vector mediator Z' emits a Higgs boson and subsequently decays into a pair of Dirac fermionic DM candidates. DM couples to SM particles only via the new Z' boson, and the new associated $\mathrm{U}(1)_B$ baryon number symmetry ensures the stability of the DM particle in a natural way. An additional scalar particle (referred to as a baryonic Higgs boson) is introduced to break this symmetry spontaneously and generate the Z' boson mass. The parameters of the Z'_B model are:

- $m_{Z'}$, the Z' boson mass;
- g_χ, the coupling of the Z' boson to the DM particle χ;
- g_q, the coupling of the Z' boson to quarks;
- $g_{hZ'Z'}$, the coupling between the Z' boson and the observed Higgs boson h;
- $\sin\theta$, the mixing angle between the baryonic Higgs boson and the observed Higgs boson; and
- m_χ, the mass of the fermionic dark-matter candidate χ.

The second and third simplified models implement different possible mediators connecting the SM spectrum to DM particles but are both derived from a general extension of the SM implementing two Higgs doublets, called 2HDM [24]. These models predict the existence of five Higgs bosons: two scalars, one being the already observed Higgs boson; one heavy pseudoscalar A; and two charged Higgs bosons $H^\pm$. The first of these two models is called the Z'-2HDM model [24], as it introduces a new vector mediator Z' whose mass is generated by the extended Higgs sector. In this model, DM particles are produced through the decay of the pseudoscalar A, giving rise to an $E_{\mathrm{T}}^{\mathrm{miss}}$ distribution that becomes harder as the mass difference between the Z' and A bosons increases. The parameters of the Z'-2HDM model are:

- m_A, the pseudoscalar boson mass;
- $m_{Z'}$, the Z' boson mass;
- m_χ, the mass of the fermionic dark-matter candidate χ;
- $\tan\beta$, the ratio of the vacuum expectation values of the two Higgs doublets;
- $g_{Z'}$ the coupling strength of the Z' boson to quarks; and
- α, the mixing angle between the two neutral scalars in the 2HDM model.

The third model considered in this analysis is called 2HDM+a [25] and offers another phenomenological option where a new pseudoscalar mediator a couples directly to both the SM fermions and dark-matter particles [26]. This model is of particular interest since it allows for gluon-gluon fusion production (figures 1(c), 1(d)), which is forbidden for the Z' mediator. This model has an extended set of 13 parameters, namely:

JHEP10(2021)013

- m_A and m_a, the pseudoscalar particle masses;
- m_H and m_h, the scalar particle masses;
- $m_{H^\pm}$, the mass of the charged Higgs bosons;
- m_χ, the fermionic DM particle mass;
- y_χ, the DM Yukawa coupling;
- $\tan\beta$, the ratio of the vacuum expectation values of the two Higgs doublets;
- α, the mixing angle between the two neutral scalars in the 2HDM model;
- θ, the mixing angle between the two pseudoscalars; and
- λ_3, the quartic coupling of the Higgs potential, and λ_{1P} and λ_{2P}, the quartic couplings of the pseudoscalar potentials.

By choosing $\cos(\alpha-\beta)=0$ and a null coupling to quarks and leptons of the a field, the 2HDM+a model can escape experimental constraints from both Higgs precision measurements and DM direct search limits.

For the particles mediating the interaction between SM and DM in these three models, it is assumed that only decays which are kinematically accessible and strictly necessary for the self-consistency of the model are considered in the decay widths [23]. In the case of the 2HDM+a model, a SM-like Higgs width is assumed for h, which restricts the possible parameter space.

The analysis reported in the present paper selects events with two photons and large $E_{\mathrm{T}}^{\mathrm{miss}}$. Searches are performed in different regions of observed diphoton transverse momentum ($p_{\mathrm{T}}^{\gamma\gamma}$) and event $E_{\mathrm{T}}^{\mathrm{miss}}$ significance, defined in section 5.

The main backgrounds in the analysis correspond to either SM Higgs boson production contributions, QCD-induced non-resonant diphoton events ($\gamma\gamma$, $V\gamma\gamma$, where V is a W or Z boson), or to reducible contributions where an electron or a jet is misidentified as a photon ('fake photons') and $E_{\mathrm{T}}^{\mathrm{miss}}$ is generated either by particles escaping the detector acceptance or by neutrinos ($V\gamma$, γ+jet). An additional background contribution dominating the low $E_{\mathrm{T}}^{\mathrm{miss}}$ region is associated with resolution effects when computing the transverse energy from high-energy objects and softer contributions measured in the ATLAS calorimeters. The $E_{\mathrm{T}}^{\mathrm{miss}}$ can therefore be either 'fake', i.e. spurious values of $E_{\mathrm{T}}^{\mathrm{miss}}$ reconstructed in the detector for events with no invisible particles, or 'true', i.e. genuine $E_{\mathrm{T}}^{\mathrm{miss}}$ associated with the presence of particles escaping detection in the event.

This paper is organized as follows. Section 2 gives a brief description of the ATLAS detector. Section 3 describes the dataset and the signal and background Monte Carlo (MC) simulation samples used. Section 4 explains the reconstruction and identification of objects, while section 5 outlines the optimization of the event selection and categorization. Section 6 summarizes the signal and background modelling. Section 7 discusses the experimental and theoretical systematic uncertainties. Section 8 presents the results and their interpretations, and finally a summary is given in section 9.

JHEP10(2021)013

2 ATLAS detector

The ATLAS detector [27–29] is a multipurpose particle physics detector with approximately forward-backward symmetric cylindrical geometry.[1] The inner detector (ID) tracking system covers $|\eta| < 2.5$ and consists of a silicon pixel detector, a silicon microstrip detector and a transition radiation tracker (TRT). The ID allows precise reconstruction of charged-particle trajectories and of decay vertices of long-lived particles. The ID is surrounded by a thin superconducting solenoid providing a 2 T axial magnetic field. A high-granularity lead/liquid-argon (LAr) sampling calorimeter measures the energy and the position of electromagnetic showers in the central ($|\eta| < 1.475$) and endcap ($1.375 < |\eta| < 3.2$) regions. It includes a presampler (for $|\eta| < 1.8$) and three sampling layers for $|\eta| < 2.5$. The longitudinal and lateral segmentation of the calorimeter allows a measurement of the shower direction without assuming that the photon originates from a specific point along the beamline. LAr sampling calorimeters with copper and tungsten absorbers are also used to measure hadronic showers in the endcap ($1.5 < |\eta| < 3.2$) and forward ($3.1 < |\eta| < 4.9$) regions, while a steel/scintillator-tile calorimeter measures hadronic showers in the central region ($|\eta| < 1.7$). The muon spectrometer surrounds the calorimeters and consists of three large superconducting air-core toroid magnets, each with eight coils, a system of precision tracking chambers ($|\eta| < 2.7$), and fast tracking chambers for triggering ($|\eta| < 2.4$). Reconstructed events are selected by a two-level trigger system. The first-level trigger is hardware-based, while the second-level trigger is implemented in software [30].

3 Data and simulation samples

The pp collision data used in the analysis correspond to the full LHC Run 2 dataset taken by the ATLAS experiment during the period 2015 to 2018 with proton beams colliding at $\sqrt{s} = 13$ TeV. The full dataset represents an integrated luminosity of $139.0 \pm 2.4\,\text{fb}^{-1}$ [31] after the application of data quality requirements checking that the ATLAS detector was fully functional and that the LHC was running in stable conditions. This dataset was recorded with a mean number of about 34 pp interactions per bunch crossing, with a peak value of 60. Events used in this analysis were selected using a diphoton trigger requiring two reconstructed photon candidates with minimum transverse energies of 35 and 25 GeV for the leading and subleading photons, respectively, where leading (subleading) refers to the photon with the highest (second-highest) transverse energy [32]. Both photons were required by the trigger to fulfil the 'Loose' photon identification criteria in 2015 and 2016, whereas the 'Medium' criteria were used in 2017–2018 to handle the higher number of pp collisions per bunch crossing resulting from the higher instantaneous luminosity in those years. The trigger selections used during 2015–2018 are estimated to be fully efficient for events satisfying the offline event selection criteria presented in section 5.

[1] ATLAS uses a right-handed coordinate system with its origin at the nominal interaction point (IP) in the centre of the detector and the z-axis along the beam pipe. The x-axis points from the IP to the centre of the LHC ring, and the y-axis points upward. Cylindrical coordinates (r, ϕ) are used in the transverse plane, ϕ being the azimuthal angle around the beam pipe. The pseudorapidity is defined in terms of the polar angle θ as $\eta = -\ln[\tan(\theta/2)]$. Angular distance is measured in units of $\Delta R \equiv \sqrt{(\Delta\eta)^2 + (\Delta\phi)^2}$. The photon transverse energy is $E_{\text{T}} = E/\cosh(\eta)$, where E is its energy.

JHEP10(2021)013

The analysis of the data sample requires the use of different types of MC generated samples to design the event selection, categorize events, and estimate systematic uncertainties applied to the statistical inference procedure used to estimate the presence of a possible DM signal in the dataset. These generated samples include the signal samples for the three models described in section 1 and the background samples for both the non-resonant contributions ($\gamma\gamma$, $V\gamma$, $V\gamma\gamma$) and the SM Higgs contributions where the Higgs boson decays into a pair of photons. Due to difficulties in correctly simulating the effect of fake photons and fake $E_{\mathrm{T}}^{\mathrm{miss}}$, the non-resonant γ+jet background is instead estimated using a data-driven method detailed in section 6. The simulated non-resonant samples and data-derived γ+jet sample are only used to calculate uncertainties affecting the background model used in the final statistical fit.

Events from gluon–gluon fusion (ggF), vector-boson fusion (VBF), Wh, and Zh processes were generated using Powheg Boxv2 [33–41] with the PDF4LHC15 parton distribution function (PDF) set [42], and interfaced to Pythia8.2 [43] for parton showering, hadronization and the underlying event, using a set of parameters tuned to data and called the AZNLO tune [44]. The ggF simulation achieves next-to-next-to-leading-order (NNLO) accuracy for arbitrary inclusive $gg \to h$ observables by reweighting the Higgs boson rapidity spectrum in Hj-MiNLO [39, 45, 46] to that of HNNLO [47]. The transverse momentum spectrum of the Higgs boson obtained with this sample is found to be compatible with the fixed-order HNNLO calculation and the HRes2.3 calculation [48, 49] performing resummation at next-to-next-to-leading-logarithm accuracy matched to a NNLO fixed-order calculation (NNLL+NNLO).

Events from $t\bar{t}h$ processes were modelled using the Powheg Boxv2 [34–36, 41, 50] generator, which provides matrix elements at next-to-leading order (NLO) in the strong coupling constant α_{s} in the five-flavour scheme with the `NNPDF3.0nlo` [51] PDF set. The functional form of the renormalization and factorization scales is set to $\sqrt[3]{m_{\mathrm{T}}(t) \cdot m_{\mathrm{T}}(\bar{t}) \cdot m_{\mathrm{T}}(h)}$.[2] The generator was interfaced to Pythia8.2 using the A14 tune [52] and the `NNPDF2.3lo` [51] PDF set. The decays of bottom and charm hadrons were simulated using the EvtGen v1.6.0 program [53].

Events from $thqb$ (tWh) processes were produced with MadGraph5_aMC@NLO in the four-flavour (five-flavour) scheme with the `NNPDF3.0nnlo` PDF [51]. The same flavour scheme is used in the matrix element calculation and the PDF. The top quark and W boson decays were handled by MadSpin [54] for the correct treatment of the spin correlations of the decay products. In the case of tWh the overlap of this process with $t\bar{t}h$ at NLO was removed following a diagram removal technique [55, 56]. The simulation of the parton shower, hadronization and underlying event was then performed by Pythia8.2 with the A14 tune for both the $thqb$ and tWh samples.

The cross sections for the SM Higgs boson processes were calculated at NLO in electroweak theory and NNLO in QCD for the VBF, Zh and Wh samples [57], and next-to-next-to-next-to-leading order plus NNLL (N^{3}LO+NNLL) in QCD for the ggF sample [57].

[2] m_{T} denotes the transverse mass of a particle, defined as $m_{\mathrm{T}} = \sqrt{m^2 + p_{\mathrm{T}}^2}$ where m and p_{T} are respectively its mass and transverse momentum.

JHEP10(2021)013

The $t\bar{t}h$ cross section was calculated with NLO accuracy in QCD with NLO electroweak corrections [58]. The $b\bar{b}h$ cross section was found to be negligible. All samples were normalized to the most precise available theoretical cross sections corresponding to a Higgs boson mass of 125.09 GeV [59]. The analysis assumes a branching ratio for the Higgs boson decay into two photons of 0.227% [57].

The $\gamma\gamma$, $V\gamma\gamma$, and $V\gamma$ processes were simulated with the Sherpa v2.2.4 [60] generator. For the $\gamma\gamma$ and $V\gamma$ processes, QCD NLO-accurate matrix elements for up to one parton, and LO-accurate matrix elements for up to three partons, were calculated with the Comix [61] and OpenLoops 1 [62–64] libraries, while for the $V\gamma\gamma$ process, QCD LO-accurate matrix elements for up to one additional parton emission were calculated. They were matched and merged with the Sherpa parton shower based on Catani–Seymour dipole factorization [61, 65] using the MEPS@NLO prescription [66–69]. Samples were generated using the `NNPDF3.0nnlo` PDF set, along with the dedicated set of tuned parton-shower parameters developed by the Sherpa authors.

MC simulated samples for the different signal models were generated using the MadGraph5 [70] generator at LO accuracy, using the `NNPDF3.0lo` PDF set [71] for the Z'_B and Z'-2HDM signal samples or the `NNPDF3.0nlo` PDF set for 2HDM+a signal samples. Parton showering and hadronization were simulated using the Pythia8.1 [72] generator for Z'_B or the Pythia8.2 generator for Z'-2HDM and 2HDM+a samples, with the A14 tune and the `NNPDF2.3lo` PDF set [71]. Multiple samples were generated in order to scan the mediator masses and the key parameters of each model, while the default values of other parameters were set to fixed values. In general the choice of parameter values follows the recommendations of the LHC DM Forum report [23] and are based on the sensitivities expected at the LHC.

For the Z'_B model, the generation scans a wide range of Z' and DM particle masses. The mass $m_{Z'}$ ranges from 10 GeV to 2000 GeV while m_χ ranges from 1 GeV to 1000 GeV. The different couplings of this model are required to fulfil perturbativity bounds that allow the choice of $g_\chi = 1.0$, $g_q = 1/3$, $g_{hZ'Z'} = m_{Z'}$, and $\sin\theta = 0.3$ to maximize the expected cross section. The couplings choice affects only the magnitude of the cross section and not the shape of the $E_{\mathrm{T}}^{\mathrm{miss}}$ and $p_{\mathrm{T}}^{\gamma\gamma}$ distributions, and in particular, a lower $\sin\theta$ value decreases the expected yield. In this model, $p_{\mathrm{T}}^{\gamma\gamma}$ and $E_{\mathrm{T}}^{\mathrm{miss}}$ grow with $m_{Z'}$ while the diphoton pair becomes more back-to-back with the $E_{\mathrm{T}}^{\mathrm{miss}}$ vector. Additionally, the photon pair is more collimated for higher $m_{Z'}$ and m_χ, since the Higgs boson is more boosted in that region of the parameter space.

For the Z'-2HDM model, the cross section and kinematics depend on the Z' and A masses but much less on the DM particle mass while $m_\chi < m_A/2$ is satisfied. Consequently, signal samples were generated for different values of $m_{Z'} \in [400, 1600]$ GeV and $m_A \in [200, 600]$ GeV and for $m_\chi = 100$ GeV. The values of other parameters which only affect the cross section were fixed to $\alpha = \beta - \pi/2$, $g_{Z'} = 0.8$, and $\tan\beta = 1$. In this model, $E_{\mathrm{T}}^{\mathrm{miss}}$ exhibits a peaked distribution arising from the fact that DM particles are produced from the pseudoscalar A. The peak position depends strongly on the mass difference $m_{Z'} - m_A$.

For the 2HDM+a model, the parameter space is more complex than for the two first models and different scans were generated to test its richer phenomenology. This includes

JHEP10(2021)013

two $\sin\theta$ scans corresponding to two sets of $(A,\ a)$ masses, a two-dimensional scan of the m_A–m_a mass plane, and a two-dimensional scan of the $\tan\beta$–m_a plane. The default parameter values were set to $\sin(\alpha-\beta)=1$, $\lambda_3=\lambda_{1P}=\lambda_{2P}=3$, $y_\chi=1$, $m_\chi=10$ GeV, and a decoupled Higgs boson spectrum with $m_A=m_H=m_{H^\pm}$ sizeably larger than that of the observed scalar Higgs boson with m_h near 125 GeV.

The effects of additional pp collisions from the same and neighbouring bunch crossings ('pile-up') were simulated by overlaying the hard-scattering event with inelastic pp events generated by Pythia8.1 using the `NNPDF2.3lo` PDF set and the A3 tune [73]. Differences between the simulated and observed distributions of the number of interactions per bunch crossing were removed by applying pile-up weights to simulated events. A full simulation of the ATLAS detector [74] based on Geant4 [75] was used to reproduce the detector response to SM Higgs boson processes and $V\gamma$ and $V\gamma\gamma$ backgrounds. The $\gamma\gamma$ background and the signal samples were simulated using AtlFastII [76], a fast simulation of the ATLAS detector response which was shown to be able to accurately simulate diphoton events.

As it is not computationally feasible to generate fully simulated samples for all interesting parameter points, an interpolation method was used to efficiently create new samples from existing fully simulated ones. First, a set of base samples covering a wide range of generator-level 'truth' values for key variables was chosen from the existing fully simulated samples. For the Z'_B and Z'-2HDM models, these variables are $p_{\mathrm{T}}^{\gamma\gamma}$ and $E_{\mathrm{T}}^{\mathrm{miss}}$, while for the 2HDM+a model, these are $p_{\mathrm{T}}^{\gamma\gamma}$, $p_{\mathrm{T}}^{\chi\chi}$ (the transverse momentum of the $\chi\chi$ system), and $|\Delta\phi(p_{\mathrm{T}}^{\gamma\gamma}, p_{\mathrm{T}}^{\chi\chi})|$ (the difference in azimuthal angle between the $\gamma\gamma$ and $\chi\chi$ systems). For any desired additional parameter point, a new sample was generated containing only these generator-level key variables. The base samples were then reweighted on an event-by-event basis to the desired new one, using the bin-by-bin ratio of the generator-level distributions from the new sample to the corresponding distribution from the base samples. Finally, for a few validation samples, the differences between the generated and reweighted samples were used to estimate a conservative uncertainty from this procedure.

4 Event reconstruction

Within the ATLAS detector, photons are reconstructed from topologically connected clusters [77] of energy deposits in the EM calorimeters in the region $|\eta|<2.37$. The transition region between the barrel and endcap EM calorimeters, $1.37<|\eta|<1.52$, is excluded. Photon candidates matched to a conversion vertex or a track, which are consistent with originating from a photon conversion, are classified as converted photons. Those without a matched conversion vertex or track are classified as unconverted photons. The efficiency of the diphoton trigger used to select the events used in the present analysis is estimated to be greater than 99.2% on average for events passing the final event selection [32].

The calibration of the photon energy is based on a multivariate regression algorithm trained with MC samples, where the input variables are corrected with data-driven techniques. The calibrated energy is then adjusted by applying energy scale factors derived from $Z\to e^+e^-$ events [78]. The photon direction is reconstructed using the longitudinal segmentation of the calorimeters and a constraint from the average collision point of

JHEP10(2021)013

the proton beams. Additionally, the conversion vertex position is included in the case of converted photons.

Events are required to have at least one reconstructed primary vertex (PV), defined as a vertex associated with at least two tracks with $p_{\mathrm{T}} > 0.5$ GeV. To select the correct PV of a given event, a neural network [79] that uses the pointing information from the selected photons is deployed. Although this neural-network-selected vertex is taken to be the nominally correct choice, an alternative 'hardest vertex', defined as the vertex with the highest sum of squares of the transverse momenta of associated tracks, is also used for certain $E_{\mathrm{T}}^{\mathrm{miss}}$-related calculations described in section 5.

Photon identification is based on the lateral shower profile of the energy deposits in the first and second EM calorimeter layers and on the energy leakage fraction in the hadronic calorimeter. 'Tight' identification criteria [78] are applied, after tuning them for converted and unconverted photons separately. These criteria reduce the misidentification of hadronic jets containing large neutral components, primarily π^0 particles, which decay into highly collimated photons. For transverse momenta between 30 GeV and 250 GeV, the identification efficiency for unconverted and converted photons ranges from 85% to 99%, while fake photons originating from jets have an identification efficiency of 25% to 40% [78].

To further improve fake-photon rejection, two isolation variables are defined to quantify the activity around a photon. The calorimeter-based isolation $E_{\mathrm{T}}^{\mathrm{iso}}$ is defined as the sum of the transverse energy in topological clusters of calorimeter cells within a cone of size $\Delta R = 0.2$ around the photon, correcting for the energy of the photon candidate itself as well as an average expected pile-up contribution. The track-based isolation $p_{\mathrm{T}}^{\mathrm{iso}}$ is defined as the scalar sum of the transverse momenta of all tracks with $p_{\mathrm{T}} > 1$ GeV that originate from the neural-network-selected vertex and are within a cone of $\Delta R = 0.2$. Isolated photons must have $E_{\mathrm{T}}^{\mathrm{iso}} < 0.065\, E_{\mathrm{T}}$ and $p_{\mathrm{T}}^{\mathrm{iso}} < 0.05\, E_{\mathrm{T}}$.

Electrons are reconstructed from energy deposits measured in the EM calorimeter which are matched to ID tracks [78]. They are required to satisfy $|\eta| < 2.47$, excluding the EM calorimeter transition region $1.37 < |\eta| < 1.52$, and have a transverse momentum $p_{\mathrm{T}} > 10$ GeV. Electrons are required to satisfy the 'Medium' identification criteria based on the use of shower shape, track-cluster matching and TRT parameters [80] in a likelihood-based algorithm. Muons are reconstructed from high-quality track segments found in the muon spectrometer [81]. A matching of these segments to ID tracks is required in the region $|\eta| < 2.5$. Muons are required to have $|\eta| < 2.7$ and $p_{\mathrm{T}} > 10$ GeV, and to satisfy the 'Medium' identification criteria [81]. Both the electrons and muons are matched to the PV via requirements on the tracks' longitudinal and transverse impact parameters, $|z_0|$ and $|d_0|$. The applied requirements are $|z_0| \sin\theta < 0.5$ mm (where θ is the polar angle of the track) for electrons and muons and $|d_0|/\sigma_{d_0} < 5(3)$ for electrons (muons).

Jets are reconstructed by a particle-flow algorithm [82] using noise-suppressed positive-energy topological clusters in the calorimeter [83] which are formed by the anti-k_t algorithm [84] with a radius parameter of $R = 0.4$. They are required to have $|\eta| < 4.4$ and $p_{\mathrm{T}} > 25$ GeV. To further suppress jets produced in pile-up interactions, each jet within the tracking acceptance, i.e. $|\eta| < 2.4$, and with $p_{\mathrm{T}} < 60$ GeV, is required to satisfy jet vertex tagger (JVT) [85] criteria used to identify the jet as originating from the PV.

JHEP10(2021)013

To resolve ambiguities between photon, electron, muon and jet reconstruction, an overlap removal procedure is applied to avoid multiple usage of the same detector signals in the same event. The prioritization of photons in this analysis requires the removal of electrons, muons and jets within $\Delta R = 0.4$ of a selected photon. Next, jets within $\Delta R = 0.2$ of electrons are removed. In the last step, electrons and muons within $\Delta R = 0.4$ of any jet are removed.

The missing transverse momentum $E_{\mathrm{T}}^{\mathrm{miss}}$ is calculated as the magnitude of the negative vectorial sum of the transverse momenta of all selected and calibrated physics objects of an event that can be matched to the PV. A so-called 'soft term' is calculated from the residual tracks that originate from the PV but are not associated with any other object and is added to the $E_{\mathrm{T}}^{\mathrm{miss}}$ [86].

5 Event selection

Events are required to have at least two photon candidates within a fiducial region of the EM calorimeter defined by $|\eta| < 2.37$, excluding the region of $1.37 < |\eta| < 1.52$. Photon candidates in this fiducial region are ordered according to their E_{T} and only the highest two are considered. These leading and subleading photon candidates must have $E_{\mathrm{T}}^{\gamma}/m_{\gamma\gamma} > 0.35$ and 0.25, respectively, where $m_{\gamma\gamma}$ is the invariant mass of the two selected photons. Furthermore, events are required to have $105 < m_{\gamma\gamma} < 160$ GeV. The data sideband is defined to consist of events in this region but excluding the region $120 < m_{\gamma\gamma} < 130$ GeV.

In the DM production models, the Higgs boson recoils against the DM pair, resulting in large $E_{\mathrm{T}}^{\mathrm{miss}}$ in the event and large p_{T} of the diphoton system, denoted by $p_{\mathrm{T}}^{\gamma\gamma}$. The $E_{\mathrm{T}}^{\mathrm{miss}}$ distribution after the aforementioned photon requirements is shown in figure 2.

After the photon requirements, events are required to pass a preselection of $E_{\mathrm{T}}^{\mathrm{miss}} > 90$ GeV and $\Delta E_{\mathrm{T}}^{\mathrm{miss}} < 30$ GeV, where $\Delta E_{\mathrm{T}}^{\mathrm{miss}}$ is the $E_{\mathrm{T}}^{\mathrm{miss}}$ calculated from the vertex selected by the neural network minus the $E_{\mathrm{T}}^{\mathrm{miss}}$ calculated from the hardest vertex. High values of $\Delta E_{\mathrm{T}}^{\mathrm{miss}}$ indicate that the $E_{\mathrm{T}}^{\mathrm{miss}}$ can simply be attributed to the misidentification of the primary vertex. In addition, events with electrons or muons are vetoed to suppress $V\gamma$ and $V\gamma\gamma$ backgrounds.

Following this preselection, a boosted decision tree (BDT) is trained using XGBoost 0.82 [87] to discriminate between DM signals and the non-resonant diphoton background, using $p_{\mathrm{T}}^{\gamma\gamma}$ and the $E_{\mathrm{T}}^{\mathrm{miss}}$ significance $S_{E_{\mathrm{T}}^{\mathrm{miss}}}$ as input variables. This latter variable is defined as the ratio of the $E_{\mathrm{T}}^{\mathrm{miss}}$ to its expected resolution: $S_{E_{\mathrm{T}}^{\mathrm{miss}}} = E_{\mathrm{T}}^{\mathrm{miss}}/\sqrt{\sum E_{\mathrm{T}}}$, where the total transverse energy $\sum E_{\mathrm{T}}$ is calculated from the scalar sum of the transverse momenta of the calibrated photons, electrons, muons, jets, and the soft term used in the $E_{\mathrm{T}}^{\mathrm{miss}}$ calculation described in section 4. $S_{E_{\mathrm{T}}^{\mathrm{miss}}}$ is used to better control the experimental uncertainties that affect the reconstruction of the different physical objects that enter the calculation of $E_{\mathrm{T}}^{\mathrm{miss}}$ and improves the impact of $E_{\mathrm{T}}^{\mathrm{miss}}$ on the search sensitivity at low $E_{\mathrm{T}}^{\mathrm{miss}}$. A study showed that very effective discriminating power between signal and backgrounds can be achieved by using only these two variables, considering both increases in sensitivity and in the size of systematic uncertainties associated with the use of additional variables.

Figure 3 shows how different signal models considered in the present search populate the phase space of these two crucial BDT training variables, after applying both the photon

JHEP10(2021)013

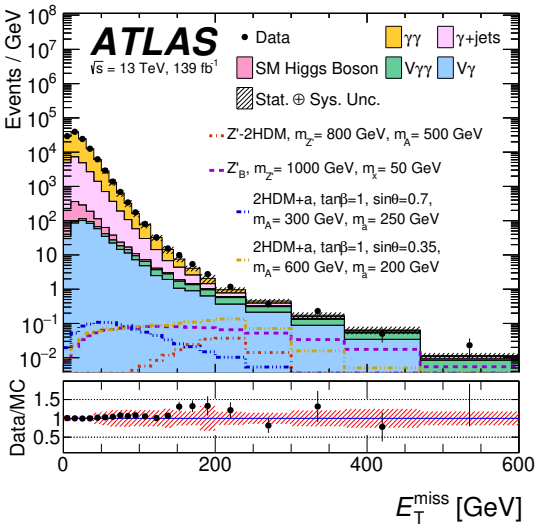

Figure 2. Comparison of the $E_{\mathrm{T}}^{\mathrm{miss}}$ distribution in MC simulation and data, shown after the photon requirements but before the preselection requirements prior to BDT training. In particular, events are required to have $105 < m_{\gamma\gamma} < 160$ GeV. In addition to the signal used for training (blue), one representative signal is also shown for each of the three signal models. The Z'-2HDM, Z'_B, 2HDM+a ($\tan\beta = 1, \sin\theta = 0.7, m_A = 300$ GeV, $m_a = 250$ GeV), and 2HDM+a ($\tan\beta = 1, \sin\theta = 0.35, m_A = 600$ GeV, $m_a = 200$ GeV) signal models are normalized to their respective theoretical cross sections times branching ratios of 0.0815 fb, 0.411 fb, 0.269 fb, and 0.533 fb. The lower panel shows the ratio of data to MC. The uncertainty bands indicate the sum of statistical and experimental systematic uncertainties.

requirements and the preselection. Combined with the $E_{\mathrm{T}}^{\mathrm{miss}}$ distribution in figure 2, these figures illustrate that high-$E_{\mathrm{T}}^{\mathrm{miss}}$ backgrounds are dominated by events with true $E_{\mathrm{T}}^{\mathrm{miss}}$ from $V\gamma$ and $V\gamma\gamma$ processes, while $\gamma\gamma$ and γ+jet backgrounds contribute significantly across the full diphoton candidate p_{T} range. The sum of statistical and experimental systematic uncertainties (indicated by the shaded bands) is relatively flat as a function of $p_{\mathrm{T}}^{\gamma\gamma}$ but decreases in the high $S_{E_{\mathrm{T}}^{\mathrm{miss}}}$ tail, due to the large jet and $E_{\mathrm{T}}^{\mathrm{miss}}$-related systematic uncertainties associated with the fake $E_{\mathrm{T}}^{\mathrm{miss}}$ in the $\gamma\gamma$ and γ+jet components.

The BDT is trained with signal taken from simulated 2HDM+a ($m_A = 300$ GeV, $m_a = 250$ GeV, $\tan\beta = 1$, $\sin\theta = 0.7$) events, while the background used in training is taken from a data control region that differs from the nominal data selection by requiring that at least one photon fails either the identification or isolation requirements, with the expectation that this will not drastically change the event kinematics. The choice of training signal is motivated by its soft $E_{\mathrm{T}}^{\mathrm{miss}}$ distribution, which is relatively close to that of the background. The trained classifier performs well for all signal models, and using a different signal model with soft $E_{\mathrm{T}}^{\mathrm{miss}}$ in the training does not appreciably affect the sensitivity. For instance, for each of the four signals shown in figure 3, the variance in sensitivity from retraining the existing classifier on a different signal is generally on the order of 10%. Figure 4 shows the distribution of the BDT score for various signals and backgrounds after training. The model trained on the data control region (dominated by γ+jet contributions) performs well

JHEP10(2021)013

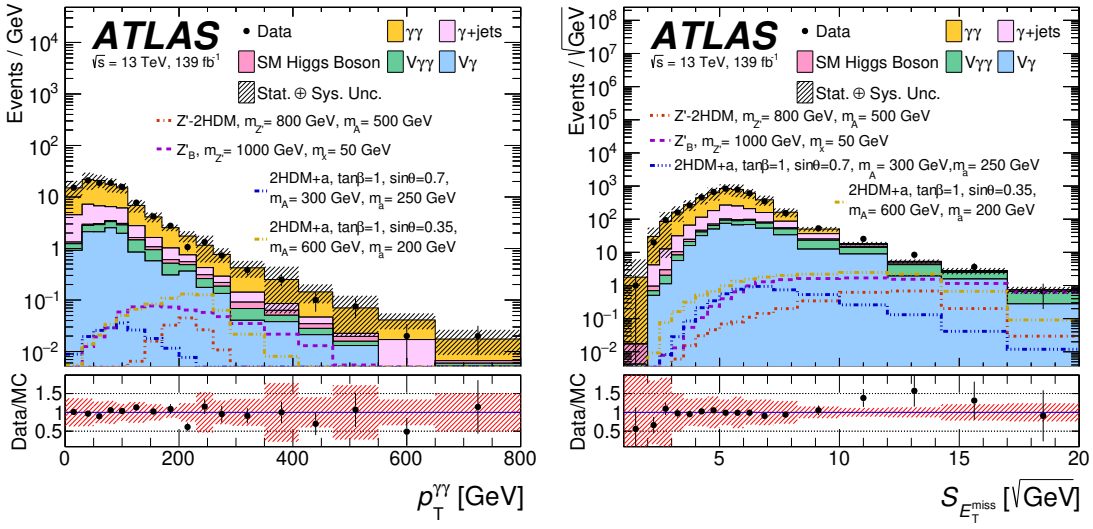

Figure 3. Data and MC distributions of the BDT input variables, $p_{\mathrm{T}}^{\gamma\gamma}$ and $S_{E_{\mathrm{T}}^{\mathrm{miss}}}$, after the photon requirements and the preselection requirements prior to BDT training. In particular, events are required to have $105 < m_{\gamma\gamma} < 160$ GeV. In addition to the signal used for training (blue), one representative signal is also shown for each of the three signal models. The Z'-2HDM, Z'_B, 2HDM+a ($\tan\beta = 1, \sin\theta = 0.7, m_A = 300$ GeV, $m_a = 250$ GeV), and 2HDM+a ($\tan\beta = 1, \sin\theta = 0.35, m_A = 600$ GeV, $m_a = 200$ GeV) signal models are normalized to their respective theoretical cross sections times branching ratios of 0.0815 fb, 0.411 fb, 0.269 fb, and 0.533 fb. The lower panel shows the ratio of data to MC. The narrow uncertainty bands (indicating the sum of statistical and experimental systematic uncertainties) at high $S_{E_{\mathrm{T}}^{\mathrm{miss}}}$ values are due to the absence of $\gamma\gamma$ and γ+jet contributions, which have large jet and $E_{\mathrm{T}}^{\mathrm{miss}}$-related systematic uncertainties.

when applied to the data sideband (dominated by true diphoton events) as the BDT is able to separate both these backgrounds from expected signals. The disagreement between the data control region and the data sideband at high BDT values is expected due to their different compositions and does not impact the final statistical results as the data control region is only used to train the BDT classifier.

Finally, events are separated into low $E_{\mathrm{T}}^{\mathrm{miss}}$ ($E_{\mathrm{T}}^{\mathrm{miss}} < 150$ GeV) and high $E_{\mathrm{T}}^{\mathrm{miss}}$ ($E_{\mathrm{T}}^{\mathrm{miss}} > 150$ GeV) regions. Such a split not only improves overall sensitivity but also complements h+$E_{\mathrm{T}}^{\mathrm{miss}}$ searches where h decays into a pair of b-quarks [15], which have low sensitivity in the $E_{\mathrm{T}}^{\mathrm{miss}} < 150$ GeV region due to trigger thresholds. In each region, two categories are defined from two sequential ranges of the BDT score, with the ranges optimized to maximize the combined signal sensitivity in the two chosen categories while discarding the remaining events. The category naming scheme and corresponding ranges are summarized in table 1, with the 'tight' categories having a higher training signal purity than the 'loose' categories. Figure 5 demonstrates that in each of the two regions, the BDT score is a non-trivial function of the input variables. The black and red contours in the figure indicate the separation between categories based on the BDT score for the high $E_{\mathrm{T}}^{\mathrm{miss}}$ and low $E_{\mathrm{T}}^{\mathrm{miss}}$ regions, respectively.

JHEP10(2021)013

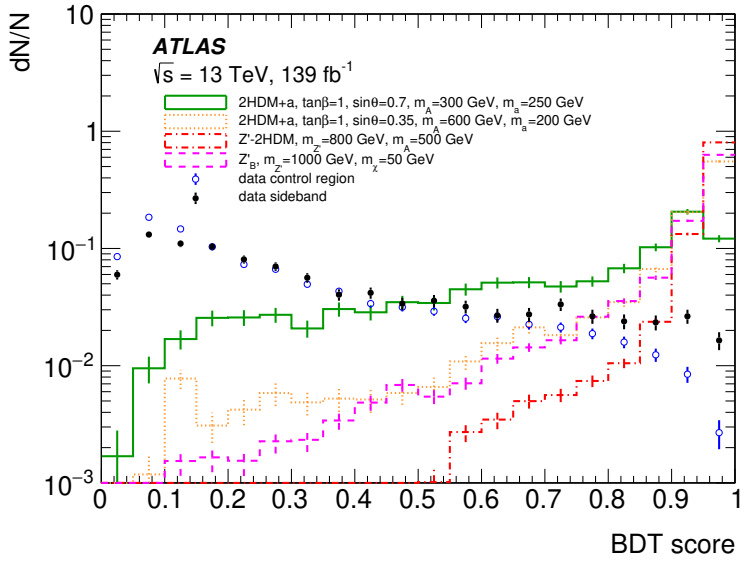

Figure 4. The BDT score for selected signals, the data control region, and the data sideband, with 1 being more signal-like and 0 being more background-like. The data sideband consists of events with two 'tight' identified and isolated photon candidates, while the data control region consists of diphoton events where at least one photon candidate fails at least one of the identification or isolation requirements. All events are required to have $105 < m_{\gamma\gamma} < 160$ GeV, and events in the $120 < m_{\gamma\gamma} < 130$ GeV region of the data sideband are vetoed. The error bars represent statistical uncertainties.

Category	$E_{\mathrm{T}}^{\mathrm{miss}}$ requirement	BDT score range
High $E_{\mathrm{T}}^{\mathrm{miss}}$ BDT tight	$E_{\mathrm{T}}^{\mathrm{miss}} > 150$ GeV	$0.950 <$ BDT score < 1
High $E_{\mathrm{T}}^{\mathrm{miss}}$ BDT loose	$E_{\mathrm{T}}^{\mathrm{miss}} > 150$ GeV	$0.694 <$ BDT score < 0.950
Low $E_{\mathrm{T}}^{\mathrm{miss}}$ BDT tight	$E_{\mathrm{T}}^{\mathrm{miss}} < 150$ GeV	$0.864 <$ BDT score < 1
Low $E_{\mathrm{T}}^{\mathrm{miss}}$ BDT loose	$E_{\mathrm{T}}^{\mathrm{miss}} < 150$ GeV	$0.386 <$ BDT score < 0.864

Table 1. The definitions of the four signal region categories.

6 Signal and background parameterization

The signal and backgrounds are extracted by fitting analytic functions to the diphoton invariant mass distribution in the range $105 < m_{\gamma\gamma} < 160$ GeV in each category. For the signal and the SM Higgs boson background, the expected normalizations are obtained from their theoretical cross sections multiplied by the product of the acceptance times efficiency from the simulation. The diphoton invariant mass distribution shapes are modelled with a double-sided Crystal Ball function (as defined in ref. [79]). The shape parameters are determined by fitting the diphoton mass distribution in simulation for each category. The width of the fitted function is largely insensitive to the specific signal model, with maximum variations of approximately 10%.

Both the normalization and the shape of the non-resonant background are obtained by fitting the diphoton invariant mass distribution in data for each category. A variety of analytic functions are considered for the non-resonant background parameterization:

JHEP10(2021)013

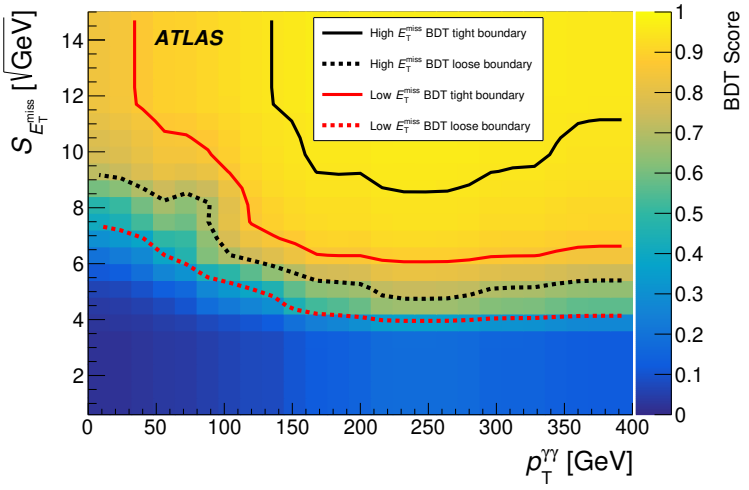

Figure 5. The BDT score as a function of the input variables, $p_{\mathrm{T}}^{\gamma\gamma}$ and $S_{E_{\mathrm{T}}^{\mathrm{miss}}}$, with 1 being more signal-like and 0 being more background-like. The plot is produced by splitting the plane into equal cells of $p_{\mathrm{T}}^{\gamma\gamma} \times S_{E_{\mathrm{T}}^{\mathrm{miss}}}$, and evaluating the corresponding BDT score. The black (red) lines indicate the minimum score boundaries for the BDT categories in the high $E_{\mathrm{T}}^{\mathrm{miss}}$ (low $E_{\mathrm{T}}^{\mathrm{miss}}$) region, as defined in table 1.

exponential functions of different-order polynomials, Bernstein polynomials of different order [88], and an adapted dijet function [89]. The potential bias associated with the choice of a specific analytic function to model the continuum background is referred to as the non-resonant background modelling uncertainty, $\Delta N_{\mathrm{sig}}^{\mathrm{bkg\ model}}$. It is estimated for each category as the signal event yield extracted from a signal-plus-background maximum-likelihood fit to a background-only diphoton invariant mass distribution, following the procedure in ref. [79]. The background-only distribution is obtained by combining $\gamma\gamma$, γ+jet, $V\gamma$, and $V\gamma\gamma$ processes so that the total template is normalized to the data sideband.

Around 80% of sideband events consist of true diphoton events, with the remaining 20% consisting of γ+jet events and a negligible number of dijet events. These fractions are determined by a two-dimensional sideband technique which counts the number of events in 16 regions defined by whether each photon passes or fails the identification or isolation requirements [90]. The final background modelling shows a negligible dependence on these fractions when varied by their respective uncertainties.

The true diphoton component is modelled by simulated $\gamma\gamma$, $V\gamma$, and $V\gamma\gamma$ samples. The $V\gamma$ sample consists mainly of V decays into electrons subsequently misidentified as photons, resulting in an $m_{\gamma\gamma}$ spectrum similar to that of the $V\gamma\gamma$ sample. Both the $V\gamma$ and $V\gamma\gamma$ templates are normalized according to their theoretical cross sections, which accounts for approximately 10% of the sideband events. The $\gamma\gamma$ template is then normalized to approximately 70% of the sideband events, so that the sum of the $\gamma\gamma$, $V\gamma$, and $V\gamma\gamma$ templates accounts for the entire true diphoton component. To represent the remaining γ+jet and dijet components, a γ+jet template derived from a data control region in which exactly one photon fails the identification requirements is normalized to 20% of sideband events and combined with the true diphoton template.

JHEP10(2021)013

Category	$\Delta N_{\text{sig}}^{\text{bkg model}}$	$\Delta N_{\text{sig}}^{\text{bkg model}} / N_{\text{bkg}}^{\text{non-res.}}$ [%]
High $E_{\text{T}}^{\text{miss}}$ BDT tight	0.54	6.8
High $E_{\text{T}}^{\text{miss}}$ BDT loose	1.07	4.2
Low $E_{\text{T}}^{\text{miss}}$ BDT tight	0.62	6.3
Low $E_{\text{T}}^{\text{miss}}$ BDT loose	2.64	2.0

Table 2. The uncertainty in the signal due to the non-resonant background modelling ($\Delta N_{\text{sig}}^{\text{bkg model}}$) per category. As a comparison of scale, its ratio to the expected non-resonant background in the signal window $120 < m_{\gamma\gamma} < 130$ GeV is also shown. In each category, the non-resonant $m_{\gamma\gamma}$ distribution is modelled by an exponential function ($\exp(a \cdot m_{\gamma\gamma})$), where a is a free parameter.

For a given functional form, several fits are tested by varying the position of the signal peak between 121 and 129 GeV. The largest number of signal events obtained in these fits to the background-only templates is taken as $\Delta N_{\text{sig}}^{\text{bkg model}}$. Among the different analytic functions that are tested, the one with $\Delta N_{\text{sig}}^{\text{bkg model}}$ smaller than 50% of the statistical uncertainty of the fitted signal yield and the least number of free parameters is chosen as the nominal background parameterization to describe the non-resonant background shape. In each category, an exponential function $\exp(a \cdot m_{\gamma\gamma})$ is found to be the best choice.

The non-resonant background modelling uncertainty $\Delta N_{\text{sig}}^{\text{bkg model}}$, which is taken as an estimate of the systematic uncertainty due to the choice of parameterization, is shown in table 2 for each category. As a comparison of scale, its ratio to the expected non-resonant background $N_{\text{bkg}}^{\text{non-res.}}$ in the signal window $120 < m_{\gamma\gamma} < 130$ GeV is also provided. This quantity is less than 7% in the most sensitive category, showing that the systematic uncertainty is under control in a category already dominated by statistical uncertainties. This uncertainty is implemented in the statistical model described in section 7 as an additional signal normalized to $\Delta N_{\text{sig}}^{\text{bkg model}}$, times a Gaussian-constrained nuisance parameter.

7 Systematic uncertainties

Uncertainties from experimental and theoretical sources affect both the shapes and yields of the signal and the SM Higgs boson background, estimated from the simulated MC samples. Of these, the largest uncertainties are due to the $E_{\text{T}}^{\text{miss}}$ reconstruction and jets, pile-up, and signal efficiency interpolation. The theoretical systematic uncertainties include uncertainties on the factorization and renormalization scale and the parton distribution function and α_{s} (PDF+α_{s}). The non-resonant background is obtained directly from the fit to the data and therefore its only systematic uncertainty is the potential bias $\Delta N_{\text{sig}}^{\text{bkg model}}$, as described in section 6. A summary of the experimental and theoretical uncertainties affecting the yields from SM Higgs boson processes, non-resonant background, and signal production is shown in table 3.

The uncertainty in the integrated luminosity of the full Run 2 dataset is 1.7% [91], obtained using the LUCID-2 detector [31] for the primary luminosity measurements.

JHEP10(2021)013

Source	Signals [%]	Backgrounds [%]	
		SM Higgs boson	Non-resonant background
Experimental			
Luminosity	1.7	1.7	– – –
Trigger efficiency	1.0	1.0	– – –
Vertex selection (inclusive cat.)	0.01	0.01	– – –
Photon energy scale	1.0	1.2	– – –
Photon energy resolution	0.3	0.4	– – –
Photon identification efficiency	1.3	1.3	– – –
Photon isolation efficiency	1.3	1.4	– – –
AtlFastII simulation	2.0	– – –	– – –
$E_{\mathrm{T}}^{\mathrm{miss}}$ reconstruction and jet uncertainty	2.8	1.7	– – –
Pile-up reweighting	2.3	2.0	– – –
Signal efficiency interpolation	< 13	– – –	– – –
Non-resonant background modelling	– – –	– – –	6.8
Theoretical			
Factorization and renormalization scale in migration	1.3	3.5	– – –
PDF+α_{s} in migration	1.2	1.0	– – –
Factorization and renormalization scale in cross section	– – –	2.8	– – –
PDF+α_{s} in cross section	– – –	2.8	– – –
Multi-parton interactions, ISR/FSR, hadronization	3.0	3.0	– – –
$B(H \to \gamma\gamma)$	1.7	1.7	– – –

Table 3. Breakdown of the dominant systematic uncertainties. The impact of uncertainties on the yield of the SM Higgs boson processes and signal samples is shown. All production modes of the SM Higgs boson are considered together. Representative values for the impact on the most sensitive category are shown, unless one of the systematic uncertainties is not applicable to the sample, in which case the value is substituted by a "---". The "<" on the signal efficiency interpolation uncertainty indicates that the value is estimated from the maximum relative difference between the fully simulated and reweighted samples over all validation points. The impact of theoretical uncertainties is split into their effects on the migration of events between different categories and on the total cross section. Here the signal is a 2HDM+a model with $m_A = 200$ GeV, $m_a = 100$ GeV, $\tan\beta = 1.0$, $\sin\theta = 0.35$, which provides a conservative estimate of the size of the uncertainties for all signal points.

The efficiency of the diphoton trigger used to select events is evaluated in MC simulation using a trigger matching technique and in data using a bootstrap method [32]. In the diphoton invariant mass window of $105 < m_{\gamma\gamma} < 160$ GeV, the trigger efficiency uncertainty affects the acceptance by 1% in each category.

The uncertainty in the vertex selection efficiency is assessed by comparing the efficiency of finding photon-pointing vertices in $Z \to e^+e^-$ events in data with that in MC simulation [92]. The resulting uncertainty is found to be negligible in the inclusive photon selection.

The systematic uncertainties due to the photon identification and isolation efficiencies are estimated following the prescriptions in ref. [78]. They are evaluated by varying the

JHEP10(2021)013

correction factors of photon selection efficiencies in MC simulation by the corresponding uncertainties. In the most sensitive category, the photon identification efficiency uncertainty is 1.3% for the SM Higgs boson and for the signal samples, while the photon isolation efficiency uncertainty is 1.4% for the SM Higgs boson and 1.3% for the signal samples. For the signal samples, an additional 2% uncertainty is added to account for photon mismodelling by the AtlFastII simulations.

The experimental uncertainties in photon scale and resolution are obtained from ref. [78]. In the most sensitive category, the uncertainty in the energy scale has an effect of 1.0% on the normalization of the signals and 1.2% on the normalization of the SM Higgs boson background. The uncertainty in the energy resolution has an effect below 0.3% on the normalization of the signals and 0.4% on the normalization of the SM Higgs boson background. The effects of photon energy scale and resolution uncertainties on the signal and SM Higgs boson background mass distributions are also evaluated and parameterized in the fit to MC simulation. In particular, the impact of the scale uncertainties on the mean of these mass distributions is 0.3%, while the impact of the energy resolution on the width is 6%. An additional uncertainty in the Higgs boson mass position of 0.24 GeV from the measurement of the Higgs boson mass is considered in the fit, although this does not significantly impact the final result [59].

The migration of events among categories results from changes in object energies and momenta, due mostly to misreconstruction of jets and $E_{\mathrm{T}}^{\mathrm{miss}}$. The experimental uncertainties in jet energy scale and resolution are propagated to the $E_{\mathrm{T}}^{\mathrm{miss}}$ calculation. In addition, the uncertainties in the scale and resolution of the $E_{\mathrm{T}}^{\mathrm{miss}}$ soft term are evaluated by using the method described in ref. [86]. The uncertainties for the $E_{\mathrm{T}}^{\mathrm{miss}}$ reconstructed from the hardest vertex and the neural-network-selected vertex are evaluated independently by using jets reconstructed relative to the respective vertices. In the most sensitive category, the uncertainties due to the $E_{\mathrm{T}}^{\mathrm{miss}}$ soft term are 0.6% for both the signal and background. The migration uncertainties due to the jet energy scale and resolution have an effect of 2.5% and 1.3% on the event yield of the signal and SM Higgs boson samples, respectively. The pile-up reweighting uncertainty is taken into account by propagating it through the event selection, and results in a 2.3% and 2.0% uncertainty in the event yield of the signal and SM Higgs boson samples, respectively, in the most sensitive category.

The uncertainty in the signal efficiency due to the interpolation method detailed in section 3 is estimated by comparing the yields from fully simulated samples and reweighted samples for certain validation parameter points. The maximum relative difference between the fully simulated and reweighted samples over all these points ranges from 9% to 13%, depending on the model, and these numbers are taken as the uncertainty.

The effects of theoretical scale uncertainties on the SM Higgs boson and 2HDM+a signal samples are estimated by varying the factorization and renormalization scales up and down from their nominal values by a factor of two, recalculating the cross section in each case, and taking the largest deviation from the nominal cross section as the uncertainty. The scale uncertainties affect the event migration between the categories by 3.5% for the SM Higgs boson processes and 1.3% for the signal processes. The uncertainties in the cross section of the SM Higgs boson processes are taken from ref. [57]. The effect of the scale

JHEP10(2021)013

uncertainty when selecting ggF Higgs boson events with high $p_{\mathrm{T}}^{\gamma\gamma}$ is estimated to be 20% for each category, but the effect is negligible in the final fit because the ggF Higgs boson contribution is small. In general, the effects of theory uncertainties on the SM Higgs boson yield are small compared to the uncertainties in the non-resonant background, and do not significantly impact the sensitivity. For signals, only the uncertainties on the 2HDM+a models are taken into account, because for the Z'_B and Z'-2HDM models, no QCD vertex is calculated in the matrix element. The uncertainties in the signal cross section are not used in the fit, but are instead shown as bands on the observed limits.

For signals, PDF+α_{s} uncertainties are estimated using the SysCalc [93] package associated with MadGraph5. The uncertainties in the migration of each category are estimated by varying the parameters of the `NNPDF3.0lo` PDF set and taking the maximum change as the uncertainty. For the SM Higgs boson, the effects of PDF+α_{s} uncertainties on the cross sections are taken from ref. [57]. The uncertainties in the migration of each category are estimated using the recommendations of PDF4LHC [42]. These uncertainties are 1.0% for the SM Higgs boson and 1.2% for signals. The effects of PDF+α_{s} uncertainties on the cross section are estimated to be 2.8% for the SM Higgs boson and up to 32% for the signals. The effects of these SM Higgs boson uncertainties are once again small compared to the impact of the non-resonant background uncertainty, while the uncertainties in the signal cross sections are not used in the fit, but are instead shown as bands on the observed limits.

The uncertainty in the branching ratio (B) of $h \to \gamma\gamma$ is 1.73% [57]. The same $h \to \gamma\gamma$ branching ratio is used for the SM Higgs boson and the signal models when setting limits. For the 2HDM+a models, the Higgs boson is only allowed to decay into $a\chi\chi$ or through a SM channel, where the $h \to a\chi\chi$ decay branching ratio is smaller than 1% when m_a is greater than 110 GeV for $m_\chi = 10$ GeV. This 1% effect is neglected when setting limits as it is small with respect to the uncertainty in the SM $h \to \gamma\gamma$ branching ratio. Similarly, the $h \to Z'Z'$ decay branching ratio is neglected in the Z'_B model for $m_{Z'} < m_h/2$.

The effects of multi-parton interactions, parton showering and hadronization are evaluated by varying the eigen-variables in Pythia for signal, by comparing Herwig 7.1.3 [94] with Pythia for ggF, VBF, and Vh, and by comparing Herwig 7.0.4 [95] with Pythia for $t\bar{t}h$. These uncertainties are of the order of 3% for both the signal and SM Higgs boson processes.

8 Results

8.1 Statistical framework

The results of the analysis are derived from a likelihood fit of the $m_{\gamma\gamma}$ distribution in the range $105 < m_{\gamma\gamma} < 160$ GeV, performed simultaneously over all four categories. The likelihood function is defined as

$$\mathcal{L} = \prod_{c=1}^{4} \left(\mathrm{Pois}(n_c | N_c(\theta)) \cdot \prod_{i=1}^{n_c} f_c(m^i_{\gamma\gamma}, \theta) \cdot G(\theta) \right)$$

where for each event i in a category c, n_c is the observed number of events, N_c is the expected number of events, f_c is the value of the probability density function, θ are nuisance parameters, and $G(\theta)$ are Gaussian constraints on the nuisance parameters.

JHEP10(2021)013

The expected number of events N_c is the sum of the expected yields from BSM signals, SM Higgs boson processes, the non-resonant background modelling uncertainty, and the non-resonant background:

$$N_c(\theta) = \mu \cdot N_{\mathrm{BSM},c}(\theta_{\mathrm{yield}}) + N_{\mathrm{Higgs},c}(\theta_{\mathrm{yield}}) + \Delta N_{\mathrm{sig},c}^{\text{bkg model}} \cdot \theta_{\mathrm{sig},c}^{\text{bkg model}} + N_{\mathrm{bkg},c}^{\text{non-res.}}$$

where μ is the signal strength, and θ_{yield} and $\theta_{\mathrm{sig},c}^{\text{bkg model}}$ represent systematic uncertainties in the resonant and non-resonant yields, as detailed in section 7.

The nominal Higgs boson mass is set to 125.09 GeV [59] and the nominal resonant yields are fixed to values from simulation. The signal strength, non-resonant background shape parameters, and the nuisance parameters representing the systematic uncertainties are free parameters in the fit.

The test statistic is based on the likelihood ratio approach, as presented in ref. [96].

The event yields and uncertainties in the observed data, signal, and backgrounds in the four categories within a window of $120 < m_{\gamma\gamma} < 130$ GeV after the fit are shown in table 4, for representative Z'_B, Z'-2HDM, and 2HDM+a signals. While the signal yields in each category depend on the specific model, the SM Higgs boson contribution comprises approximately 30% of the total background in the High $E_{\mathrm{T}}^{\mathrm{miss}}$ BDT tight and Low $E_{\mathrm{T}}^{\mathrm{miss}}$ BDT tight categories, due primarily to the presence of Vh events with high genuine $E_{\mathrm{T}}^{\mathrm{miss}}$. The uncertainties in the SM Higgs backgrounds reflect the impact of systematic uncertainties, while the uncertainties in the non-resonant background are constrained by the full diphoton mass range and the given analytic form, giving a lower uncertainty relative to the background contribution. On the other hand, the uncertainties in the signal yields reflect the fact that the fitted signal is driven mainly by the High $E_{\mathrm{T}}^{\mathrm{miss}}$ BDT tight category, where there is a large statistical uncertainty in the data.

Figure 6 shows the $m_{\gamma\gamma}$ distribution in each BDT category as well as the analytic fits to the data for the 2HDM+a model with $\tan\beta = 1.0$, $\sin\theta = 0.35$, $m_A = 600$ GeV, and $m_a = 200$ GeV. Different signal models have similar $m_{\gamma\gamma}$ shapes and therefore will mainly differ in the relative signal contributions in the various categories. The fit demonstrates sensitivity to the SM Higgs boson expected production yield, with the Vh channel providing sensitivity in the high $E_{\mathrm{T}}^{\mathrm{miss}}$ region. For each $m_{\gamma\gamma}$ distribution, the residual between data observed in each bin and the fitted non-resonant and SM Higgs boson backgrounds is shown in the lower panel. The experimental data distribution clearly exhibits no excess with respect to the total background and the fit result is then interpreted to set 95% confidence level (CL) limits on the different models discussed in section 1.

8.2 Interpretation

The observed and expected exclusion contours at 95% CL for the Z'_B model in the m_χ–$m_{Z'}$ plane are shown in figure 7 for $\sin\theta = 0.3$, $g_q = 1/3$, and $g_\chi = 1$. Compared to the results of previous h+$E_{\mathrm{T}}^{\mathrm{miss}}$ searches in the $\gamma\gamma$ decay channel, the limit from the full LHC Run 2 dataset extends up to 1150 GeV in $m_{Z'}$ while it was lower than 1000 GeV in the previous ATLAS publication in this search channel [17] with early Run 2 data. The increase in the limit is only 150 GeV despite the four times larger dataset, because the signal cross

JHEP10(2021)013

Category	High $E_{\mathrm{T}}^{\mathrm{miss}}$ BDT tight	High $E_{\mathrm{T}}^{\mathrm{miss}}$ BDT loose	Low $E_{\mathrm{T}}^{\mathrm{miss}}$ BDT tight	Low $E_{\mathrm{T}}^{\mathrm{miss}}$ BDT loose
Data	12	29	11	143
Backgrounds				
SM Higgs boson	3.74 ± 0.25	3.40 ± 0.28	3.12 ± 0.23	9.9 ± 1.5
Non-resonant	7.8 ± 1.3	25.3 ± 2.3	9.8 ± 1.5	130 ± 5
Total	11.6 ± 1.3	28.7 ± 2.3	12.9 ± 1.5	140 ± 5
Z'_B model, $m_{Z'} = 1000$ GeV, $m_\chi = 50$ GeV				
Signal yields	0.7 ± 3.1	0.1 ± 0.6	0.1 ± 0.6	0.1 ± 0.6
Z'-2HDM model, $m_A = 800$ GeV and $m_\chi = 500$ GeV				
Signal yields	0.6 ± 3.1	0.1 ± 0.4	0.05 ± 0.26	0.03 ± 0.17
2HDM+a model, $m_A = 600$ GeV, $m_a = 200$ GeV, $\tan\beta = 1.0$, $\sin\theta = 0.35$				
Signal yields	0.6 ± 3.1	0.2 ± 1.2	0.1 ± 0.5	0.1 ± 0.7

Table 4. Event yields and uncertainties after a fit to data in the range of $120 < m_{\gamma\gamma} < 130$ GeV for data, signal models, the SM Higgs boson background, and non-resonant background in each analysis category, for an integrated luminosity of 139 fb^{-1}. The signal samples shown correspond to a Z'_B signal with $m_{Z'} = 1000$ GeV and $m_\chi = 50$ GeV, a Z'-2HDM signal with $m_A = 800$ GeV and $m_\chi = 500$ GeV, and a 2HDM+a signal with $m_A = 600$ GeV, $m_a = 200$ GeV, $\tan\beta = 1.0$, and $\sin\theta = 0.35$. The uncertainties correspond to the quadrature sum of the statistical and systematic uncertainties.

section decreases strongly with increasing Z' mass. In addition, the maximum limit on m_χ increases by more than 100 GeV to reach 280 GeV for $m_{Z'}$ in the range 700–950 GeV.

Figure 8 shows a comparison of the inferred limits at 90% CL with the constraints from direct detection experiments on the spin-independent DM-nucleon cross section in the context of the Z'_B simplified model with vector couplings using the relation

$$\sigma_{N\chi}^{\mathrm{SI}} = \frac{\mu_{N\chi}^2}{\pi A^2}\left[Zf_p + (A-Z)f_n\right]^2 ,$$

in which $\mu_{N\chi} = m_\chi m_N/(m_\chi + m_N)$ is the reduced mass of the DM-nucleon system, and $f_p = f_n = 3g_q g_\chi/m_{Z'}^2$ are the couplings between DM particles and protons and neutrons, respectively [12]. In the above expression, Z and A are the numbers of protons and nucleons in the considered nucleus, set to 1 in this case. Results from the XENON [97–99] and DarkSide-50 [100] direct detection experiments are overlaid for the comparison. The diagonal upper branch of the limit curve reflects the fact that there are no parameters of the model that predict a cross section larger than this limit. Consequently, an observed cross section greater than this limit cannot be interpreted in this model. On the contrary, the horizontal branch delimits the sensitivity of the analysis to this model. This result improves the upper limit on the spin-independent cross section for $m_\chi < 2$ GeV by a factor of two relative to the previous publication [17]. LHC data offers a unique window on low-mass DM candidates that complements direct DM searches in an interesting way but provides results that are more model-dependent than direct search results. The ability of each result to constrain new physics depends crucially on the model parameters. For instance, the results for the Z'_B model, with model parameters $\sin\theta = 0.3$, $g_q = 1/3$, and $g_\chi = 1$ for this

JHEP10(2021)013

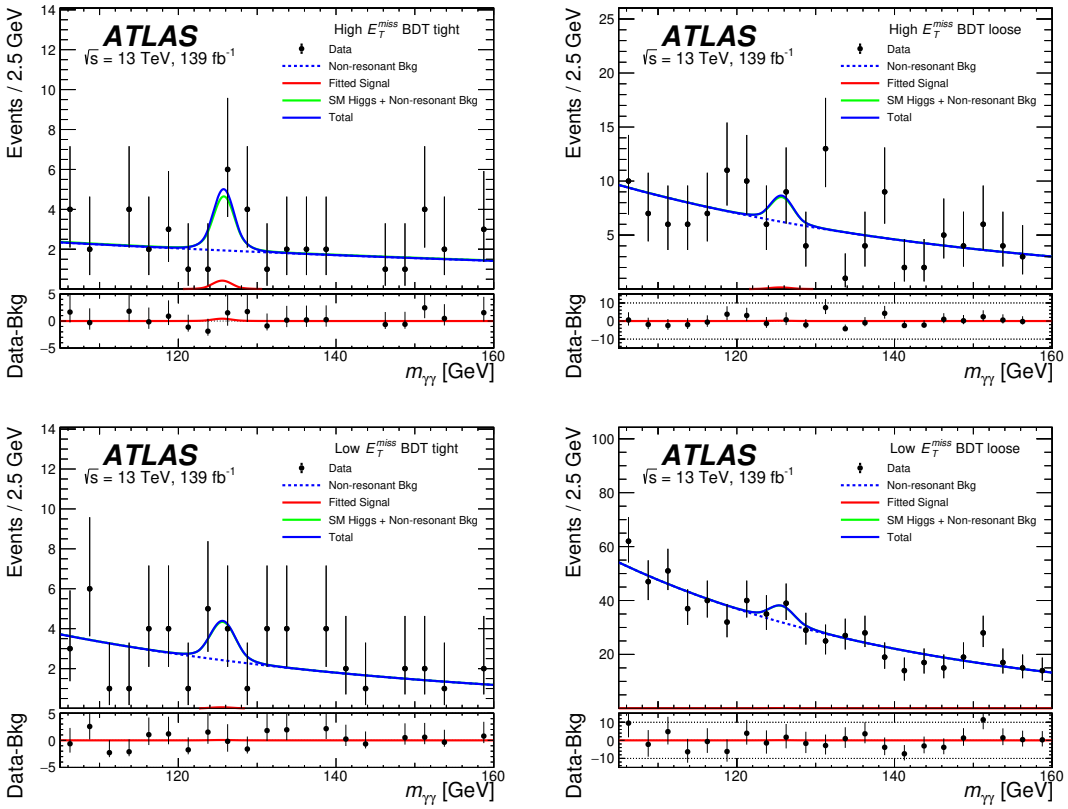

Figure 6. The diphoton invariant mass spectra from the data and the corresponding fitted signal and background in each BDT category. The signal is the 2HDM+a model with $\tan\beta = 1.0$, $\sin\theta = 0.35$, $m_A = 600$ GeV, and $m_a = 200$ GeV. Different signal models have similar $m_{\gamma\gamma}$ shapes and therefore will mainly differ in the relative signal contributions in the various categories. The non-resonant background and the predicted SM Higgs boson contribution are shown. The blue curve shows the sum of the signal, SM Higgs boson, and non-resonant background after the fit. The subplot shows the residual between the observed number of events and the fitted non-resonant and SM Higgs boson backgrounds. The error bars represent statistical uncertainties.

search, are more stringent than direct detection experiments for $m_\chi < 2$ GeV and extend to DM masses well below 1 GeV, while in the case of a much lower coupling between DM and SM particles, the direct search limits may provide the more stringent constraints on this possible phenomenology. The impact of renormalization-group evolution effects [101, 102] when comparing collider and direct detection limits is not considered here.

The observed and expected exclusion contours at 95% CL for the Z'-2HDM model in the m_A–$m_{Z'}$ plane are shown in figure 9 for $m_{H^{0,\pm}} = m_A$, $m_\chi = 100$ GeV, $\tan\beta = 1.0$, and $g'_Z = 0.8$. The maximum limit on m_A reaches 420 GeV for a Z' mass of $m_{Z'} = 825$ GeV. Above $m_A = 350$ GeV, competing decays from $A \to t\bar{t}$ cause the $A \to \chi\chi$ branching ratio to decrease quickly with increasing m_A, resulting in the feature near $m_{Z'} = 1300$ GeV. Changes in the DM mass m_χ would not significantly affect these results; such variations would only become important for very high DM masses which are not accessible to the current analysis [23].

JHEP10(2021)013

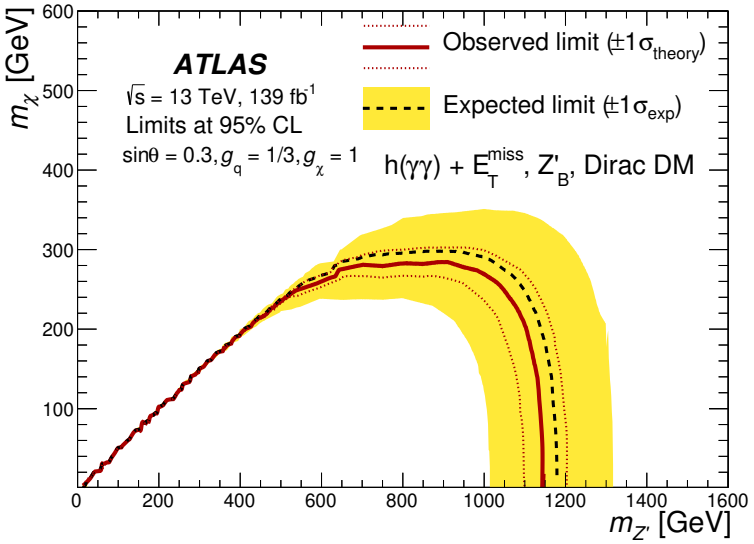

Figure 7. The observed (solid line) and expected (dashed lines) exclusion limit contours at 95% CL for the Z'_B model in the m_χ–$m_{Z'}$ plane, for $\sin\theta = 0.3$, $g_q = 1/3$, and $g_\chi = 1$. The dotted lines represent the $\pm1\sigma$ theoretical uncertainty for the observed limit. The $\pm1\sigma$ expected exclusion limit contour is shown as the yellow band.

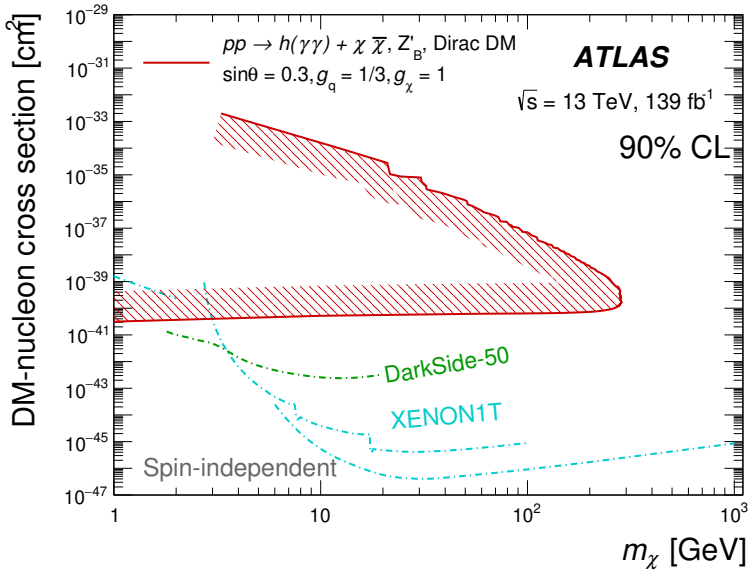

Figure 8. A comparison of the inferred limits with the constraints from direct detection experiments on the spin-independent DM-nucleon cross section in the context of the Z'_B simplified model with vector couplings. Limits are shown at 90% CL. The results from this analysis, in which the region on the side of the hatched band inside the contour is excluded, are compared with limits from the XENON [97–99] and DarkSide-50 [100] experiments. The comparison is model-dependent and solely valid in the context of this model, assuming Dirac fermion DM, mixing angle $\sin\theta = 0.3$, and the coupling values $g_q = 1/3$ and $g_\chi = 1$. The diagonal upper branch of the limit curve reflects the fact that there are no parameters of the model that predict a cross section larger than this limit. The impact of renormalization-group evolution effects [101, 102] when comparing collider and direct detection limits is not taken into consideration here.

JHEP10(2021)013

Figures 10 and 11 show the observed and expected exclusion contours at 95% CL for the 2HDM+a model in the m_A–m_a and $\tan\beta$–m_a planes, respectively, for $\sin\theta = 0.35$ and $m_\chi = 10$ GeV. In the m_A–m_a scan for this benchmark point, the highest excluded m_A is 800 GeV for $m_a = 110$ GeV while the maximum excluded m_a reaches about 260 GeV for $m_A = 600$ GeV. The scan of m_a starts from 110 GeV to avoid opening the decay of $h \to a\chi\chi$ for $\chi = 10$ GeV. In the $\tan\beta$–m_a scan, the region $\tan\beta < 0.4$ is covered with a hatched band because there the decay width of the low-mass Higgs boson is greater than 20% of its mass, which renders the cross-section calculation unreliable [22]. The shape of the limit curve closely follows the signal cross section, which is dominated by ggF for low $\tan\beta$ and $b\bar{b}$-fusion for high $\tan\beta$. Figure 12 shows the observed and expected limits on the 2HDM+a model as a function of $\sin\theta$ for $m_{A,H^\pm,H} = 600$ GeV, $m_a = 200$ GeV, and $\tan\beta = 1.0$, showing that for this benchmark point the ATLAS data excludes a vast domain of possible mixing angle θ values.

9 Summary

A search for dark matter in association with a Higgs boson decaying into two photons is presented. This study is based on data collected with the ATLAS detector during 2015-2018, corresponding to an integrated luminosity of 139 fb^{-1} of proton-proton collisions at the LHC at a centre-of-mass energy of 13 TeV. No significant excess over the expected background is observed. Upper limits at 95% CL are set on the possible contributions to the cross sections times branching fraction of the Higgs boson decaying into two photons in association with missing transverse momentum for three models: a Z'_B model, a Z'-2HDM model, and a 2HDM+a model. The Z'_B and Z'-2HDM models provide interesting information complementary to leptophobic vector or axial-vector Z' models, which are already largely excluded by dijet searches [22]. Limits at 95% CL are set on the observed signal strength in the m_χ–$m_{Z'}$ plane for the Z'_B model, the m_A–$m_{Z'}$ plane for the Z'-2HDM model, and the m_A–m_a and $\tan\beta$–m_a planes for the 2HDM+a model. A one-dimensional scan of the mixing parameter $\sin\theta$ for $m_{A,H^\pm,H} = 600$ GeV, $m_a = 200$ GeV and $\tan\beta = 1.0$ in the 2HDM+a model is performed as well. Additionally, the results for the Z'_B model are interpreted in terms of 90% CL limits on the DM-nucleon scattering cross section, as a function of the DM particle mass, for a spin-independent scenario. For a DM mass lower than 2 GeV, the constraint with couplings $\sin\theta = 0.3$, $g_q = 1/3$, and $g_\chi = 1$ placed on the DM-nucleon cross section is more stringent than limits from direct detection experiments at low DM mass, showing the complementarity between the several approaches trying to unveil the microscopic nature of DM.

Acknowledgments

We thank CERN for the very successful operation of the LHC, as well as the support staff from our institutions without whom ATLAS could not be operated efficiently.

We acknowledge the support of ANPCyT, Argentina; YerPhI, Armenia; ARC, Australia; BMWFW and FWF, Austria; ANAS, Azerbaijan; SSTC, Belarus; CNPq and

JHEP10(2021)013

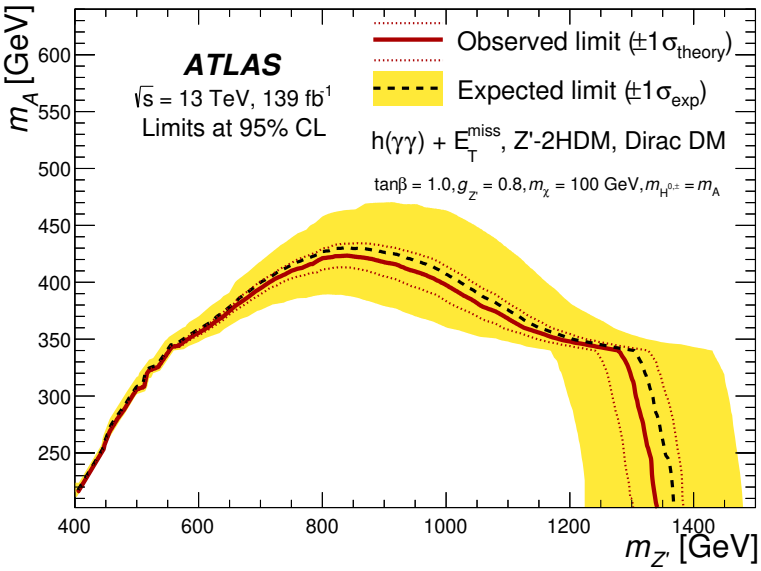

Figure 9. The observed (solid line) and expected (dashed lines) exclusion limit contours at 95% CL for the Z'-2HDM model in the m_A–$m_{Z'}$ plane, for $\tan\beta = 1.0$, $g_{Z'} = 0.8$, $m_\chi = 100$ GeV, and $m_{H^{0,\pm}} = m_A$. The dotted lines represent the $\pm 1\sigma$ theoretical uncertainty for the observed limit. The $\pm 1\sigma$ expected exclusion limit contour is shown as the yellow band. Above $m_A = 350$ GeV, competing decays from $A \to t\bar{t}$ cause the $A \to \chi\chi$ branching ratio to decrease quickly with increasing m_A, resulting in the feature near $m_{Z'} = 1300$ GeV.

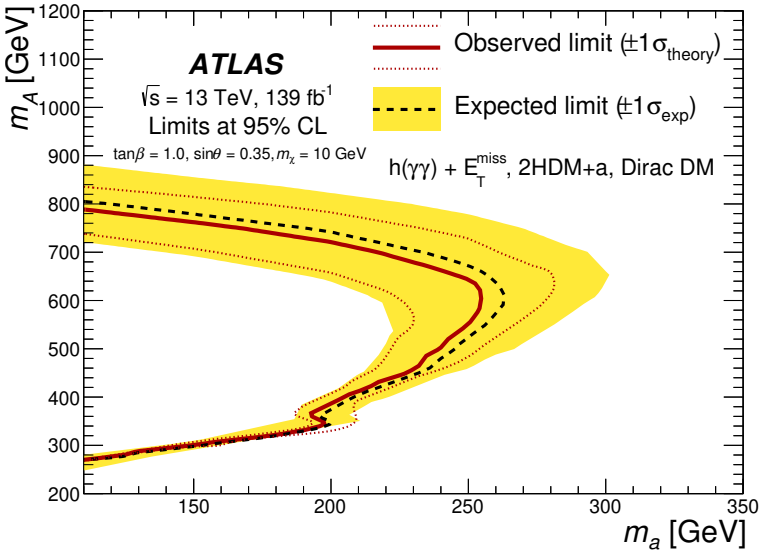

Figure 10. The observed (solid line) and expected (dashed lines) exclusion limit contours at 95% CL for the 2HDM+a model in the m_A–m_a plane, for $\tan\beta = 1.0$, $\sin\theta = 0.35$, and $m_\chi = 10$ GeV. The dotted lines represent the $\pm 1\sigma$ theoretical uncertainty for the observed limit. The $\pm 1\sigma$ expected exclusion limit contour is shown as the yellow band. Around the threshold $m_A = 350$ GeV, the competition between the resonant decay $A \to t\bar{t}$ and $A \to ah$ causes the $A \to ah$ branching ratio to decrease suddenly with a limited increase of m_A, resulting in the feature near $m_a = 200$ GeV. Above $m_A = 350$ GeV, the limit is mainly driven by the increased selection efficiency due to the harder signal $E_{\mathrm{T}}^{\mathrm{miss}}$ distribution.

JHEP10(2021)013

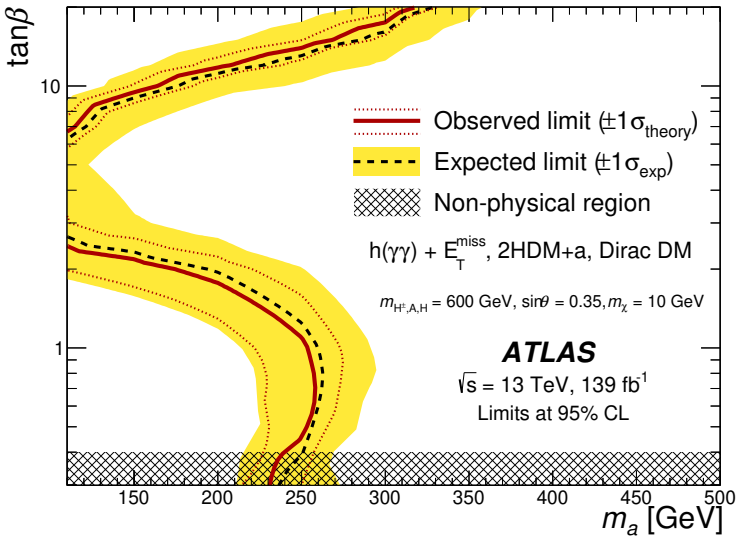

Figure 11. The observed (solid line) and expected (dashed lines) exclusion limit contours at 95% CL for the 2HDM+a model in the $\tan\beta$–m_a plane, for $m_{A,H^\pm,H} = 600$ GeV, $\sin\theta = 0.35$, and $m_\chi = 10$ GeV. The dotted lines represent the $\pm1\sigma$ theoretical uncertainty for the observed limit. The $\pm1\sigma$ expected exclusion limit contour is shown as the yellow band. The region $\tan\beta < 0.4$ is covered with a hatched band because there the decay width of the low-mass Higgs boson is greater than 20% of its mass, which renders the cross-section calculation unreliable [22]. The shape of the limit curve closely follows the signal cross section, which is dominated by ggF for low $\tan\beta$ and $b\bar{b}$-fusion for high $\tan\beta$.

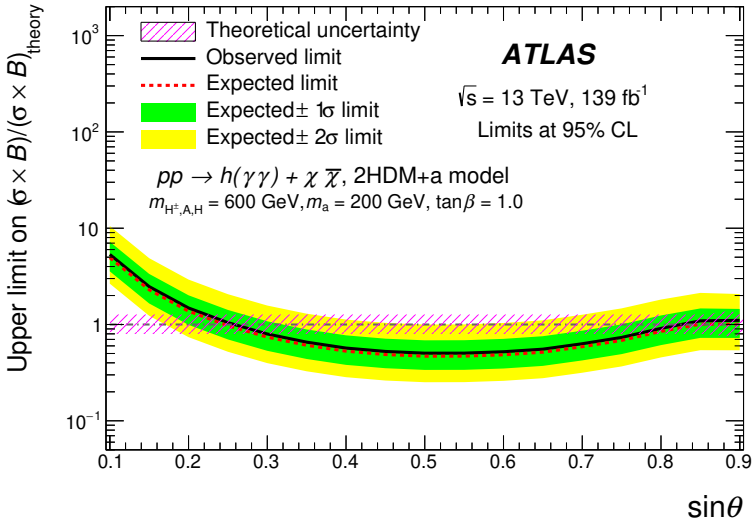

Figure 12. The observed (solid line) and expected (dashed lines) exclusion limits at 95% CL for the 2HDM+a model as a function of $\sin\theta$, for $m_{A,H^\pm,H} = 600$ GeV, $m_a = 200$ GeV, and $\tan\beta = 1.0$. Since the predicted yield for this model vanishes at mixing angles of $\theta = 0$ and $\theta = \pi/2$, $\sin\theta$ is limited to the range $[0.1, 0.9]$.

JHEP10(2021)013

FAPESP, Brazil; NSERC, NRC and CFI, Canada; CERN; ANID, Chile; CAS, MOST and NSFC, China; Minciencias, Colombia; MSMT CR, MPO CR and VSC CR, Czech Republic; DNRF and DNSRC, Denmark; IN2P3-CNRS and CEA-DRF/IRFU, France; SRNSFG, Georgia; BMBF, HGF and MPG, Germany; GSRT, Greece; RGC and Hong Kong SAR, China; ISF and Benoziyo Center, Israel; INFN, Italy; MEXT and JSPS, Japan; CNRST, Morocco; NWO, Netherlands; RCN, Norway; MNiSW and NCN, Poland; FCT, Portugal; MNE/IFA, Romania; JINR; MES of Russia and NRC KI, Russian Federation; MESTD, Serbia; MSSR, Slovakia; ARRS and MIZŠ, Slovenia; DST/NRF, South Africa; MICINN, Spain; SRC and Wallenberg Foundation, Sweden; SERI, SNSF and Cantons of Bern and Geneva, Switzerland; MOST, Taiwan; TAEK, Turkey; STFC, United Kingdom; DOE and NSF, United States of America. In addition, individual groups and members have received support from BCKDF, CANARIE, Compute Canada, CRC and IVADO, Canada; Beijing Municipal Science & Technology Commission, China; COST, ERC, ERDF, Horizon 2020 and Marie Skłodowska-Curie Actions, European Union; Investissements d'Avenir Labex, Investissements d'Avenir Idex and ANR, France; DFG and AvH Foundation, Germany; Herakleitos, Thales and Aristeia programmes co-financed by EU-ESF and the Greek NSRF, Greece; BSF-NSF and GIF, Israel; La Caixa Banking Foundation, CERCA Programme Generalitat de Catalunya and PROMETEO and GenT Programmes Generalitat Valenciana, Spain; Göran Gustafssons Stiftelse, Sweden; The Royal Society and Leverhulme Trust, United Kingdom.

The crucial computing support from all WLCG partners is acknowledged gratefully, in particular from CERN, the ATLAS Tier-1 facilities at TRIUMF (Canada), NDGF (Denmark, Norway, Sweden), CC-IN2P3 (France), KIT/GridKA (Germany), INFN-CNAF (Italy), NL-T1 (Netherlands), PIC (Spain), ASGC (Taiwan), RAL (U.K.) and BNL (U.S.A.), the Tier-2 facilities worldwide and large non-WLCG resource providers. Major contributors of computing resources are listed in ref. [103].

References

[1] ATLAS collaboration, *Observation of a new particle in the search for the Standard Model Higgs boson with the ATLAS detector at the LHC*, *Phys. Lett. B* **716** (2012) 1 [arXiv:1207.7214] [INSPIRE].

[2] CMS collaboration, *Observation of a new boson at a mass of* 125 *GeV with the CMS experiment at the LHC*, *Phys. Lett. B* **716** (2012) 30 [arXiv:1207.7235] [INSPIRE].

[3] ATLAS collaboration, *Combined measurements of Higgs boson production and decay using up to* 80 fb^{-1} *of proton-proton collision data at* $\sqrt{s} = 13\,TeV$ *collected with the ATLAS experiment*, *Phys. Rev. D* **101** (2020) 012002 [arXiv:1909.02845] [INSPIRE].

[4] CMS collaboration, *Measurements of Higgs boson production cross sections and couplings in the diphoton decay channel at* $\sqrt{s} = 13$ *TeV*, *JHEP* **07** (2021) 027 [arXiv:2103.06956] [INSPIRE].

JHEP10(2021)013

[5] Particle Data Group collaboration, *Review of particle physics*, *PTEP* **2020** (2020) 083C01 [INSPIRE].

[6] G. Bertone, D. Hooper and J. Silk, *Particle dark matter: evidence, candidates and constraints*, *Phys. Rept.* **405** (2005) 279 [hep-ph/0404175] [INSPIRE].

[7] ATLAS collaboration, *Search for dark matter at $\sqrt{s} = 13$ TeV in final states containing an energetic photon and large missing transverse momentum with the ATLAS detector*, *Eur. Phys. J. C* **77** (2017) 393 [arXiv:1704.03848] [INSPIRE].

[8] ATLAS collaboration, *Search for dark matter in events with a hadronically decaying vector boson and missing transverse momentum in pp collisions at $\sqrt{s} = 13$ TeV with the ATLAS detector*, *JHEP* **10** (2018) 180 [arXiv:1807.11471] [INSPIRE].

[9] ATLAS collaboration, *Search for dark matter and other new phenomena in events with an energetic jet and large missing transverse momentum using the ATLAS detector*, *JHEP* **01** (2018) 126 [arXiv:1711.03301] [INSPIRE].

[10] ATLAS collaboration, *Search for large missing transverse momentum in association with one top-quark in proton-proton collisions at $\sqrt{s} = 13$ TeV with the ATLAS detector*, *JHEP* **05** (2019) 041 [arXiv:1812.09743] [INSPIRE].

[11] ATLAS collaboration, *Search for new phenomena in events with two opposite-charge leptons, jets and missing transverse momentum in pp collisions at $\sqrt{s} = 13$ TeV with the ATLAS detector*, *JHEP* **04** (2021) 165 [arXiv:2102.01444] [INSPIRE].

[12] L. Carpenter, A. DiFranzo, M. Mulhearn, C. Shimmin, S. Tulin and D. Whiteson, *Mono-Higgs-boson: a new collider probe of dark matter*, *Phys. Rev. D* **89** (2014) 075017 [arXiv:1312.2592] [INSPIRE].

[13] ATLAS collaboration, *Search for dark matter in events with missing transverse momentum and a Higgs boson decaying to two photons in pp collisions at $\sqrt{s} = 8$ TeV with the ATLAS detector*, *Phys. Rev. Lett.* **115** (2015) 131801 [arXiv:1506.01081] [INSPIRE].

[14] ATLAS collaboration, *Search for dark matter produced in association with a Higgs boson decaying to two bottom quarks in pp collisions at $\sqrt{s} = 8$ TeV with the ATLAS detector*, *Phys. Rev. D* **93** (2016) 072007 [arXiv:1510.06218] [INSPIRE].

[15] ATLAS collaboration, *Search for dark matter in association with a Higgs boson decaying to b-quarks in pp collisions at $\sqrt{s} = 13$ TeV with the ATLAS detector*, *Phys. Lett. B* **765** (2017) 11 [arXiv:1609.04572] [INSPIRE].

[16] CMS collaboration, *Search for associated production of dark matter with a Higgs boson decaying to $b\bar{b}$ or $\gamma\gamma$ at $\sqrt{s} = 13$ TeV*, *JHEP* **10** (2017) 180 [arXiv:1703.05236] [INSPIRE].

[17] ATLAS collaboration, *Search for dark matter in association with a Higgs boson decaying to two photons at $\sqrt{s} = 13$ TeV with the ATLAS detector*, *Phys. Rev. D* **96** (2017) 112004 [arXiv:1706.03948] [INSPIRE].

[18] ATLAS collaboration, *Search for new phenomena in high-mass diphoton final states using 37 fb^{-1} of proton–proton collisions collected at $\sqrt{s} = 13$ TeV with the ATLAS detector*, *Phys. Lett. B* **775** (2017) 105 [arXiv:1707.04147] [INSPIRE].

[19] CMS collaboration, *Search for dark matter produced in association with a Higgs boson decaying to a pair of bottom quarks in proton-proton collisions at $\sqrt{s} = 13$ TeV*, *Eur. Phys. J. C* **79** (2019) 280 [arXiv:1811.06562] [INSPIRE].

JHEP10(2021)013

[20] CMS collaboration, *Search for dark matter produced in association with a Higgs boson decaying to $\gamma\gamma$ or $\tau^+\tau^-$ at $\sqrt{s} = 13$ TeV*, *JHEP* **09** (2018) 046 [arXiv:1806.04771] [INSPIRE].

[21] CMS collaboration, *Search for dark matter particles produced in association with a Higgs boson in proton-proton collisions at $\sqrt{s} = 13$ TeV*, *JHEP* **03** (2020) 025 [arXiv:1908.01713] [INSPIRE].

[22] ATLAS collaboration, *Constraints on mediator-based dark matter and scalar dark energy models using $\sqrt{s} = 13$ TeV pp collision data collected by the ATLAS detector*, *JHEP* **05** (2019) 142 [arXiv:1903.01400] [INSPIRE].

[23] D. Abercrombie et al., *Dark matter benchmark models for early LHC run-2 searches: report of the ATLAS/CMS dark matter forum*, *Phys. Dark Univ.* **27** (2020) 100371 [arXiv:1507.00966] [INSPIRE].

[24] A. Berlin, T. Lin and L.-T. Wang, *Mono-Higgs detection of dark matter at the LHC*, *JHEP* **06** (2014) 078 [arXiv:1402.7074] [INSPIRE].

[25] M. Bauer, U. Haisch and F. Kahlhoefer, *Simplified dark matter models with two Higgs doublets: I. Pseudoscalar mediators*, *JHEP* **05** (2017) 138 [arXiv:1701.07427] [INSPIRE].

[26] LHC Dark Matter Working Group collaboration, *LHC dark matter working group: next-generation spin-0 dark matter models*, *Phys. Dark Univ.* **27** (2020) 100351 [arXiv:1810.09420] [INSPIRE].

[27] ATLAS collaboration, *The ATLAS experiment at the CERN Large Hadron Collider*, 2008 *JINST* **3** S08003 [INSPIRE].

[28] ATLAS collaboration, *ATLAS insertable B-layer technical design report*, ATLAS-TDR-19 (2010).

[29] ATLAS IBL collaboration, *Production and integration of the ATLAS insertable B-layer*, 2018 *JINST* **13** T05008 [arXiv:1803.00844] [INSPIRE].

[30] ATLAS collaboration, *Performance of the ATLAS trigger system in 2015*, *Eur. Phys. J. C* **77** (2017) 317 [arXiv:1611.09661] [INSPIRE].

[31] G. Avoni et al., *The new LUCID-2 detector for luminosity measurement and monitoring in ATLAS*, 2018 *JINST* **13** P07017 [INSPIRE].

[32] ATLAS collaboration, *Performance of electron and photon triggers in ATLAS during LHC Run 2*, *Eur. Phys. J. C* **80** (2020) 47 [arXiv:1909.00761] [INSPIRE].

[33] K. Hamilton, P. Nason, E. Re and G. Zanderighi, *NNLOPS simulation of Higgs boson production*, *JHEP* **10** (2013) 222 [arXiv:1309.0017] [INSPIRE].

[34] P. Nason, *A new method for combining NLO QCD with shower Monte Carlo algorithms*, *JHEP* **11** (2004) 040 [hep-ph/0409146] [INSPIRE].

[35] S. Frixione, P. Nason and C. Oleari, *Matching NLO QCD computations with Parton Shower simulations: the POWHEG method*, *JHEP* **11** (2007) 070 [arXiv:0709.2092] [INSPIRE].

[36] S. Alioli, P. Nason, C. Oleari and E. Re, *A general framework for implementing NLO calculations in shower Monte Carlo programs: the POWHEG BOX*, *JHEP* **06** (2010) 043 [arXiv:1002.2581] [INSPIRE].

[37] P. Nason and C. Oleari, *NLO Higgs boson production via vector-boson fusion matched with shower in POWHEG*, *JHEP* **02** (2010) 037 [arXiv:0911.5299] [INSPIRE].

JHEP10(2021)013

[38] K. Mimasu, V. Sanz and C. Williams, *Higher Order QCD predictions for Associated Higgs production with anomalous couplings to gauge bosons*, *JHEP* **08** (2016) 039 [arXiv:1512.02572] [INSPIRE].

[39] J.M. Campbell, R.K. Ellis, R. Frederix, P. Nason, C. Oleari and C. Williams, *NLO Higgs boson production plus one and two jets using the POWHEG BOX, MadGraph4 and MCFM*, *JHEP* **07** (2012) 092 [arXiv:1202.5475] [INSPIRE].

[40] G. Luisoni, P. Nason, C. Oleari and F. Tramontano, $HW^{\pm}/HZ + 0$ *and* 1 *jet at NLO with the POWHEG BOX interfaced to GoSam and their merging within MiNLO*, *JHEP* **10** (2013) 083 [arXiv:1306.2542] [INSPIRE].

[41] H.B. Hartanto, B. Jager, L. Reina and D. Wackeroth, *Higgs boson production in association with top quarks in the POWHEG BOX*, *Phys. Rev. D* **91** (2015) 094003 [arXiv:1501.04498] [INSPIRE].

[42] J. Butterworth et al., *PDF4LHC recommendations for LHC Run II*, *J. Phys. G* **43** (2016) 023001 [arXiv:1510.03865] [INSPIRE].

[43] T. Sjöstrand et al., *An introduction to PYTHIA 8.2*, *Comput. Phys. Commun.* **191** (2015) 159 [arXiv:1410.3012] [INSPIRE].

[44] ATLAS collaboration, *Measurement of the Z/γ^* boson transverse momentum distribution in pp collisions at $\sqrt{s} = 7$ TeV with the ATLAS detector*, *JHEP* **09** (2014) 145 [arXiv:1406.3660] [INSPIRE].

[45] K. Hamilton, P. Nason and G. Zanderighi, *MINLO: Multi-Scale Improved NLO*, *JHEP* **10** (2012) 155 [arXiv:1206.3572] [INSPIRE].

[46] K. Hamilton, P. Nason, C. Oleari and G. Zanderighi, *Merging $H/W/Z + 0$ and* 1 *jet at NLO with no merging scale: a path to parton shower + NNLO matching*, *JHEP* **05** (2013) 082 [arXiv:1212.4504] [INSPIRE].

[47] S. Catani and M. Grazzini, *An NNLO subtraction formalism in hadron collisions and its application to Higgs boson production at the LHC*, *Phys. Rev. Lett.* **98** (2007) 222002 [hep-ph/0703012] [INSPIRE].

[48] G. Bozzi, S. Catani, D. de Florian and M. Grazzini, *Transverse-momentum resummation and the spectrum of the Higgs boson at the LHC*, *Nucl. Phys. B* **737** (2006) 73 [hep-ph/0508068] [INSPIRE].

[49] D. de Florian, G. Ferrera, M. Grazzini and D. Tommasini, *Transverse-momentum resummation: Higgs boson production at the Tevatron and the LHC*, *JHEP* **11** (2011) 064 [arXiv:1109.2109] [INSPIRE].

[50] S. Frixione, P. Nason and G. Ridolfi, *A positive-weight next-to-leading-order Monte Carlo for heavy flavour hadroproduction*, *JHEP* **09** (2007) 126 [arXiv:0707.3088] [INSPIRE].

[51] NNPDF collaboration, *Parton distributions for the LHC Run II*, *JHEP* **04** (2015) 040 [arXiv:1410.8849] [INSPIRE].

[52] *ATLAS PYTHIA 8 tunes to 7 TeV data*, ATL-PHYS-PUB-2014-021 (2014).

[53] D.J. Lange, *The EvtGen particle decay simulation package*, *Nucl. Instrum. Meth. A* **462** (2001) 152 [INSPIRE].

[54] P. Artoisenet, R. Frederix, O. Mattelaer and R. Rietkerk, *Automatic spin-entangled decays*

JHEP10(2021)013

of heavy resonances in Monte Carlo simulations, *JHEP* **03** (2013) 015 [arXiv:1212.3460] [INSPIRE].

[55] S. Frixione, E. Laenen, P. Motylinski, B.R. Webber and C.D. White, *Single-top hadroproduction in association with a W boson*, *JHEP* **07** (2008) 029 [arXiv:0805.3067] [INSPIRE].

[56] F. Demartin, B. Maier, F. Maltoni, K. Mawatari and M. Zaro, *tWH associated production at the LHC*, *Eur. Phys. J. C* **77** (2017) 34 [arXiv:1607.05862] [INSPIRE].

[57] LHC Higgs Cross Section Working Group collaboration, *Handbook of LHC Higgs Cross sections: 4. Deciphering the nature of the Higgs sector*, arXiv:1610.07922 [INSPIRE].

[58] W. Beenakker, S. Dittmaier, M. Krämer, B. Plumper, M. Spira and P.M. Zerwas, *NLO QCD corrections to $t\bar{t}H$ production in hadron collisions*, *Nucl. Phys. B* **653** (2003) 151 [hep-ph/0211352] [INSPIRE].

[59] ATLAS, CMS collaboration, *Combined measurement of the Higgs boson mass in pp collisions at $\sqrt{s} = 7$ and 8 TeV with the ATLAS and CMS experiments*, *Phys. Rev. Lett.* **114** (2015) 191803 [arXiv:1503.07589] [INSPIRE].

[60] Sherpa collaboration, *Event generation with Sherpa 2.2*, *SciPost Phys.* **7** (2019) 034 [arXiv:1905.09127] [INSPIRE].

[61] T. Gleisberg and S. Hoeche, *Comix, a new matrix element generator*, *JHEP* **12** (2008) 039 [arXiv:0808.3674] [INSPIRE].

[62] F. Buccioni et al., *OpenLoops 2*, *Eur. Phys. J. C* **79** (2019) 866 [arXiv:1907.13071] [INSPIRE].

[63] F. Cascioli, P. Maierhofer and S. Pozzorini, *Scattering amplitudes with open loops*, *Phys. Rev. Lett.* **108** (2012) 111601 [arXiv:1111.5206] [INSPIRE].

[64] A. Denner, S. Dittmaier and L. Hofer, *Collier: a Fortran-based Complex One-Loop LIbrary in Extended Regularizations*, *Comput. Phys. Commun.* **212** (2017) 220 [arXiv:1604.06792] [INSPIRE].

[65] S. Schumann and F. Krauss, *A parton shower algorithm based on Catani-Seymour dipole factorisation*, *JHEP* **03** (2008) 038 [arXiv:0709.1027] [INSPIRE].

[66] S. Hoeche, F. Krauss, M. Schonherr and F. Siegert, *A critical appraisal of NLO+PS matching methods*, *JHEP* **09** (2012) 049 [arXiv:1111.1220] [INSPIRE].

[67] S. Hoeche, F. Krauss, M. Schonherr and F. Siegert, *QCD matrix elements + parton showers: The NLO case*, *JHEP* **04** (2013) 027 [arXiv:1207.5030] [INSPIRE].

[68] S. Catani, F. Krauss, R. Kuhn and B.R. Webber, *QCD matrix elements + parton showers*, *JHEP* **11** (2001) 063 [hep-ph/0109231] [INSPIRE].

[69] S. Hoeche, F. Krauss, S. Schumann and F. Siegert, *QCD matrix elements and truncated showers*, *JHEP* **05** (2009) 053 [arXiv:0903.1219] [INSPIRE].

[70] J. Alwall et al., *The automated computation of tree-level and next-to-leading order differential cross sections, and their matching to parton shower simulations*, *JHEP* **07** (2014) 079 [arXiv:1405.0301] [INSPIRE].

[71] R.D. Ball et al., *Parton distributions with LHC data*, *Nucl. Phys. B* **867** (2013) 244 [arXiv:1207.1303] [INSPIRE].

JHEP10(2021)013

[72] T. Sjöstrand, S. Mrenna and P.Z. Skands, *A brief introduction to PYTHIA 8.1*, *Comput. Phys. Commun.* **178** (2008) 852 [arXiv:0710.3820] [INSPIRE].

[73] ATLAS collaboration, *The PYTHIA 8 A3 tune description of ATLAS minimum bias and inelastic measurements incorporating the Donnachie-Landshoff diffractive model*, ATL-PHYS-PUB-2016-017 (2016).

[74] ATLAS collaboration, *The ATLAS simulation infrastructure*, *Eur. Phys. J. C* **70** (2010) 823 [arXiv:1005.4568] [INSPIRE].

[75] GEANT4 collaboration, *GEANT4 — a simulation toolkit*, *Nucl. Instrum. Meth. A* **506** (2003) 250 [INSPIRE].

[76] ATLAS collaboration, *The simulation principle and performance of the ATLAS fast calorimeter simulation FastCaloSim*, ATL-PHYS-PUB-2010-013 (2010).

[77] ATLAS collaboration, *Electron and photon reconstruction and performance in ATLAS using a dynamical, topological cell clustering-based approach*, ATL-PHYS-PUB-2017-022 (2017).

[78] ATLAS collaboration, *Electron and photon performance measurements with the ATLAS detector using the 2015–2017 LHC proton-proton collision data*, 2019 *JINST* **14** P12006 [arXiv:1908.00005] [INSPIRE].

[79] ATLAS collaboration, *Measurement of Higgs boson production in the diphoton decay channel in pp collisions at center-of-mass energies of* 7 *and* 8 *TeV with the ATLAS detector*, *Phys. Rev. D* **90** (2014) 112015 [arXiv:1408.7084] [INSPIRE].

[80] ATLAS collaboration, *Electron reconstruction and identification in the ATLAS experiment using the 2015 and 2016 LHC proton-proton collision data at* $\sqrt{s} = 13$ *TeV*, *Eur. Phys. J. C* **79** (2019) 639 [arXiv:1902.04655] [INSPIRE].

[81] ATLAS collaboration, *Muon reconstruction performance of the ATLAS detector in proton-proton collision data at* $\sqrt{s} = 13$ *TeV*, *Eur. Phys. J. C* **76** (2016) 292 [arXiv:1603.05598] [INSPIRE].

[82] ATLAS collaboration, *Jet reconstruction and performance using particle flow with the ATLAS Detector*, *Eur. Phys. J. C* **77** (2017) 466 [arXiv:1703.10485] [INSPIRE].

[83] ATLAS collaboration, *Topological cell clustering in the ATLAS calorimeters and its performance in LHC Run 1*, *Eur. Phys. J. C* **77** (2017) 490 [arXiv:1603.02934] [INSPIRE].

[84] M. Cacciari, G.P. Salam and G. Soyez, *The anti-k_t jet clustering algorithm*, *JHEP* **04** (2008) 063 [arXiv:0802.1189] [INSPIRE].

[85] *Tagging and suppression of pileup jets with the ATLAS detector*, ATLAS-CONF-2014-018 (2014).

[86] ATLAS collaboration, *Performance of missing transverse momentum reconstruction with the ATLAS detector using proton-proton collisions at* $\sqrt{s} = 13$ *TeV*, *Eur. Phys. J. C* **78** (2018) 903 [arXiv:1802.08168] [INSPIRE].

[87] T. Chen and C. Guestrin, *XGBoost: a scalable tree boosting system*, arXiv:1603.02754 [INSPIRE].

[88] S. Bernstein, *Démonstration du Théorème de Weierstrass fondée sur le calcul des Probabilités*, *Comm. Soc. Math. Kharkov* **13** (1912) 1.

JHEP10(2021)013

[89] CDF collaboration, *Search for new particles decaying into dijets in proton-antiproton collisions at* $\sqrt{s} = 1.96$ *TeV*, *Phys. Rev. D* **79** (2009) 112002 [arXiv:0812.4036] [INSPIRE].

[90] ATLAS collaboration, *Measurement of isolated-photon pair production in pp collisions at* $\sqrt{s} = 7$ *TeV with the ATLAS detector*, *JHEP* **01** (2013) 086 [arXiv:1211.1913] [INSPIRE].

[91] ATLAS collaboration, *Luminosity determination in pp collisions at* $\sqrt{s} = 13$ *TeV using the ATLAS detector at the LHC*, ATLAS-CONF-2019-021 (2019).

[92] ATLAS collaboration, *Search for resonances in diphoton events at* $\sqrt{s} = 13$ *TeV with the ATLAS detector*, *JHEP* **09** (2016) 001 [arXiv:1606.03833] [INSPIRE].

[93] A. Kalogeropoulos and J. Alwall, *The syscalc code: A tool to derive theoretical systematic uncertainties*, arXiv:1801.08401.

[94] J. Bellm et al., *HERWIG 7.1 release note*, arXiv:1705.06919 [INSPIRE].

[95] J. Bellm et al., *HERWIG 7.0/HERWIG++ 3.0 release note*, *Eur. Phys. J. C* **76** (2016) 196 [arXiv:1512.01178] [INSPIRE].

[96] G. Cowan, K. Cranmer, E. Gross and O. Vitells, *Asymptotic formulae for likelihood-based tests of new physics*, *Eur. Phys. J. C* **71** (2011) 1554 [*Erratum ibid.* **73** (2013) 2501] [arXiv:1007.1727] [INSPIRE].

[97] XENON collaboration, *Light dark matter search with ionization signals in XENON1T*, *Phys. Rev. Lett.* **123** (2019) 251801 [arXiv:1907.11485] [INSPIRE].

[98] XENON collaboration, *Search for light dark matter interactions enhanced by the Migdal effect or Bremsstrahlung in XENON1T*, *Phys. Rev. Lett.* **123** (2019) 241803 [arXiv:1907.12771] [INSPIRE].

[99] XENON collaboration, *Dark matter search results from a one ton-year exposure of XENON1T*, *Phys. Rev. Lett.* **121** (2018) 111302 [arXiv:1805.12562] [INSPIRE].

[100] DarkSide collaboration, *Low-mass dark matter search with the DarkSide-50 experiment*, *Phys. Rev. Lett.* **121** (2018) 081307 [arXiv:1802.06994] [INSPIRE].

[101] A. Crivellin, F. D'Eramo and M. Procura, *New constraints on dark matter effective theories from standard model loops*, *Phys. Rev. Lett.* **112** (2014) 191304 [arXiv:1402.1173] [INSPIRE].

[102] F. D'Eramo and M. Procura, *Connecting dark matter UV complete models to direct detection rates via effective field theory*, *JHEP* **04** (2015) 054 [arXiv:1411.3342] [INSPIRE].

[103] ATLAS collaboration, *ATLAS computing acknowledgements*, ATL-SOFT-PUB-2020-001 (2020).

JHEP10(2021)013

The ATLAS collaboration

G. Aad[101], B. Abbott[127], D.C. Abbott[102], A. Abed Abud[36], K. Abeling[53], D.K. Abhayasinghe[93], S.H. Abidi[29], O.S. AbouZeid[40], N.L. Abraham[155], H. Abramowicz[160], H. Abreu[159], Y. Abulaiti[6], B.S. Acharya[66a,66b,o], B. Achkar[53], L. Adam[99], C. Adam Bourdarios[5], L. Adamczyk[83a], L. Adamek[165], J. Adelman[120], A. Adiguzel[12c,ad], S. Adorni[54], T. Adye[142], A.A. Affolder[144], Y. Afik[159], C. Agapopoulou[64], M.N. Agaras[38], A. Aggarwal[118], C. Agheorghiesei[27c], J.A. Aguilar-Saavedra[138f,138a,ac], A. Ahmad[36], F. Ahmadov[79], W.S. Ahmed[103], X. Ai[18], G. Aielli[73a,73b], S. Akatsuka[85], M. Akbiyik[99], T.P.A. Åkesson[96], E. Akilli[54], A.V. Akimov[110], K. Al Khoury[64], G.L. Alberghi[23b,23a], J. Albert[174], M.J. Alconada Verzini[160], S. Alderweireldt[36], M. Aleksa[36], I.N. Aleksandrov[79], C. Alexa[27b], T. Alexopoulos[10], A. Alfonsi[119], F. Alfonsi[23b,23a], M. Alhroob[127], B. Ali[140], S. Ali[157], M. Aliev[164], G. Alimonti[68a], C. Allaire[36], B.M.M. Allbrooke[155], P.P. Allport[21], A. Aloisio[69a,69b], F. Alonso[88], C. Alpigiani[147], E. Alunno Camelia[73a,73b], M. Alvarez Estevez[98], M.G. Alviggi[69a,69b], Y. Amaral Coutinho[80b], A. Ambler[103], L. Ambroz[133], C. Amelung[36], D. Amidei[105], S.P. Amor Dos Santos[138a], S. Amoroso[46], C.S. Amrouche[54], C. Anastopoulos[148], N. Andari[143], T. Andeen[11], J.K. Anders[20], S.Y. Andrean[45a,45b], A. Andreazza[68a,68b], V. Andrei[61a], C.R. Anelli[174], S. Angelidakis[9], A. Angerami[39], A.V. Anisenkov[121b,121a], A. Annovi[71a], C. Antel[54], M.T. Anthony[148], E. Antipov[128], M. Antonelli[51], D.J.A. Antrim[18], F. Anulli[72a], M. Aoki[81], J.A. Aparisi Pozo[172], M.A. Aparo[155], L. Aperio Bella[46], N. Aranzabal[36], V. Araujo Ferraz[80a], R. Araujo Pereira[80b], C. Arcangeletti[51], A.T.H. Arce[49], J-F. Arguin[109], S. Argyropoulos[52], J.-H. Arling[46], A.J. Armbruster[36], A. Armstrong[169], O. Arnaez[165], H. Arnold[119], Z.P. Arrubarrena Tame[113], G. Artoni[133], H. Asada[116], K. Asai[125], S. Asai[162], T. Asawatavonvanich[163], N.A. Asbah[59], E.M. Asimakopoulou[170], L. Asquith[155], J. Assahsah[35d], K. Assamagan[29], R. Astalos[28a], R.J. Atkin[33a], M. Atkinson[171], N.B. Atlay[19], H. Atmani[64], P.A. Atmasiddha[105], K. Augsten[140], V.A. Austrup[180], G. Avolio[36], M.K. Ayoub[15c], G. Azuelos[109,ak], D. Babal[28a], H. Bachacou[143], K. Bachas[161], F. Backman[45a,45b], P. Bagnaia[72a,72b], H. Bahrasemani[151], A.J. Bailey[172], V.R. Bailey[171], J.T. Baines[142], C. Bakalis[10], O.K. Baker[181], P.J. Bakker[119], E. Bakos[16], D. Bakshi Gupta[8], S. Balaji[156], R. Balasubramanian[119], E.M. Baldin[121b,121a], P. Balek[178], F. Balli[143], W.K. Balunas[133], J. Balz[99], E. Banas[84], M. Bandieramonte[137], A. Bandyopadhyay[19], L. Barak[160], W.M. Barbe[38], E.L. Barberio[104], D. Barberis[55b,55a], M. Barbero[101], G. Barbour[94], T. Barillari[114], M-S. Barisits[36], J. Barkeloo[130], T. Barklow[152], B.M. Barnett[142], R.M. Barnett[18], Z. Barnovska-Blenessy[60a], A. Baroncelli[60a], G. Barone[29], A.J. Barr[133], L. Barranco Navarro[45a,45b], F. Barreiro[98], J. Barreiro Guimarães da Costa[15a], U. Barron[160], S. Barsov[136], F. Bartels[61a], R. Bartoldus[152], G. Bartolini[101], A.E. Barton[89], P. Bartos[28a], A. Basalaev[46], A. Basan[99], A. Bassalat[64,ah], M.J. Basso[165], C.R. Basson[100], R.L. Bates[57], S. Batlamous[35e], J.R. Batley[32], B. Batool[150], M. Battaglia[144], M. Bauce[72a,72b], F. Bauer[143,*], P. Bauer[24], H.S. Bawa[31], A. Bayirli[12c], J.B. Beacham[49], T. Beau[134], P.H. Beauchemin[168], F. Becherer[52], P. Bechtle[24], H.P. Beck[20,q], K. Becker[176], C. Becot[46], A.J. Beddall[12a], V.A. Bednyakov[79], C.P. Bee[154], T.A. Beermann[180], M. Begalli[80b], M. Begel[29], A. Behera[154], J.K. Behr[46], F. Beisiegel[24], M. Belfkir[5], G. Bella[160], L. Bellagamba[23b], A. Bellerive[34], P. Bellos[21], K. Beloborodov[121b,121a], K. Belotskiy[111], N.L. Belyaev[111], D. Benchekroun[35a], N. Benekos[10], Y. Benhammou[160], D.P. Benjamin[6], M. Benoit[29], J.R. Bensinger[26], S. Bentvelsen[119], L. Beresford[133], M. Beretta[51], D. Berge[19], E. Bergeaas Kuutmann[170], N. Berger[5], B. Bergmann[140], L.J. Bergsten[26], J. Beringer[18], S. Berlendis[7], G. Bernardi[134], C. Bernius[152], F.U. Bernlochner[24], T. Berry[93], P. Berta[99], A. Berthold[48], I.A. Bertram[89], O. Bessidskaia Bylund[180], S. Bethke[114], A. Betti[42], A.J. Bevan[92], S. Bhatta[154], D.S. Bhattacharya[175], P. Bhattarai[26], V.S. Bhopatkar[6], R. Bi[137], R.M. Bianchi[137], O. Biebel[113], D. Biedermann[19], R. Bielski[36], K. Bierwagen[99], N.V. Biesuz[71a,71b],

JHEP10(2021)013

M. Biglietti[74a], T.R.V. Billoud[140], M. Bindi[53], A. Bingul[12d], C. Bini[72a,72b], S. Biondi[23b,23a], C.J. Birch-sykes[100], M. Birman[178], T. Bisanz[36], J.P. Biswal[3], D. Biswas[179,j], A. Bitadze[100], C. Bittrich[48], K. Bjørke[132], T. Blazek[28a], I. Bloch[46], C. Blocker[26], A. Blue[57], U. Blumenschein[92], G.J. Bobbink[119], V.S. Bobrovnikov[121b,121a], D. Bogavac[14], A.G. Bogdanchikov[121b,121a], C. Bohm[45a], V. Boisvert[93], P. Bokan[170,53], T. Bold[83a], M. Bomben[134], M. Bona[92], J.S. Bonilla[130], M. Boonekamp[143], C.D. Booth[93], A.G. Borbély[57], H.M. Borecka-Bielska[90], L.S. Borgna[94], A. Borisov[122], G. Borissov[89], D. Bortoletto[133], D. Boscherini[23b], M. Bosman[14], J.D. Bossio Sola[103], K. Bouaouda[35a], J. Boudreau[137], E.V. Bouhova-Thacker[89], D. Boumediene[38], R. Bouquet[134], A. Boveia[126], J. Boyd[36], D. Boye[29], I.R. Boyko[79], A.J. Bozson[93], J. Bracinik[21], N. Brahimi[60d,60c], G. Brandt[180], O. Brandt[32], F. Braren[46], B. Brau[102], J.E. Brau[130], W.D. Breaden Madden[57], K. Brendlinger[46], R. Brener[159], L. Brenner[36], R. Brenner[170], S. Bressler[178], B. Brickwedde[99], D.L. Briglin[21], D. Britton[57], D. Britzger[114], I. Brock[24], R. Brock[106], G. Brooijmans[39], W.K. Brooks[145d], E. Brost[29], P.A. Bruckman de Renstrom[84], B. Brüers[46], D. Bruncko[28b], A. Bruni[23b], G. Bruni[23b], M. Bruschi[23b], N. Bruscino[72a,72b], L. Bryngemark[152], T. Buanes[17], Q. Buat[154], P. Buchholz[150], A.G. Buckley[57], I.A. Budagov[79], M.K. Bugge[132], O. Bulekov[111], B.A. Bullard[59], T.J. Burch[120], S. Burdin[90], C.D. Burgard[46], A.M. Burger[128], B. Burghgrave[8], J.T.P. Burr[46], C.D. Burton[11], J.C. Burzynski[102], V. Büscher[99], E. Buschmann[53], P.J. Bussey[57], J.M. Butler[25], C.M. Buttar[57], J.M. Butterworth[94], W. Buttinger[142], C.J. Buxo Vazquez[106], A.R. Buzykaev[121b,121a], G. Cabras[23b,23a], S. Cabrera Urbán[172], D. Caforio[56], H. Cai[137], V.M.M. Cairo[152], O. Cakir[4a], N. Calace[36], P. Calafiura[18], G. Calderini[134], P. Calfayan[65], G. Callea[57], L.P. Caloba[80b], A. Caltabiano[73a,73b], S. Calvente Lopez[98], D. Calvet[38], S. Calvet[38], T.P. Calvet[101], M. Calvetti[71a,71b], R. Camacho Toro[134], S. Camarda[36], D. Camarero Munoz[98], P. Camarri[73a,73b], M.T. Camerlingo[74a,74b], D. Cameron[132], C. Camincher[36], M. Campanelli[94], A. Camplani[40], V. Canale[69a,69b], A. Canesse[103], M. Cano Bret[77], J. Cantero[128], Y. Cao[171], M. Capua[41b,41a], R. Cardarelli[73a], F. Cardillo[172], G. Carducci[41b,41a], T. Carli[36], G. Carlino[69a], B.T. Carlson[137], E.M. Carlson[174,166a], L. Carminati[68a,68b], R.M.D. Carney[152], S. Caron[118], E. Carquin[145d], S. Carrá[46], G. Carratta[23b,23a], J.W.S. Carter[165], T.M. Carter[50], M.P. Casado[14,g], A.F. Casha[165], E.G. Castiglia[181], F.L. Castillo[172], L. Castillo Garcia[14], V. Castillo Gimenez[172], N.F. Castro[138a,138e], A. Catinaccio[36], J.R. Catmore[132], A. Cattai[36], V. Cavaliere[29], V. Cavasinni[71a,71b], E. Celebi[12b], F. Celli[133], K. Cerny[129], A.S. Cerqueira[80a], A. Cerri[155], L. Cerrito[73a,73b], F. Cerutti[18], A. Cervelli[23b,23a], S.A. Cetin[12b], Z. Chadi[35a], D. Chakraborty[120], J. Chan[179], W.S. Chan[119], W.Y. Chan[90], J.D. Chapman[32], B. Chargeishvili[158b], D.G. Charlton[21], T.P. Charman[92], M. Chatterjee[20], C.C. Chau[34], S. Chekanov[6], S.V. Chekulaev[166a], G.A. Chelkov[79,af], B. Chen[78], C. Chen[60a], C.H. Chen[78], H. Chen[15c], H. Chen[29], J. Chen[60a], J. Chen[39], J. Chen[26], S. Chen[135], S.J. Chen[15c], X. Chen[15b], Y. Chen[60a], Y-H. Chen[46], H.C. Cheng[62a], H.J. Cheng[15a], A. Cheplakov[79], E. Cheremushkina[122], R. Cherkaoui El Moursli[35e], E. Cheu[7], K. Cheung[63], T.J.A. Chevalérias[143], L. Chevalier[143], V. Chiarella[51], G. Chiarelli[71a], G. Chiodini[67a], A.S. Chisholm[21], A. Chitan[27b], I. Chiu[162], Y.H. Chiu[174], M.V. Chizhov[79], K. Choi[11], A.R. Chomont[72a,72b], Y. Chou[102], Y.S. Chow[119], L.D. Christopher[33f], M.C. Chu[62a], X. Chu[15a,15d], J. Chudoba[139], J.J. Chwastowski[84], D. Cieri[114], K.M. Ciesla[84], V. Cindro[91], I.A. Cioară[27b], A. Ciocio[18], F. Cirotto[69a,69b], Z.H. Citron[178,k], M. Citterio[68a], D.A. Ciubotaru[27b], B.M. Ciungu[165], A. Clark[54], P.J. Clark[50], S.E. Clawson[100], C. Clement[45a,45b], L. Clissa[23b,23a], Y. Coadou[101], M. Cobal[66a,66c], A. Coccaro[55b], J. Cochran[78], R. Coelho Lopes De Sa[102], H. Cohen[160], A.E.C. Coimbra[36], B. Cole[39], J. Collot[58], P. Conde Muiño[138a,138h], S.H. Connell[33c], I.A. Connelly[57], F. Conventi[69a,al], A.M. Cooper-Sarkar[133], F. Cormier[173], L.D. Corpe[94], M. Corradi[72a,72b], E.E. Corrigan[96], F. Corriveau[103,aa], M.J. Costa[172], F. Costanza[5], D. Costanzo[148], G. Cowan[93], J.W. Cowley[32], J. Crane[100], K. Cranmer[124], R.A. Creager[135],

JHEP10(2021)013

S. Crépé-Renaudin[58], F. Crescioli[134], M. Cristinziani[24], M. Cristoforetti[75a,75b], V. Croft[168], G. Crosetti[41b,41a], A. Cueto[5], T. Cuhadar Donszelmann[169], H. Cui[15a,15d], A.R. Cukierman[152], W.R. Cunningham[57], S. Czekierda[84], P. Czodrowski[36], M.M. Czurylo[61b], M.J. Da Cunha Sargedas De Sousa[60b], J.V. Da Fonseca Pinto[80b], C. Da Via[100], W. Dabrowski[83a], F. Dachs[36], T. Dado[47], S. Dahbi[33f], T. Dai[105], C. Dallapiccola[102], M. Dam[40], G. D'amen[29], V. D'Amico[74a,74b], J. Damp[99], J.R. Dandoy[135], M.F. Daneri[30], M. Danninger[151], V. Dao[36], G. Darbo[55b], O. Dartsi[5], A. Dattagupta[130], S. D'Auria[68a,68b], C. David[166b], T. Davidek[141], D.R. Davis[49], I. Dawson[148], K. De[8], R. De Asmundis[69a], M. De Beurs[119], S. De Castro[23b,23a], N. De Groot[118], P. de Jong[119], H. De la Torre[106], A. De Maria[15c], D. De Pedis[72a], A. De Salvo[72a], U. De Sanctis[73a,73b], M. De Santis[73a,73b], A. De Santo[155], J.B. De Vivie De Regie[58], D.V. Dedovich[79], A.M. Deiana[42], J. Del Peso[98], Y. Delabat Diaz[46], D. Delgove[64], F. Deliot[143], C.M. Delitzsch[7], M. Della Pietra[69a,69b], D. Della Volpe[54], A. Dell'Acqua[36], L. Dell'Asta[73a,73b], M. Delmastro[5], C. Delporte[64], P.A. Delsart[58], S. Demers[181], M. Demichev[79], G. Demontigny[109], S.P. Denisov[122], L. D'Eramo[120], D. Derendarz[84], J.E. Derkaoui[35d], F. Derue[134], P. Dervan[90], K. Desch[24], K. Dette[165], C. Deutsch[24], P.O. Deviveiros[36], F.A. Di Bello[72a,72b], A. Di Ciaccio[73a,73b], L. Di Ciaccio[5], C. Di Donato[69a,69b], A. Di Girolamo[36], G. Di Gregorio[71a,71b], A. Di Luca[75a,75b], B. Di Micco[74a,74b], R. Di Nardo[74a,74b], R. Di Sipio[165], C. Diaconu[101], F.A. Dias[119], T. Dias Do Vale[138a], M.A. Diaz[145a], F.G. Diaz Capriles[24], J. Dickinson[18], M. Didenko[164], E.B. Diehl[105], J. Dietrich[19], S. Díez Cornell[46], C. Diez Pardos[150], A. Dimitrievska[18], W. Ding[15b], J. Dingfelder[24], S.J. Dittmeier[61b], F. Dittus[36], F. Djama[101], T. Djobava[158b], J.I. Djuvsland[17], M.A.B. Do Vale[146], M. Dobre[27b], D. Dodsworth[26], C. Doglioni[96], J. Dolejsi[141], Z. Dolezal[141], M. Donadelli[80c], B. Dong[60c], J. Donini[38], A. D'onofrio[15c], M. D'Onofrio[90], J. Dopke[142], A. Doria[69a], M.T. Dova[88], A.T. Doyle[57], E. Drechsler[151], E. Dreyer[151], T. Dreyer[53], A.S. Drobac[168], D. Du[60b], T.A. du Pree[119], Y. Duan[60d], F. Dubinin[110], M. Dubovsky[28a], A. Dubreuil[54], E. Duchovni[178], G. Duckeck[113], O.A. Ducu[36,27b], D. Duda[114], A. Dudarev[36], A.C. Dudder[99], M. D'uffizi[100], L. Duflot[64], M. Dührssen[36], C. Dülsen[180], M. Dumancic[178], A.E. Dumitriu[27b], M. Dunford[61a], S. Dungs[47], A. Duperrin[101], H. Duran Yildiz[4a], M. Düren[56], A. Durglishvili[158b], B. Dutta[46], D. Duvnjak[1], G.I. Dyckes[135], M. Dyndal[36], S. Dysch[100], B.S. Dziedzic[84], M.G. Eggleston[49], T. Eifert[8], G. Eigen[17], K. Einsweiler[18], T. Ekelof[170], H. El Jarrari[35e], A. El Moussaouy[35a], V. Ellajosyula[170], M. Ellert[170], F. Ellinghaus[180], A.A. Elliot[92], N. Ellis[36], J. Elmsheuser[29], M. Elsing[36], D. Emeliyanov[142], A. Emerman[39], Y. Enari[162], J. Erdmann[47], A. Ereditato[20], P.A. Erland[84], M. Errenst[180], M. Escalier[64], C. Escobar[172], O. Estrada Pastor[172], E. Etzion[160], G. Evans[138a], H. Evans[65], M.O. Evans[155], A. Ezhilov[136], F. Fabbri[57], L. Fabbri[23b,23a], V. Fabiani[118], G. Facini[176], R.M. Fakhrutdinov[122], S. Falciano[72a], P.J. Falke[24], S. Falke[36], J. Faltova[141], Y. Fang[15a], Y. Fang[15a], G. Fanourakis[44], M. Fanti[68a,68b], M. Faraj[60c], A. Farbin[8], A. Farilla[74a], E.M. Farina[70a,70b], T. Farooque[106], S.M. Farrington[50], P. Farthouat[36], F. Fassi[35e], D. Fassouliotis[9], M. Faucci Giannelli[50], W.J. Fawcett[32], L. Fayard[64], O.L. Fedin[136,p], A. Fehr[20], M. Feickert[171], L. Feligioni[101], A. Fell[148], C. Feng[60b], M. Feng[49], M.J. Fenton[169], A.B. Fenyuk[122], S.W. Ferguson[43], J. Ferrando[46], A. Ferrari[170], P. Ferrari[119], R. Ferrari[70a], D. Ferrere[54], C. Ferretti[105], F. Fiedler[99], A. Filipčič[91], F. Filthaut[118], K.D. Finelli[25], M.C.N. Fiolhais[138a,138c,a], L. Fiorini[172], F. Fischer[113], J. Fischer[99], W.C. Fisher[106], T. Fitschen[21], I. Fleck[150], P. Fleischmann[105], T. Flick[180], B.M. Flierl[113], L. Flores[135], L.R. Flores Castillo[62a], F.M. Follega[75a,75b], N. Fomin[17], J.H. Foo[165], G.T. Forcolin[75a,75b], B.C. Forland[65], A. Formica[143], F.A. Förster[14], A.C. Forti[100], E. Fortin[101], M.G. Foti[133], D. Fournier[64], H. Fox[89], P. Francavilla[71a,71b], S. Francescato[72a,72b], M. Franchini[23b,23a], S. Franchino[61a], D. Francis[36], L. Franco[5], L. Franconi[20], M. Franklin[59], G. Frattari[72a,72b], P.M. Freeman[21], B. Freund[109], W.S. Freund[80b], E.M. Freundlich[47], D.C. Frizzell[127], D. Froidevaux[36], J.A. Frost[133],

JHEP10(2021)013

M. Fujimoto[125], E. Fullana Torregrosa[172], T. Fusayasu[115], J. Fuster[172], A. Gabrielli[23b,23a], A. Gabrielli[36], P. Gadow[114], G. Gagliardi[55b,55a], L.G. Gagnon[109], G.E. Gallardo[133], E.J. Gallas[133], B.J. Gallop[142], R. Gamboa Goni[92], K.K. Gan[126], S. Ganguly[178], J. Gao[60a], Y. Gao[50], Y.S. Gao[31,m], F.M. Garay Walls[145a], C. García[172], J.E. García Navarro[172], J.A. García Pascual[15a], M. Garcia-Sciveres[18], R.W. Gardner[37], S. Gargiulo[52], C.A. Garner[165], V. Garonne[132], S.J. Gasiorowski[147], P. Gaspar[80b], G. Gaudio[70a], P. Gauzzi[72a,72b], I.L. Gavrilenko[110], A. Gavrilyuk[123], C. Gay[173], G. Gaycken[46], E.N. Gazis[10], A.A. Geanta[27b], C.M. Gee[144], C.N.P. Gee[142], J. Geisen[96], M. Geisen[99], C. Gemme[55b], M.H. Genest[58], C. Geng[105], S. Gentile[72a,72b], S. George[93], T. Geralis[44], L.O. Gerlach[53], P. Gessinger-Befurt[99], G. Gessner[47], M. Ghasemi Bostanabad[174], M. Ghneimat[150], A. Ghosh[64], A. Ghosh[77], B. Giacobbe[23b], S. Giagu[72a,72b], N. Giangiacomi[165], P. Giannetti[71a], A. Giannini[69a,69b], G. Giannini[14], S.M. Gibson[93], M. Gignac[144], D.T. Gil[83b], B.J. Gilbert[39], D. Gillberg[34], G. Gilles[180], N.E.K. Gillwald[46], D.M. Gingrich[3,ak], M.P. Giordani[66a,66c], P.F. Giraud[143], G. Giugliarelli[66a,66c], D. Giugni[68a], F. Giuli[73a,73b], S. Gkaitatzis[161], I. Gkialas[9,h], E.L. Gkougkousis[14], P. Gkountoumis[10], L.K. Gladilin[112], C. Glasman[98], G.R. Gledhill[130], I. Gnesi[41b,c], M. Goblirsch-Kolb[26], D. Godin[109], S. Goldfarb[104], T. Golling[54], D. Golubkov[122], A. Gomes[138a,138b], R. Goncalves Gama[53], R. Gonçalo[138a,138c], G. Gonella[130], L. Gonella[21], A. Gongadze[79], F. Gonnella[21], J.L. Gonski[39], S. González de la Hoz[172], S. Gonzalez Fernandez[14], R. Gonzalez Lopez[90], C. Gonzalez Renteria[18], R. Gonzalez Suarez[170], S. Gonzalez-Sevilla[54], G.R. Gonzalvo Rodriguez[172], L. Goossens[36], N.A. Gorasia[21], P.A. Gorbounov[123], H.A. Gordon[29], B. Gorini[36], E. Gorini[67a,67b], A. Gorišek[91], A.T. Goshaw[49], M.I. Gostkin[79], C.A. Gottardo[118], M. Gouighri[35b], A.G. Goussiou[147], N. Govender[33c], C. Goy[5], I. Grabowska-Bold[83a], E. Gramstad[132], S. Grancagnolo[19], M. Grandi[155], V. Gratchev[136], P.M. Gravila[27f], F.G. Gravili[67a,67b], C. Gray[57], H.M. Gray[18], C. Grefe[24], I.M. Gregor[46], P. Grenier[152], K. Grevtsov[46], C. Grieco[14], N.A. Grieser[127], A.A. Grillo[144], K. Grimm[31,l], S. Grinstein[14,w], J.-F. Grivaz[64], S. Groh[99], E. Gross[178], J. Grosse-Knetter[53], Z.J. Grout[94], C. Grud[105], A. Grummer[117], J.C. Grundy[133], L. Guan[105], W. Guan[179], C. Gubbels[173], J. Guenther[36], J.G.R. Guerrero Rojas[172], F. Guescini[114], D. Guest[76,19], R. Gugel[99], A. Guida[46], T. Guillemin[5], S. Guindon[36], J. Guo[60c], Z. Guo[101], R. Gupta[46], S. Gurbuz[24], G. Gustavino[127], M. Guth[52], P. Gutierrez[127], L.F. Gutierrez Zagazeta[135], C. Gutschow[94], C. Guyot[143], C. Gwenlan[133], C.B. Gwilliam[90], E.S. Haaland[132], A. Haas[124], C. Haber[18], H.K. Hadavand[8], A. Hadef[99], M. Haleem[175], J. Haley[128], J.J. Hall[148], G. Halladjian[106], G.D. Hallewell[101], K. Hamano[174], H. Hamdaoui[35e], M. Hamer[24], G.N. Hamity[50], K. Han[60a], L. Han[15c], L. Han[60a], S. Han[18], Y.F. Han[165], K. Hanagaki[81,u], M. Hance[144], M.D. Hank[37], R. Hankache[100], E. Hansen[96], J.B. Hansen[40], J.D. Hansen[40], M.C. Hansen[24], P.H. Hansen[40], E.C. Hanson[100], K. Hara[167], T. Harenberg[180], S. Harkusha[107], P.F. Harrison[176], N.M. Hartman[152], N.M. Hartmann[113], Y. Hasegawa[149], A. Hasib[50], S. Hassani[143], S. Haug[20], R. Hauser[106], M. Havranek[140], C.M. Hawkes[21], R.J. Hawkings[36], S. Hayashida[116], D. Hayden[106], C. Hayes[105], R.L. Hayes[173], C.P. Hays[133], J.M. Hays[92], H.S. Hayward[90], S.J. Haywood[142], F. He[60a], Y. He[163], M.P. Heath[50], V. Hedberg[96], A.L. Heggelund[132], N.D. Hehir[92], C. Heidegger[52], K.K. Heidegger[52], W.D. Heidorn[78], J. Heilman[34], S. Heim[46], T. Heim[18], B. Heinemann[46,ai], J.G. Heinlein[135], J.J. Heinrich[130], L. Heinrich[36], J. Hejbal[139], L. Helary[46], A. Held[124], S. Hellesund[132], C.M. Helling[144], S. Hellman[45a,45b], C. Helsens[36], R.C.W. Henderson[89], L. Henkelmann[32], A.M. Henriques Correia[36], H. Herde[152], Y. Hernández Jiménez[33f], H. Herr[99], M.G. Herrmann[113], T. Herrmann[48], G. Herten[52], R. Hertenberger[113], L. Hervas[36], N.P. Hessey[166a], H. Hibi[82], S. Higashino[81], E. Higón-Rodriguez[172], K. Hildebrand[37], J.C. Hill[32], K.K. Hill[29], K.H. Hiller[46], S.J. Hillier[21], M. Hils[48], I. Hinchliffe[18], F. Hinterkeuser[24], M. Hirose[131], S. Hirose[167], D. Hirschbuehl[180], B. Hiti[91], O. Hladik[139], J. Hobbs[154], R. Hobincu[27e], N. Hod[178],

JHEP10(2021)013

M.C. Hodgkinson[148], A. Hoecker[36], D. Hohn[52], D. Hohov[64], T. Holm[24], T.R. Holmes[37], M. Holzbock[114], L.B.A.H. Hommels[32], T.M. Hong[137], J.C. Honig[52], A. Hönle[114], B.H. Hooberman[171], W.H. Hopkins[6], Y. Horii[116], P. Horn[48], L.A. Horyn[37], S. Hou[157], J. Howarth[57], J. Hoya[88], M. Hrabovsky[129], A. Hrynevich[108], T. Hryn'ova[5], P.J. Hsu[63], S.-C. Hsu[147], Q. Hu[39], S. Hu[60c], Y.F. Hu[15a,15d,am], D.P. Huang[94], X. Huang[15c], Y. Huang[60a], Y. Huang[15a], Z. Hubacek[140], F. Hubaut[101], M. Huebner[24], F. Huegging[24], T.B. Huffman[133], M. Huhtinen[36], R. Hulsken[58], R.F.H. Hunter[34], N. Huseynov[79,ab], J. Huston[106], J. Huth[59], R. Hyneman[152], S. Hyrych[28a], G. Iacobucci[54], G. Iakovidis[29], I. Ibragimov[150], L. Iconomidou-Fayard[64], P. Iengo[36], R. Ignazzi[40], R. Iguchi[162], T. Iizawa[54], Y. Ikegami[81], N. Ilic[165,165], H. Imam[35a], G. Introzzi[70a,70b], M. Iodice[74a], K. Iordanidou[166a], V. Ippolito[72a,72b], M.F. Isacson[170], M. Ishino[162], W. Islam[128], C. Issever[19,46], S. Istin[12c], J.M. Iturbe Ponce[62a], R. Iuppa[75a,75b], A. Ivina[178], J.M. Izen[43], V. Izzo[69a], P. Jacka[139], P. Jackson[1], R.M. Jacobs[46], B.P. Jaeger[151], G. Jäkel[180], K.B. Jakobi[99], K. Jakobs[52], T. Jakoubek[178], J. Jamieson[57], K.W. Janas[83a], R. Jansky[54], P.A. Janus[83a], G. Jarlskog[96], A.E. Jaspan[90], N. Javadov[79,ab], T. Javůrek[36], M. Javurkova[102], F. Jeanneau[143], L. Jeanty[130], J. Jejelava[158a], P. Jenni[52,d], S. Jézéquel[5], J. Jia[154], Z. Jia[15c], Y. Jiang[60a], S. Jiggins[52], F.A. Jimenez Morales[38], J. Jimenez Pena[114], S. Jin[15c], A. Jinaru[27b], O. Jinnouchi[163], H. Jivan[33f], P. Johansson[148], K.A. Johns[7], C.A. Johnson[65], E. Jones[176], R.W.L. Jones[89], S.D. Jones[155], T.J. Jones[90], J. Jovicevic[36], X. Ju[18], J.J. Junggeburth[114], A. Juste Rozas[14,w], A. Kaczmarska[84], M. Kado[72a,72b], H. Kagan[126], M. Kagan[152], A. Kahn[39], C. Kahra[99], T. Kaji[177], E. Kajomovitz[159], C.W. Kalderon[29], A. Kaluza[99], A. Kamenshchikov[122], M. Kaneda[162], N.J. Kang[144], S. Kang[78], Y. Kano[116], J. Kanzaki[81], D. Kar[33f], K. Karava[133], M.J. Kareem[166b], I. Karkanias[161], S.N. Karpov[79], Z.M. Karpova[79], V. Kartvelishvili[89], A.N. Karyukhin[122], E. Kasimi[161], C. Kato[60d], J. Katzy[46], K. Kawade[149], K. Kawagoe[87], T. Kawaguchi[116], T. Kawamoto[143], G. Kawamura[53], E.F. Kay[174], F.I. Kaya[168], S. Kazakos[14], V.F. Kazanin[121b,121a], J.M. Keaveney[33a], R. Keeler[174], J.S. Keller[34], D. Kelsey[155], J.J. Kempster[21], J. Kendrick[21], K.E. Kennedy[39], O. Kepka[139], S. Kersten[180], B.P. Kerševan[91], S. Ketabchi Haghighat[165], F. Khalil-Zada[13], M. Khandoga[143], A. Khanov[128], A.G. Kharlamov[121b,121a], T. Kharlamova[121b,121a], E.E. Khoda[173], T.J. Khoo[76,19], G. Khoriauli[175], E. Khramov[79], J. Khubua[158b], S. Kido[82], M. Kiehn[36], A. Kilgallon[130], E. Kim[163], Y.K. Kim[37], N. Kimura[94], A. Kirchhoff[53], D. Kirchmeier[48], J. Kirk[142], A.E. Kiryunin[114], T. Kishimoto[162], D.P. Kisliuk[165], V. Kitali[46], C. Kitsaki[10], O. Kivernyk[24], T. Klapdor-Kleingrothaus[52], M. Klassen[61a], C. Klein[34], L. Klein[175], M.H. Klein[105], M. Klein[90], U. Klein[90], P. Klimek[36], A. Klimentov[29], F. Klimpel[36], T. Klingl[24], T. Klioutchnikova[36], F.F. Klitzner[113], P. Kluit[119], S. Kluth[114], E. Kneringer[76], A. Knue[52], D. Kobayashi[87], M. Kobel[48], M. Kocian[152], T. Kodama[162], P. Kodys[141], D.M. Koeck[155], P.T. Koenig[24], T. Koffas[34], N.M. Köhler[36], M. Kolb[143], I. Koletsou[5], T. Komarek[129], K. Köneke[52], A.X.Y. Kong[1], T. Kono[125], V. Konstantinides[94], N. Konstantinidis[94], B. Konya[96], R. Kopeliansky[65], S. Koperny[83a], K. Korcyl[84], K. Kordas[161], G. Koren[160], A. Korn[94], I. Korolkov[14], E.V. Korolkova[148], N. Korotkova[112], O. Kortner[114], S. Kortner[114], V.V. Kostyukhin[148,164], A. Kotsokechagia[64], A. Kotwal[49], A. Koulouris[10], A. Kourkoumeli-Charalampidi[70a,70b], C. Kourkoumelis[9], E. Kourlitis[6], R. Kowalewski[174], W. Kozanecki[143], A.S. Kozhin[122], V.A. Kramarenko[112], G. Kramberger[91], D. Krasnopevtsev[60a], M.W. Krasny[134], A. Krasznahorkay[36], J.A. Kremer[99], J. Kretzschmar[90], K. Kreul[19], P. Krieger[165], F. Krieter[113], S. Krishnamurthy[102], A. Krishnan[61b], M. Krivos[141], K. Krizka[18], K. Kroeninger[47], H. Kroha[114], J. Kroll[139], J. Kroll[135], K.S. Krowpman[106], U. Kruchonak[79], H. Krüger[24], N. Krumnack[78], M.C. Kruse[49], J.A. Krzysiak[84], A. Kubota[163], O. Kuchinskaia[164], S. Kuday[4b], D. Kuechler[46], J.T. Kuechler[46], S. Kuehn[36], T. Kuhl[46], V. Kukhtin[79], Y. Kulchitsky[107,ae], S. Kuleshov[145b], Y.P. Kulinich[171], M. Kumar[33f], M. Kuna[58], A. Kupco[139],

JHEP10(2021)013

T. Kupfer[47], O. Kuprash[52], H. Kurashige[82], L.L. Kurchaninov[166a], Y.A. Kurochkin[107], A. Kurova[111], M.G. Kurth[15a,15d], E.S. Kuwertz[36], M. Kuze[163], A.K. Kvam[147], J. Kvita[129], T. Kwan[103], C. Lacasta[172], F. Lacava[72a,72b], D.P.J. Lack[100], H. Lacker[19], D. Lacour[134], E. Ladygin[79], R. Lafaye[5], B. Laforge[134], T. Lagouri[145c], S. Lai[53], I.K. Lakomiec[83a], J.E. Lambert[127], S. Lammers[65], W. Lampl[7], C. Lampoudis[161], E. Lançon[29], U. Landgraf[52], M.P.J. Landon[92], V.S. Lang[52], J.C. Lange[53], R.J. Langenberg[102], A.J. Lankford[169], F. Lanni[29], K. Lantzsch[24], A. Lanza[70a], A. Lapertosa[55b,55a], J.F. Laporte[143], T. Lari[68a], F. Lasagni Manghi[23b,23a], M. Lassnig[36], V. Latonova[139], T.S. Lau[62a], A. Laudrain[99], A. Laurier[34], M. Lavorgna[69a,69b], S.D. Lawlor[93], M. Lazzaroni[68a,68b], B. Le[100], A. Lebedev[78], M. LeBlanc[7], T. LeCompte[6], F. Ledroit-Guillon[58], A.C.A. Lee[94], C.A. Lee[29], G.R. Lee[17], L. Lee[59], S.C. Lee[157], S. Lee[78], B. Lefebvre[166a], H.P. Lefebvre[93], M. Lefebvre[174], C. Leggett[18], K. Lehmann[151], N. Lehmann[20], G. Lehmann Miotto[36], W.A. Leight[46], A. Leisos[161,v], M.A.L. Leite[80c], C.E. Leitgeb[113], R. Leitner[141], K.J.C. Leney[42], T. Lenz[24], S. Leone[71a], C. Leonidopoulos[50], A. Leopold[134], C. Leroy[109], R. Les[106], C.G. Lester[32], M. Levchenko[136], J. Levêque[5], D. Levin[105], L.J. Levinson[178], D.J. Lewis[21], B. Li[15b], B. Li[105], C-Q. Li[60c,60d], F. Li[60c], H. Li[60a], H. Li[60b], J. Li[60c], K. Li[147], L. Li[60c], M. Li[15a,15d], Q.Y. Li[60a], S. Li[60d,60c,b], X. Li[46], Y. Li[46], Z. Li[60b], Z. Li[133], Z. Li[103], Z. Li[90], Z. Liang[15a], M. Liberatore[46], B. Liberti[73a], K. Lie[62c], C.Y. Lin[32], K. Lin[106], R.A. Linck[65], R.E. Lindley[7], J.H. Lindon[21], A. Linss[46], A.L. Lionti[54], E. Lipeles[135], A. Lipniacka[17], T.M. Liss[171,aj], A. Lister[173], J.D. Little[8], B. Liu[78], B.X. Liu[151], J.B. Liu[60a], J.K.K. Liu[37], K. Liu[60d,60c], M. Liu[60a], M.Y. Liu[60a], P. Liu[15a], X. Liu[60a], Y. Liu[46], Y. Liu[15a,15d], Y.L. Liu[105], Y.W. Liu[60a], M. Livan[70a,70b], A. Lleres[58], J. Llorente Merino[151], S.L. Lloyd[92], E.M. Lobodzinska[46], P. Loch[7], S. Loffredo[73a,73b], T. Lohse[19], K. Lohwasser[148], M. Lokajicek[139], J.D. Long[171], R.E. Long[89], I. Longarini[72a,72b], L. Longo[36], R. Longo[171], I. Lopez Paz[100], A. Lopez Solis[148], J. Lorenz[113], N. Lorenzo Martinez[5], A.M. Lory[113], A. Lösle[52], X. Lou[45a,45b], X. Lou[15a], A. Lounis[64], J. Love[6], P.A. Love[89], J.J. Lozano Bahilo[172], M. Lu[60a], S. Lu[135], Y.J. Lu[63], H.J. Lubatti[147], C. Luci[72a,72b], F.L. Lucio Alves[15c], A. Lucotte[58], F. Luehring[65], I. Luise[154], L. Luminari[72a], B. Lund-Jensen[153], N.A. Luongo[130], M.S. Lutz[160], D. Lynn[29], H. Lyons[90], R. Lysak[139], E. Lytken[96], F. Lyu[15a], V. Lyubushkin[79], T. Lyubushkina[79], H. Ma[29], L.L. Ma[60b], Y. Ma[94], D.M. Mac Donell[174], G. Maccarrone[51], C.M. Macdonald[148], J.C. MacDonald[148], J. Machado Miguens[135], R. Madar[38], W.F. Mader[48], M. Madugoda Ralalage Don[128], N. Madysa[48], J. Maeda[82], T. Maeno[29], M. Maerker[48], V. Magerl[52], J. Magro[66a,66c,r], D.J. Mahon[39], C. Maidantchik[80b], A. Maio[138a,138b,138d], K. Maj[83a], O. Majersky[28a], S. Majewski[130], N. Makovec[64], B. Malaescu[134], Pa. Malecki[84], V.P. Maleev[136], F. Malek[58], D. Malito[41b,41a], U. Mallik[77], C. Malone[32], S. Maltezos[10], S. Malyukov[79], J. Mamuzic[172], G. Mancini[51], J.P. Mandalia[92], I. Mandić[91], L. Manhaes de Andrade Filho[80a], I.M. Maniatis[161], J. Manjarres Ramos[48], K.H. Mankinen[96], A. Mann[113], A. Manousos[76], B. Mansoulie[143], I. Manthos[161], S. Manzoni[119], A. Marantis[161,v], L. Marchese[133], G. Marchiori[134], M. Marcisovsky[139], L. Marcoccia[73a,73b], C. Marcon[96], M. Marjanovic[127], Z. Marshall[18], M.U.F. Martensson[170], S. Marti-Garcia[172], T.A. Martin[176], V.J. Martin[50], B. Martin dit Latour[17], L. Martinelli[74a,74b], M. Martinez[14,w], P. Martinez Agullo[172], V.I. Martinez Outschoorn[102], S. Martin-Haugh[142], V.S. Martoiu[27b], A.C. Martyniuk[94], A. Marzin[36], S.R. Maschek[114], L. Masetti[99], T. Mashimo[162], R. Mashinistov[110], J. Masik[100], A.L. Maslennikov[121b,121a], L. Massa[23b,23a], P. Massarotti[69a,69b], P. Mastrandrea[71a,71b], A. Mastroberardino[41b,41a], T. Masubuchi[162], D. Matakias[29], T. Mathisen[170], A. Matic[113], N. Matsuzawa[162], J. Maurer[27b], B. Maček[91], D.A. Maximov[121b,121a], R. Mazini[157], I. Maznas[161], S.M. Mazza[144], C. Mc Ginn[29], J.P. Mc Gowan[103], S.P. Mc Kee[105], T.G. McCarthy[114], W.P. McCormack[18], E.F. McDonald[104], A.E. McDougall[119], J.A. Mcfayden[18], G. Mchedlidze[158b], M.A. McKay[42], K.D. McLean[174], S.J. McMahon[142], P.C. McNamara[104], C.J. McNicol[176], R.A. McPherson[174,aa], J.E. Mdhluli[33f],

JHEP10(2021)013

Z.A. Meadows[102], S. Meehan[36], T. Megy[38], S. Mehlhase[113], A. Mehta[90], B. Meirose[43], D. Melini[159], B.R. Mellado Garcia[33f], F. Meloni[46], A. Melzer[24], E.D. Mendes Gouveia[138a,138e], A.M. Mendes Jacques Da Costa[21], H.Y. Meng[165], L. Meng[36], S. Menke[114], E. Meoni[41b,41a], S. Mergelmeyer[19], S.A.M. Merkt[137], C. Merlassino[133], P. Mermod[54,*], L. Merola[69a,69b], C. Meroni[68a], G. Merz[105], O. Meshkov[112,110], J.K.R. Meshreki[150], J. Metcalfe[6], A.S. Mete[6], C. Meyer[65], J-P. Meyer[143], M. Michetti[19], R.P. Middleton[142], L. Mijović[50], G. Mikenberg[178], M. Mikestikova[139], M. Mikuž[91], H. Mildner[148], A. Milic[165], C.D. Milke[42], D.W. Miller[37], L.S. Miller[34], A. Milov[178], D.A. Milstead[45a,45b], A.A. Minaenko[122], I.A. Minashvili[158b], L. Mince[57], A.I. Mincer[124], B. Mindur[83a], M. Mineev[79], Y. Minegishi[162], Y. Mino[85], L.M. Mir[14], M. Mironova[133], T. Mitani[177], J. Mitrevski[113], V.A. Mitsou[172], M. Mittal[60c], O. Miu[165], A. Miucci[20], P.S. Miyagawa[92], A. Mizukami[81], J.U. Mjörnmark[96], T. Mkrtchyan[61a], M. Mlynarikova[120], T. Moa[45a,45b], S. Mobius[53], K. Mochizuki[109], P. Moder[46], P. Mogg[113], S. Mohapatra[39], G. Mokgatitswane[33f], B. Mondal[150], S. Mondal[140], K. Mönig[46], E. Monnier[101], A. Montalbano[151], J. Montejo Berlingen[36], M. Montella[94], F. Monticelli[88], N. Morange[64], A.L. Moreira De Carvalho[138a], M. Moreno Llácer[172], C. Moreno Martinez[14], P. Morettini[55b], M. Morgenstern[159], S. Morgenstern[176], D. Mori[151], M. Morii[59], M. Morinaga[177], V. Morisbak[132], A.K. Morley[36], A.P. Morris[94], L. Morvaj[36], P. Moschovakos[36], B. Moser[119], M. Mosidze[158b], T. Moskalets[143], P. Moskvitina[118], J. Moss[31,n], E.J.W. Moyse[102], S. Muanza[101], J. Mueller[137], D. Muenstermann[89], G.A. Mullier[96], J.J. Mullin[135], D.P. Mungo[68a,68b], J.L. Munoz Martinez[14], F.J. Munoz Sanchez[100], P. Murin[28b], W.J. Murray[176,142], A. Murrone[68a,68b], J.M. Muse[127], M. Muškinja[18], C. Mwewa[33a], A.G. Myagkov[122,af], A.A. Myers[137], G. Myers[65], J. Myers[130], M. Myska[140], B.P. Nachman[18], O. Nackenhorst[47], A.Nag Nag[48], K. Nagai[133], K. Nagano[81], J.L. Nagle[29], E. Nagy[101], A.M. Nairz[36], Y. Nakahama[116], K. Nakamura[81], H. Nanjo[131], F. Napolitano[61a], R.F. Naranjo Garcia[46], R. Narayan[42], I. Naryshkin[136], M. Naseri[34], T. Naumann[46], G. Navarro[22a], J. Navarro-Gonzalez[172], P.Y. Nechaeva[110], F. Nechansky[46], T.J. Neep[21], A. Negri[70a,70b], M. Negrini[23b], C. Nellist[118], C. Nelson[103], M.E. Nelson[45a,45b], S. Nemecek[139], M. Nessi[36,f], M.S. Neubauer[171], F. Neuhaus[99], M. Neumann[180], R. Newhouse[173], P.R. Newman[21], C.W. Ng[137], Y.S. Ng[19], Y.W.Y. Ng[169], B. Ngair[35e], H.D.N. Nguyen[101], T. Nguyen Manh[109], E. Nibigira[38], R.B. Nickerson[133], R. Nicolaidou[143], D.S. Nielsen[40], J. Nielsen[144], M. Niemeyer[53], N. Nikiforou[11], V. Nikolaenko[122,af], I. Nikolic-Audit[134], K. Nikolopoulos[21], P. Nilsson[29], H.R. Nindhito[54], A. Nisati[72a], N. Nishu[60c], R. Nisius[114], I. Nitsche[47], T. Nitta[177], T. Nobe[162], D.L. Noel[32], Y. Noguchi[85], I. Nomidis[134], M.A. Nomura[29], R.R.B. Norisam[94], J. Novak[91], T. Novak[91], O. Novgorodova[48], R. Novotny[117], L. Nozka[129], K. Ntekas[169], E. Nurse[94], F.G. Oakham[34,ak], J. Ocariz[134], A. Ochi[82], I. Ochoa[138a], J.P. Ochoa-Ricoux[145a], K. O'Connor[26], S. Oda[87], S. Odaka[81], S. Oerdek[53], A. Ogrodnik[83a], A. Oh[100], C.C. Ohm[153], H. Oide[163], R. Oishi[162], M.L. Ojeda[165], Y. Okazaki[85], M.W. O'Keefe[90], Y. Okumura[162], A. Olariu[27b], L.F. Oleiro Seabra[138a], S.A. Olivares Pino[145a], D. Oliveira Damazio[29], J.L. Oliver[1], M.J.R. Olsson[169], A. Olszewski[84], J. Olszowska[84], Ö.O. Öncel[24], D.C. O'Neil[151], A.P. O'neill[133], A. Onofre[138a,138e], P.U.E. Onyisi[11], H. Oppen[132], R.G. Oreamuno Madriz[120], M.J. Oreglia[37], G.E. Orellana[88], D. Orestano[74a,74b], N. Orlando[14], R.S. Orr[165], V. O'Shea[57], R. Ospanov[60a], G. Otero y Garzon[30], H. Otono[87], P.S. Ott[61a], G.J. Ottino[18], M. Ouchrif[35d], J. Ouellette[29], F. Ould-Saada[132], A. Ouraou[143,*], Q. Ouyang[15a], M. Owen[57], R.E. Owen[142], V.E. Ozcan[12c], N. Ozturk[8], J. Pacalt[129], H.A. Pacey[32], K. Pachal[49], A. Pacheco Pages[14], C. Padilla Aranda[14], S. Pagan Griso[18], G. Palacino[65], S. Palazzo[50], S. Palestini[36], M. Palka[83b], P. Palni[83a], D.K. Panchal[11], C.E. Pandini[54], J.G. Panduro Vazquez[93], P. Pani[46], G. Panizzo[66a,66c], L. Paolozzi[54], C. Papadatos[109], S. Parajuli[42], A. Paramonov[6], C. Paraskevopoulos[10], D. Paredes Hernandez[62b], S.R. Paredes Saenz[133], B. Parida[178], T.H. Park[165], A.J. Parker[31], M.A. Parker[32], F. Parodi[55b,55a], E.W. Parrish[120], J.A. Parsons[39],

JHEP10(2021)013

U. Parzefall[52], L. Pascual Dominguez[134], V.R. Pascuzzi[18], J.M.P. Pasner[144], F. Pasquali[119], E. Pasqualucci[72a], S. Passaggio[55b], F. Pastore[93], P. Pasuwan[45a,45b], J.R. Pater[100], A. Pathak[179,j], J. Patton[90], T. Pauly[36], J. Pearkes[152], M. Pedersen[132], L. Pedraza Diaz[118], R. Pedro[138a], T. Peiffer[53], S.V. Peleganchuk[121b,121a], O. Penc[139], C. Peng[62b], H. Peng[60a], B.S. Peralva[80a], M.M. Perego[64], A.P. Pereira Peixoto[138a], L. Pereira Sanchez[45a,45b], D.V. Perepelitsa[29], E. Perez Codina[166a], L. Perini[68a,68b], H. Pernegger[36], S. Perrella[36], A. Perrevoort[119], K. Peters[46], R.F.Y. Peters[100], B.A. Petersen[36], T.C. Petersen[40], E. Petit[101], V. Petousis[140], C. Petridou[161], P. Petroff[64], F. Petrucci[74a,74b], M. Pettee[181], N.E. Pettersson[102], K. Petukhova[141], A. Peyaud[143], R. Pezoa[145d], L. Pezzotti[70a,70b], G. Pezzullo[181], T. Pham[104], P.W. Phillips[142], M.W. Phipps[171], G. Piacquadio[154], E. Pianori[18], A. Picazio[102], R. Piegaia[30], D. Pietreanu[27b], J.E. Pilcher[37], A.D. Pilkington[100], M. Pinamonti[66a,66c], J.L. Pinfold[3], C. Pitman Donaldson[94], L. Pizzimento[73a,73b], A. Pizzini[119], M.-A. Pleier[29], V. Plesanovs[52], V. Pleskot[141], E. Plotnikova[79], P. Podberezko[121b,121a], R. Poettgen[96], R. Poggi[54], L. Poggioli[134], I. Pogrebnyak[106], D. Pohl[24], I. Pokharel[53], G. Polesello[70a], A. Poley[151,166a], A. Policicchio[72a,72b], R. Polifka[141], A. Polini[23b], C.S. Pollard[46], V. Polychronakos[29], D. Ponomarenko[111], L. Pontecorvo[36], S. Popa[27a], G.A. Popeneciu[27d], L. Portales[5], D.M. Portillo Quintero[58], S. Pospisil[140], P. Postolache[27c], K. Potamianos[133], I.N. Potrap[79], C.J. Potter[32], H. Potti[11], T. Poulsen[96], J. Poveda[172], T.D. Powell[148], G. Pownall[46], M.E. Pozo Astigarraga[36], A. Prades Ibanez[172], P. Pralavorio[101], M.M. Prapa[44], S. Prell[78], D. Price[100], M. Primavera[67a], M.L. Proffitt[147], N. Proklova[111], K. Prokofiev[62c], F. Prokoshin[79], S. Protopopescu[29], J. Proudfoot[6], M. Przybycien[83a], D. Pudzha[136], A. Puri[171], P. Puzo[64], D. Pyatiizbyantseva[111], J. Qian[105], Y. Qian[179], Y. Qin[100], A. Quadt[53], M. Queitsch-Maitland[36], G. Rabanal Bolanos[59], M. Racko[28a], F. Ragusa[68a,68b], G. Rahal[97], J.A. Raine[54], S. Rajagopalan[29], K. Ran[15a,15d], D.F. Rassloff[61a], D.M. Rauch[46], S. Rave[99], B. Ravina[57], I. Ravinovich[178], M. Raymond[36], A.L. Read[132], N.P. Readioff[148], M. Reale[67a,67b], D.M. Rebuzzi[70a,70b], G. Redlinger[29], K. Reeves[43], D. Reikher[160], A. Reiss[99], A. Rej[150], C. Rembser[36], A. Renardi[46], M. Renda[27b], M.B. Rendel[114], A.G. Rennie[57], S. Resconi[68a], E.D. Resseguie[18], S. Rettie[94], B. Reynolds[126], E. Reynolds[21], O.L. Rezanova[121b,121a], P. Reznicek[141], E. Ricci[75a,75b], R. Richter[114], S. Richter[46], E. Richter-Was[83b], M. Ridel[134], P. Rieck[114], O. Rifki[46], M. Rijssenbeek[154], A. Rimoldi[70a,70b], M. Rimoldi[46], L. Rinaldi[23b], T.T. Rinn[171], G. Ripellino[153], I. Riu[14], P. Rivadeneira[46], J.C. Rivera Vergara[174], F. Rizatdinova[128], E. Rizvi[92], C. Rizzi[36], S.H. Robertson[103,aa], M. Robin[46], D. Robinson[32], C.M. Robles Gajardo[145d], M. Robles Manzano[99], A. Robson[57], A. Rocchi[73a,73b], C. Roda[71a,71b], S. Rodriguez Bosca[172], A. Rodriguez Rodriguez[52], A.M. Rodríguez Vera[166b], S. Roe[36], J. Roggel[180], O. Røhne[132], R.A. Rojas[145d], B. Roland[52], C.P.A. Roland[65], J. Roloff[29], A. Romaniouk[111], M. Romano[23b,23a], N. Rompotis[90], M. Ronzani[124], L. Roos[134], S. Rosati[72a], G. Rosin[102], B.J. Rosser[135], E. Rossi[46], E. Rossi[74a,74b], E. Rossi[69a,69b], L.P. Rossi[55b], L. Rossini[46], R. Rosten[126], M. Rotaru[27b], B. Rottler[52], D. Rousseau[64], G. Rovelli[70a,70b], A. Roy[11], A. Rozanov[101], Y. Rozen[159], X. Ruan[33f], A.J. Ruby[90], T.A. Ruggeri[1], F. Rühr[52], A. Ruiz-Martinez[172], A. Rummler[36], Z. Rurikova[52], N.A. Rusakovich[79], H.L. Russell[103], L. Rustige[38,47], J.P. Rutherfoord[7], E.M. Rüttinger[148], M. Rybar[141], E.B. Rye[132], A. Ryzhov[122], J.A. Sabater Iglesias[46], P. Sabatini[172], L. Sabetta[72a,72b], S. Sacerdoti[64], H.F-W. Sadrozinski[144], R. Sadykov[79], F. Safai Tehrani[72a], B. Safarzadeh Samani[155], M. Safdari[152], P. Saha[120], S. Saha[103], M. Sahinsoy[114], A. Sahu[180], M. Saimpert[36], M. Saito[162], T. Saito[162], D. Salamani[54], G. Salamanna[74a,74b], A. Salnikov[152], J. Salt[172], A. Salvador Salas[14], D. Salvatore[41b,41a], F. Salvatore[155], A. Salzburger[36], D. Sammel[52], D. Sampsonidis[161], D. Sampsonidou[60d,60c], J. Sánchez[172], A. Sanchez Pineda[66a,36,66c], H. Sandaker[132], C.O. Sander[46], I.G. Sanderswood[89], M. Sandhoff[180], C. Sandoval[22b], D.P.C. Sankey[142], M. Sannino[55b,55a], Y. Sano[116], A. Sansoni[51], C. Santoni[38], H. Santos[138a,138b], S.N. Santpur[18], A. Santra[178],

JHEP10(2021)013

K.A. Saoucha[148], A. Sapronov[79], J.G. Saraiva[138a,138d], O. Sasaki[81], K. Sato[167], F. Sauerburger[52], E. Sauvan[5], P. Savard[165,ak], R. Sawada[162], C. Sawyer[142], L. Sawyer[95], I. Sayago Galvan[172], C. Sbarra[23b], A. Sbrizzi[66a,66c], T. Scanlon[94], J. Schaarschmidt[147], P. Schacht[114], D. Schaefer[37], L. Schaefer[135], U. Schäfer[99], A.C. Schaffer[64], D. Schaile[113], R.D. Schamberger[154], E. Schanet[113], C. Scharf[19], N. Scharmberg[100], V.A. Schegelsky[136], D. Scheirich[141], F. Schenck[19], M. Schernau[169], C. Schiavi[55b,55a], L.K. Schildgen[24], Z.M. Schillaci[26], E.J. Schioppa[67a,67b], M. Schioppa[41b,41a], K.E. Schleicher[52], S. Schlenker[36], K.R. Schmidt-Sommerfeld[114], K. Schmieden[99], C. Schmitt[99], S. Schmitt[46], L. Schoeffel[143], A. Schoening[61b], P.G. Scholer[52], E. Schopf[133], M. Schott[99], J.F.P. Schouwenberg[118], J. Schovancova[36], S. Schramm[54], F. Schroeder[180], A. Schulte[99], H-C. Schultz-Coulon[61a], M. Schumacher[52], B.A. Schumm[144], Ph. Schune[143], A. Schwartzman[152], T.A. Schwarz[105], Ph. Schwemling[143], R. Schwienhorst[106], A. Sciandra[144], G. Sciolla[26], F. Scuri[71a], F. Scutti[104], L.M. Scyboz[114], C.D. Sebastiani[90], K. Sedlaczek[47], P. Seema[19], S.C. Seidel[117], A. Seiden[144], B.D. Seidlitz[29], T. Seiss[37], C. Seitz[46], J.M. Seixas[80b], G. Sekhniaidze[69a], S.J. Sekula[42], N. Semprini-Cesari[23b,23a], S. Sen[49], C. Serfon[29], L. Serin[64], L. Serkin[66a,66b], M. Sessa[60a], H. Severini[127], S. Sevova[152], F. Sforza[55b,55a], A. Sfyrla[54], E. Shabalina[53], J.D. Shahinian[135], N.W. Shaikh[45a,45b], D. Shaked Renous[178], L.Y. Shan[15a], M. Shapiro[18], A. Sharma[36], A.S. Sharma[1], P.B. Shatalov[123], K. Shaw[155], S.M. Shaw[100], M. Shehade[178], Y. Shen[127], P. Sherwood[94], L. Shi[94], C.O. Shimmin[181], Y. Shimogama[177], M. Shimojima[115], J.D. Shinner[93], I.P.J. Shipsey[133], S. Shirabe[163], M. Shiyakova[79,y], J. Shlomi[178], M.J. Shochet[37], J. Shojaii[104], D.R. Shope[153], S. Shrestha[126], E.M. Shrif[33f], M.J. Shroff[174], E. Shulga[178], P. Sicho[139], A.M. Sickles[171], E. Sideras Haddad[33f], O. Sidiropoulou[36], A. Sidoti[23b,23a], F. Siegert[48], Dj. Sijacki[16], M.V. Silva Oliveira[36], S.B. Silverstein[45a], S. Simion[64], R. Simoniello[99], C.J. Simpson-allsop[21], S. Simsek[12b], P. Sinervo[165], V. Sinetckii[112], S. Singh[151], S. Sinha[33f], M. Sioli[23b,23a], I. Siral[130], S.Yu. Sivoklokov[112], J. Sjölin[45a,45b], A. Skaf[53], E. Skorda[96], P. Skubic[127], M. Slawinska[84], K. Sliwa[168], V. Smakhtin[178], B.H. Smart[142], J. Smiesko[28b], N. Smirnov[111], S.Yu. Smirnov[111], Y. Smirnov[111], L.N. Smirnova[112,s], O. Smirnova[96], E.A. Smith[37], H.A. Smith[133], M. Smizanska[89], K. Smolek[140], A. Smykiewicz[84], A.A. Snesarev[110], H.L. Snoek[119], I.M. Snyder[130], S. Snyder[29], R. Sobie[174,aa], A. Soffer[160], A. Søgaard[50], F. Sohns[53], C.A. Solans Sanchez[36], E.Yu. Soldatov[111], U. Soldevila[172], A.A. Solodkov[122], A. Soloshenko[79], O.V. Solovyanov[122], V. Solovyev[136], P. Sommer[148], H. Son[168], A. Sonay[14], W.Y. Song[166b], A. Sopczak[140], A.L. Sopio[94], F. Sopkova[28b], S. Sottocornola[70a,70b], R. Soualah[66a,66c], A.M. Soukharev[121b,121a], D. South[46], S. Spagnolo[67a,67b], M. Spalla[114], M. Spangenberg[176], F. Spanò[93], D. Sperlich[52], T.M. Spieker[61a], G. Spigo[36], M. Spina[155], D.P. Spiteri[57], M. Spousta[141], A. Stabile[68a,68b], B.L. Stamas[120], R. Stamen[61a], M. Stamenkovic[119], A. Stampekis[21], E. Stanecka[84], B. Stanislaus[133], M.M. Stanitzki[46], M. Stankaityte[133], B. Stapf[119], E.A. Starchenko[122], G.H. Stark[144], J. Stark[58], P. Staroba[139], P. Starovoitov[61a], S. Stärz[103], R. Staszewski[84], G. Stavropoulos[44], P. Steinberg[29], A.L. Steinhebel[130], B. Stelzer[151,166a], H.J. Stelzer[137], O. Stelzer-Chilton[166a], H. Stenzel[56], T.J. Stevenson[155], G.A. Stewart[36], M.C. Stockton[36], G. Stoicea[27b], M. Stolarski[138a], S. Stonjek[114], A. Straessner[48], J. Strandberg[153], S. Strandberg[45a,45b], M. Strauss[127], T. Strebler[101], P. Strizenec[28b], R. Ströhmer[175], D.M. Strom[130], R. Stroynowski[42], A. Strubig[45a,45b], S.A. Stucci[29], B. Stugu[17], J. Stupak[127], N.A. Styles[46], D. Su[152], W. Su[60d,147,60c], X. Su[60a], N.B. Suarez[137], V.V. Sulin[110], M.J. Sullivan[90], D.M.S. Sultan[54], S. Sultansoy[4c], T. Sumida[85], S. Sun[105], X. Sun[100], C.J.E. Suster[156], M.R. Sutton[155], M. Svatos[139], M. Swiatlowski[166a], S.P. Swift[2], T. Swirski[175], A. Sydorenko[99], I. Sykora[28a], M. Sykora[141], T. Sykora[141], D. Ta[99], K. Tackmann[46,x], J. Taenzer[160], A. Taffard[169], R. Tafirout[166a], E. Tagiev[122], R.H.M. Taibah[134], R. Takashima[86], K. Takeda[82], T. Takeshita[149], E.P. Takeva[50], Y. Takubo[81], M. Talby[101], A.A. Talyshev[121b,121a], K.C. Tam[62b], N.M. Tamir[160], J. Tanaka[162], R. Tanaka[64], S. Tapia Araya[171], S. Tapprogge[99], A. Tarek Abouelfadl Mohamed[106],

JHEP10(2021)013

S. Tarem[159], K. Tariq[60b], G. Tarna[27b,e], G.F. Tartarelli[68a], P. Tas[141], M. Tasevsky[139], E. Tassi[41b,41a], G. Tateno[162], Y. Tayalati[35e], G.N. Taylor[104], W. Taylor[166b], H. Teagle[90], A.S. Tee[89], R. Teixeira De Lima[152], P. Teixeira-Dias[93], H. Ten Kate[36], J.J. Teoh[119], K. Terashi[162], J. Terron[98], S. Terzo[14], M. Testa[51], R.J. Teuscher[165,aa], N. Themistokleous[50], T. Theveneaux-Pelzer[19], D.W. Thomas[93], J.P. Thomas[21], E.A. Thompson[46], P.D. Thompson[21], E. Thomson[135], E.J. Thorpe[92], V.O. Tikhomirov[110,ag], Yu.A. Tikhonov[121b,121a], S. Timoshenko[111], P. Tipton[181], S. Tisserant[101], K. Todome[23b,23a], S. Todorova-Nova[141], S. Todt[48], J. Tojo[87], S. Tokár[28a], K. Tokushuku[81], E. Tolley[126], R. Tombs[32], M. Tomoto[81,116], L. Tompkins[152], P. Tornambe[102], E. Torrence[130], H. Torres[48], E. Torró Pastor[172], M. Toscani[30], C. Tosciri[37], J. Toth[101,z], D.R. Tovey[148], A. Traeet[17], C.J. Treado[124], T. Trefzger[175], F. Tresoldi[155], A. Tricoli[29], I.M. Trigger[166a], S. Trincaz-Duvoid[134], D.A. Trischuk[173], W. Trischuk[165], B. Trocmé[58], A. Trofymov[64], C. Troncon[68a], F. Trovato[155], L. Truong[33c], M. Trzebinski[84], A. Trzupek[84], F. Tsai[46], P.V. Tsiareshka[107,ae], A. Tsirigotis[161,v], V. Tsiskaridze[154], E.G. Tskhadadze[158a], M. Tsopoulou[161], I.I. Tsukerman[123], V. Tsulaia[18], S. Tsuno[81], D. Tsybychev[154], Y. Tu[62b], A. Tudorache[27b], V. Tudorache[27b], A.N. Tuna[36], S. Turchikhin[79], D. Turgeman[178], I. Turk Cakir[4b,t], R.J. Turner[21], R. Turra[68a], P.M. Tuts[39], S. Tzamarias[161], E. Tzovara[99], K. Uchida[162], F. Ukegawa[167], G. Unal[36], M. Unal[11], A. Undrus[29], G. Unel[169], F.C. Ungaro[104], K. Uno[162], J. Urban[28b], P. Urquijo[104], G. Usai[8], Z. Uysal[12d], V. Vacek[140], B. Vachon[103], K.O.H. Vadla[132], T. Vafeiadis[36], A. Vaidya[94], C. Valderanis[113], E. Valdes Santurio[45a,45b], M. Valente[166a], S. Valentinetti[23b,23a], A. Valero[172], L. Valéry[46], R.A. Vallance[21], A. Vallier[36], J.A. Valls Ferrer[172], T.R. Van Daalen[14], P. Van Gemmeren[6], S. Van Stroud[94], I. Van Vulpen[119], M. Vanadia[73a,73b], W. Vandelli[36], M. Vandenbroucke[143], E.R. Vandewall[128], D. Vannicola[72a,72b], R. Vari[72a], E.W. Varnes[7], C. Varni[55b,55a], T. Varol[157], D. Varouchas[64], K.E. Varvell[156], M.E. Vasile[27b], G.A. Vasquez[174], F. Vazeille[38], D. Vazquez Furelos[14], T. Vazquez Schroeder[36], J. Veatch[53], V. Vecchio[100], M.J. Veen[119], L.M. Veloce[165], F. Veloso[138a,138c], S. Veneziano[72a], A. Ventura[67a,67b], A. Verbytskyi[114], M. Verducci[71a,71b], C. Vergis[24], W. Verkerke[119], A.T. Vermeulen[119], J.C. Vermeulen[119], C. Vernieri[152], P.J. Verschuuren[93], M.L. Vesterbacka[124], M.C. Vetterli[151,ak], N. Viaux Maira[145d], T. Vickey[148], O.E. Vickey Boeriu[148], G.H.A. Viehhauser[133], L. Vigani[61b], M. Villa[23b,23a], M. Villaplana Perez[172], E.M. Villhauer[50], E. Vilucchi[51], M.G. Vincter[34], G.S. Virdee[21], A. Vishwakarma[50], C. Vittori[23b,23a], I. Vivarelli[155], M. Vogel[180], P. Vokac[140], J. Von Ahnen[46], S.E. von Buddenbrock[33f], E. Von Toerne[24], V. Vorobel[141], K. Vorobev[111], M. Vos[172], J.H. Vossebeld[90], M. Vozak[100], N. Vranjes[16], M. Vranjes Milosavljevic[16], V. Vrba[140,*], M. Vreeswijk[119], N.K. Vu[101], R. Vuillermet[36], I. Vukotic[37], S. Wada[167], C. Wagner[102], P. Wagner[24], W. Wagner[180], S. Wahdan[180], H. Wahlberg[88], R. Wakasa[167], V.M. Walbrecht[114], J. Walder[142], R. Walker[113], S.D. Walker[93], W. Walkowiak[150], V. Wallangen[45a,45b], A.M. Wang[59], A.Z. Wang[179], C. Wang[60a], C. Wang[60c], H. Wang[18], J. Wang[62a], P. Wang[42], R.-J. Wang[99], R. Wang[60a], R. Wang[120], S.M. Wang[157], S. Wang[60b], T. Wang[60a], W.T. Wang[60a], W.X. Wang[60a], Y. Wang[60a], Z. Wang[105], C. Wanotayaroj[36], A. Warburton[103], C.P. Ward[32], R.J. Ward[21], N. Warrack[57], A.T. Watson[21], M.F. Watson[21], G. Watts[147], B.M. Waugh[94], A.F. Webb[11], C. Weber[29], M.S. Weber[20], S.A. Weber[34], S.M. Weber[61a], Y. Wei[133], A.R. Weidberg[133], J. Weingarten[47], M. Weirich[99], C. Weiser[52], P.S. Wells[36], T. Wenaus[29], B. Wendland[47], T. Wengler[36], S. Wenig[36], N. Wermes[24], M. Wessels[61a], T.D. Weston[20], K. Whalen[130], A.M. Wharton[89], A.S. White[105], A. White[8], M.J. White[1], D. Whiteson[169], B.W. Whitmore[89], W. Wiedenmann[179], C. Wiel[48], M. Wielers[142], N. Wieseotte[99], C. Wiglesworth[40], L.A.M. Wiik-Fuchs[52], H.G. Wilkens[36], L.J. Wilkins[93], D.M. Williams[39], H.H. Williams[135], S. Williams[32], S. Willocq[102], P.J. Windischhofer[133], I. Wingerter-Seez[5], E. Winkels[155], F. Winklmeier[130], B.T. Winter[52], M. Wittgen[152], M. Wobisch[95], A. Wolf[99], R. Wölker[133],

JHEP10(2021)013

J. Wollrath[52], M.W. Wolter[84], H. Wolters[138a,138c], V.W.S. Wong[173], A.F. Wongel[46], N.L. Woods[144], S.D. Worm[46], B.K. Wosiek[84], K.W. Woźniak[84], K. Wraight[57], J. Wu[15a,15d], S.L. Wu[179], X. Wu[54], Y. Wu[60a], J. Wuerzinger[133], T.R. Wyatt[100], B.M. Wynne[50], S. Xella[40], J. Xiang[62c], X. Xiao[105], X. Xie[60a], I. Xiotidis[155], D. Xu[15a], H. Xu[60a], H. Xu[60a], L. Xu[29], R. Xu[135], T. Xu[143], W. Xu[105], Y. Xu[15b], Z. Xu[60b], Z. Xu[152], B. Yabsley[156], S. Yacoob[33a], D.P. Yallup[94], N. Yamaguchi[87], Y. Yamaguchi[163], M. Yamatani[162], H. Yamauchi[167], T. Yamazaki[18], Y. Yamazaki[82], J. Yan[60c], Z. Yan[25], H.J. Yang[60c,60d], H.T. Yang[18], S. Yang[60a], T. Yang[62c], X. Yang[60a], X. Yang[15a], Y. Yang[162], Z. Yang[105,60a], W-M. Yao[18], Y.C. Yap[46], H. Ye[15c], J. Ye[42], S. Ye[29], I. Yeletskikh[79], M.R. Yexley[89], P. Yin[39], K. Yorita[177], K. Yoshihara[78], C.J.S. Young[36], C. Young[152], R. Yuan[60b,i], X. Yue[61a], M. Zaazoua[35e], B. Zabinski[84], G. Zacharis[10], E. Zaffaroni[54], J. Zahreddine[134], A.M. Zaitsev[122,af], T. Zakareishvili[158b], N. Zakharchuk[34], S. Zambito[36], D. Zanzi[52], S.V. Zeißner[47], C. Zeitnitz[180], G. Zemaityte[133], J.C. Zeng[171], O. Zenin[122], T. Ženiš[28a], S. Zenz[92], S. Zerradi[35a], D. Zerwas[64], M. Zgubič[133], B. Zhang[15c], D.F. Zhang[15b], G. Zhang[15b], J. Zhang[6], K. Zhang[15a], L. Zhang[15c], L. Zhang[60a], M. Zhang[171], R. Zhang[179], S. Zhang[105], X. Zhang[60c], X. Zhang[60b], Y. Zhang[15a,15d], Z. Zhang[64], P. Zhao[49], Y. Zhao[144], Z. Zhao[60a], A. Zhemchugov[79], Z. Zheng[105], D. Zhong[171], B. Zhou[105], C. Zhou[179], H. Zhou[7], M. Zhou[154], N. Zhou[60c], Y. Zhou[7], C.G. Zhu[60b], C. Zhu[15a,15d], H.L. Zhu[60a], H. Zhu[15a], J. Zhu[105], Y. Zhu[60a], X. Zhuang[15a], K. Zhukov[110], V. Zhulanov[121b,121a], D. Zieminska[65], N.I. Zimine[79], S. Zimmermann[52,*], Z. Zinonos[114], M. Ziolkowski[150], L. Živković[16], A. Zoccoli[23b,23a], K. Zoch[53], T.G. Zorbas[148], R. Zou[37], L. Zwalinski[36]

[1] *Department of Physics, University of Adelaide, Adelaide; Australia*
[2] *Physics Department, SUNY Albany, Albany NY; U.S.A.*
[3] *Department of Physics, University of Alberta, Edmonton AB; Canada*
[4] *Department of Physics[(a)], Ankara University, Ankara; Istanbul Aydin University[(b)], Application and Research Center for Advanced Studies, Istanbul; Division of Physics[(c)], TOBB University of Economics and Technology, Ankara; Turkey*
[5] *LAPP, Univ. Savoie Mont Blanc, CNRS/IN2P3, Annecy ; France*
[6] *High Energy Physics Division, Argonne National Laboratory, Argonne IL; U.S.A.*
[7] *Department of Physics, University of Arizona, Tucson AZ; U.S.A.*
[8] *Department of Physics, University of Texas at Arlington, Arlington TX; U.S.A.*
[9] *Physics Department, National and Kapodistrian University of Athens, Athens; Greece*
[10] *Physics Department, National Technical University of Athens, Zografou; Greece*
[11] *Department of Physics, University of Texas at Austin, Austin TX; U.S.A.*
[12] *Bahcesehir University[(a)], Faculty of Engineering and Natural Sciences, Istanbul; Istanbul Bilgi University[(b)], Faculty of Engineering and Natural Sciences, Istanbul; Department of Physics[(c)], Bogazici University, Istanbul; Department of Physics Engineering[(d)], Gaziantep University, Gaziantep; Turkey*
[13] *Institute of Physics, Azerbaijan Academy of Sciences, Baku; Azerbaijan*
[14] *Institut de Física d'Altes Energies (IFAE), Barcelona Institute of Science and Technology, Barcelona; Spain*
[15] *Institute of High Energy Physics[(a)], Chinese Academy of Sciences, Beijing; Physics Department[(b)], Tsinghua University, Beijing; Department of Physics[(c)], Nanjing University, Nanjing; University of Chinese Academy of Science (UCAS)[(d)], Beijing; China*
[16] *Institute of Physics, University of Belgrade, Belgrade; Serbia*
[17] *Department for Physics and Technology, University of Bergen, Bergen; Norway*
[18] *Physics Division, Lawrence Berkeley National Laboratory and University of California, Berkeley CA; U.S.A.*
[19] *Institut für Physik, Humboldt Universität zu Berlin, Berlin; Germany*
[20] *Albert Einstein Center for Fundamental Physics and Laboratory for High Energy Physics, University of Bern, Bern; Switzerland*

JHEP10(2021)013

[21] School of Physics and Astronomy, University of Birmingham, Birmingham; United Kingdom
[22] Facultad de Ciencias y Centro de Investigaciónes[(a)], Universidad Antonio Nariño, Bogotá; Departamento de Física[(b)], Universidad Nacional de Colombia, Bogotá, Colombia; Colombia
[23] INFN Bologna and Università di Bologna[(a)], Dipartimento di Fisica; INFN Sezione di Bologna[(b)]; Italy
[24] Physikalisches Institut, Universität Bonn, Bonn; Germany
[25] Department of Physics, Boston University, Boston MA; U.S.A.
[26] Department of Physics, Brandeis University, Waltham MA; U.S.A.
[27] Transilvania University of Brasov[(a)], Brasov; Horia Hulubei National Institute of Physics and Nuclear Engineering[(b)], Bucharest; Department of Physics[(c)], Alexandru Ioan Cuza University of Iasi, Iasi; National Institute for Research and Development of Isotopic and Molecular Technologies[(d)], Physics Department, Cluj-Napoca; University Politehnica Bucharest[(e)], Bucharest; West University in Timisoara[(f)], Timisoara; Romania
[28] Faculty of Mathematics[(a)], Physics and Informatics, Comenius University, Bratislava; Department of Subnuclear Physics[(b)], Institute of Experimental Physics of the Slovak Academy of Sciences, Kosice; Slovak Republic
[29] Physics Department, Brookhaven National Laboratory, Upton NY; U.S.A.
[30] Departamento de Física, Universidad de Buenos Aires, Buenos Aires; Argentina
[31] California State University, CA; U.S.A.
[32] Cavendish Laboratory, University of Cambridge, Cambridge; United Kingdom
[33] Department of Physics[(a)], University of Cape Town, Cape Town;[(b)] iThemba Labs, Western Cape; Department of Mechanical Engineering Science[(c)], University of Johannesburg, Johannesburg; National Institute of Physics[(d)], University of the Philippines Diliman (Philippines); University of South Africa[(e)], Department of Physics, Pretoria; School of Physics[(f)], University of the Witwatersrand, Johannesburg; South Africa
[34] Department of Physics, Carleton University, Ottawa ON; Canada
[35] Faculté des Sciences Ain Chock[(a)], Réseau Universitaire de Physique des Hautes Energies — Université Hassan II, Casablanca; Faculté des Sciences[(b)], Université Ibn-Tofail, Kénitra; Faculté des Sciences Semlalia[(c)], Université Cadi Ayyad, LPHEA-Marrakech; LPMR[(d)], Faculté des Sciences, Université Mohamed Premier, Oujda; Faculté des sciences[(e)], Université Mohammed V, Rabat; Morocco
[36] CERN, Geneva; Switzerland
[37] Enrico Fermi Institute, University of Chicago, Chicago IL; U.S.A.
[38] LPC, Université Clermont Auvergne, CNRS/IN2P3, Clermont-Ferrand; France
[39] Nevis Laboratory, Columbia University, Irvington NY; U.S.A.
[40] Niels Bohr Institute, University of Copenhagen, Copenhagen; Denmark
[41] Dipartimento di Fisica[(a)], Università della Calabria, Rende; INFN Gruppo Collegato di Cosenza[(b)], Laboratori Nazionali di Frascati; Italy
[42] Physics Department, Southern Methodist University, Dallas TX; U.S.A.
[43] Physics Department, University of Texas at Dallas, Richardson TX; U.S.A.
[44] National Centre for Scientific Research "Demokritos", Agia Paraskevi; Greece
[45] Department of Physics[(a)], Stockholm University; Oskar Klein Centre[(b)], Stockholm; Sweden
[46] Deutsches Elektronen-Synchrotron DESY, Hamburg and Zeuthen; Germany
[47] Lehrstuhl für Experimentelle Physik IV, Technische Universität Dortmund, Dortmund; Germany
[48] Institut für Kern- und Teilchenphysik, Technische Universität Dresden, Dresden; Germany
[49] Department of Physics, Duke University, Durham NC; U.S.A.
[50] SUPA — School of Physics and Astronomy, University of Edinburgh, Edinburgh; United Kingdom
[51] INFN e Laboratori Nazionali di Frascati, Frascati; Italy
[52] Physikalisches Institut, Albert-Ludwigs-Universität Freiburg, Freiburg; Germany
[53] II. Physikalisches Institut, Georg-August-Universität Göttingen, Göttingen; Germany
[54] Département de Physique Nucléaire et Corpusculaire, Université de Genève, Genève; Switzerland
[55] Dipartimento di Fisica[(a)], Università di Genova, Genova; INFN Sezione di Genova[(b)]; Italy

JHEP10(2021)013

[56] *II. Physikalisches Institut, Justus-Liebig-Universität Giessen, Giessen; Germany*
[57] *SUPA — School of Physics and Astronomy, University of Glasgow, Glasgow; United Kingdom*
[58] *LPSC, Université Grenoble Alpes, CNRS/IN2P3, Grenoble INP, Grenoble; France*
[59] *Laboratory for Particle Physics and Cosmology, Harvard University, Cambridge MA; U.S.A.*
[60] *Department of Modern Physics and State Key Laboratory of Particle Detection and Electronics*[(a)], *University of Science and Technology of China, Hefei; Institute of Frontier and Interdisciplinary Science and Key Laboratory of Particle Physics and Particle Irradiation (MOE)*[(b)], *Shandong University, Qingdao; School of Physics and Astronomy*[(c)], *Shanghai Jiao Tong University, Key Laboratory for Particle Astrophysics and Cosmology (MOE), SKLPPC, Shanghai; Tsung-Dao Lee Institute*[(d)], *Shanghai; China*
[61] *Kirchhoff-Institut für Physik*[(a)], *Ruprecht-Karls-Universität Heidelberg, Heidelberg; Physikalisches Institut*[(b)], *Ruprecht-Karls-Universität Heidelberg, Heidelberg; Germany*
[62] *Department of Physics*[(a)], *Chinese University of Hong Kong, Shatin, N.T., Hong Kong; Department of Physics*[(b)], *University of Hong Kong, Hong Kong; Department of Physics and Institute for Advanced Study*[(c)], *Hong Kong University of Science and Technology, Clear Water Bay, Kowloon, Hong Kong; China*
[63] *Department of Physics, National Tsing Hua University, Hsinchu; Taiwan*
[64] *IJCLab, Université Paris-Saclay, CNRS/IN2P3, 91405, Orsay; France*
[65] *Department of Physics, Indiana University, Bloomington IN; U.S.A.*
[66] *INFN Gruppo Collegato di Udine*[(a)], *Sezione di Trieste, Udine; ICTP*[(b)], *Trieste; Dipartimento Politecnico di Ingegneria e Architettura*[(c)], *Università di Udine, Udine; Italy*
[67] *INFN Sezione di Lecce*[(a)]*; Dipartimento di Matematica e Fisica*[(b)], *Università del Salento, Lecce; Italy*
[68] *INFN Sezione di Milano*[(a)]*; Dipartimento di Fisica*[(b)], *Università di Milano, Milano; Italy*
[69] *INFN Sezione di Napoli*[(a)]*; Dipartimento di Fisica*[(b)], *Università di Napoli, Napoli; Italy*
[70] *INFN Sezione di Pavia*[(a)]*; Dipartimento di Fisica*[(b)], *Università di Pavia, Pavia; Italy*
[71] *INFN Sezione di Pisa*[(a)]*; Dipartimento di Fisica E. Fermi*[(b)], *Università di Pisa, Pisa; Italy*
[72] *INFN Sezione di Roma*[(a)]*; Dipartimento di Fisica*[(b)], *Sapienza Università di Roma, Roma; Italy*
[73] *INFN Sezione di Roma Tor Vergata*[(a)]*; Dipartimento di Fisica*[(b)], *Università di Roma Tor Vergata, Roma; Italy*
[74] *INFN Sezione di Roma Tre*[(a)]*; Dipartimento di Matematica e Fisica*[(b)], *Università Roma Tre, Roma; Italy*
[75] *INFN-TIFPA*[(a)]*; Università degli Studi di Trento*[(b)], *Trento; Italy*
[76] *Institut für Astro- und Teilchenphysik, Leopold-Franzens-Universität, Innsbruck; Austria*
[77] *University of Iowa, Iowa City IA; U.S.A.*
[78] *Department of Physics and Astronomy, Iowa State University, Ames IA; U.S.A.*
[79] *Joint Institute for Nuclear Research, Dubna; Russia*
[80] *Departamento de Engenharia Elétrica*[(a)], *Universidade Federal de Juiz de Fora (UFJF), Juiz de Fora; Universidade Federal do Rio De Janeiro COPPE/EE/IF*[(b)], *Rio de Janeiro; Instituto de Física*[(c)], *Universidade de São Paulo, São Paulo; Brazil*
[81] *KEK, High Energy Accelerator Research Organization, Tsukuba; Japan*
[82] *Graduate School of Science, Kobe University, Kobe; Japan*
[83] *AGH University of Science and Technology*[(a)], *Faculty of Physics and Applied Computer Science, Krakow; Marian Smoluchowski Institute of Physics*[(b)], *Jagiellonian University, Krakow; Poland*
[84] *Institute of Nuclear Physics Polish Academy of Sciences, Krakow; Poland*
[85] *Faculty of Science, Kyoto University, Kyoto; Japan*
[86] *Kyoto University of Education, Kyoto; Japan*
[87] *Research Center for Advanced Particle Physics and Department of Physics, Kyushu University, Fukuoka ; Japan*
[88] *Instituto de Física La Plata, Universidad Nacional de La Plata and CONICET, La Plata; Argentina*
[89] *Physics Department, Lancaster University, Lancaster; United Kingdom*
[90] *Oliver Lodge Laboratory, University of Liverpool, Liverpool; United Kingdom*

JHEP10(2021)013

[91] *Department of Experimental Particle Physics, Jožef Stefan Institute and Department of Physics, University of Ljubljana, Ljubljana; Slovenia*
[92] *School of Physics and Astronomy, Queen Mary University of London, London; United Kingdom*
[93] *Department of Physics, Royal Holloway University of London, Egham; United Kingdom*
[94] *Department of Physics and Astronomy, University College London, London; United Kingdom*
[95] *Louisiana Tech University, Ruston LA; U.S.A.*
[96] *Fysiska institutionen, Lunds universitet, Lund; Sweden*
[97] *Centre de Calcul de l'Institut National de Physique Nucléaire et de Physique des Particules (IN2P3), Villeurbanne; France*
[98] *Departamento de Física Teorica C-15 and CIAFF, Universidad Autónoma de Madrid, Madrid; Spain*
[99] *Institut für Physik, Universität Mainz, Mainz; Germany*
[100] *School of Physics and Astronomy, University of Manchester, Manchester; United Kingdom*
[101] *CPPM, Aix-Marseille Université, CNRS/IN2P3, Marseille; France*
[102] *Department of Physics, University of Massachusetts, Amherst MA; U.S.A.*
[103] *Department of Physics, McGill University, Montreal QC; Canada*
[104] *School of Physics, University of Melbourne, Victoria; Australia*
[105] *Department of Physics, University of Michigan, Ann Arbor MI; U.S.A.*
[106] *Department of Physics and Astronomy, Michigan State University, East Lansing MI; U.S.A.*
[107] *B.I. Stepanov Institute of Physics, National Academy of Sciences of Belarus, Minsk; Belarus*
[108] *Research Institute for Nuclear Problems of Byelorussian State University, Minsk; Belarus*
[109] *Group of Particle Physics, University of Montreal, Montreal QC; Canada*
[110] *P.N. Lebedev Physical Institute of the Russian Academy of Sciences, Moscow; Russia*
[111] *National Research Nuclear University MEPhI, Moscow; Russia*
[112] *D.V. Skobeltsyn Institute of Nuclear Physics, M.V. Lomonosov Moscow State University, Moscow; Russia*
[113] *Fakultät für Physik, Ludwig-Maximilians-Universität München, München; Germany*
[114] *Max-Planck-Institut für Physik (Werner-Heisenberg-Institut), München; Germany*
[115] *Nagasaki Institute of Applied Science, Nagasaki; Japan*
[116] *Graduate School of Science and Kobayashi-Maskawa Institute, Nagoya University, Nagoya; Japan*
[117] *Department of Physics and Astronomy, University of New Mexico, Albuquerque NM; U.S.A.*
[118] *Institute for Mathematics, Astrophysics and Particle Physics, Radboud University/Nikhef, Nijmegen; Netherlands*
[119] *Nikhef National Institute for Subatomic Physics and University of Amsterdam, Amsterdam; Netherlands*
[120] *Department of Physics, Northern Illinois University, DeKalb IL; U.S.A.*
[121] *Budker Institute of Nuclear Physics and NSU[(a)], SB RAS, Novosibirsk; Novosibirsk State University Novosibirsk[(b)]; Russia*
[122] *Institute for High Energy Physics of the National Research Centre Kurchatov Institute, Protvino; Russia*
[123] *Institute for Theoretical and Experimental Physics named by A.I. Alikhanov of National Research Centre "Kurchatov Institute", Moscow; Russia*
[124] *Department of Physics, New York University, New York NY; U.S.A.*
[125] *Ochanomizu University, Otsuka, Bunkyo-ku, Tokyo; Japan*
[126] *Ohio State University, Columbus OH; U.S.A.*
[127] *Homer L. Dodge Department of Physics and Astronomy, University of Oklahoma, Norman OK; U.S.A.*
[128] *Department of Physics, Oklahoma State University, Stillwater OK; U.S.A.*
[129] *Palacký University, Joint Laboratory of Optics, Olomouc; Czech Republic*
[130] *Institute for Fundamental Science, University of Oregon, Eugene, OR; U.S.A.*
[131] *Graduate School of Science, Osaka University, Osaka; Japan*
[132] *Department of Physics, University of Oslo, Oslo; Norway*

JHEP10(2021)013

[133] Department of Physics, Oxford University, Oxford; United Kingdom
[134] LPNHE, Sorbonne Université, Université de Paris, CNRS/IN2P3, Paris; France
[135] Department of Physics, University of Pennsylvania, Philadelphia PA; U.S.A.
[136] Konstantinov Nuclear Physics Institute of National Research Centre "Kurchatov Institute", PNPI, St. Petersburg; Russia
[137] Department of Physics and Astronomy, University of Pittsburgh, Pittsburgh PA; U.S.A.
[138] Laboratório de Instrumentação e Física Experimental de Partículas — LIP[(a)], Lisboa; Departamento de Física[(b)], Faculdade de Ciências, Universidade de Lisboa, Lisboa; Departamento de Física[(c)], Universidade de Coimbra, Coimbra; Centro de Física Nuclear da Universidade de Lisboa[(d)], Lisboa; Departamento de Física[(e)], Universidade do Minho, Braga; Departamento de Física Teórica y del Cosmos[(f)], Universidad de Granada, Granada (Spain); Dep Física and CEFITEC of Faculdade de Ciências e Tecnologia[(g)], Universidade Nova de Lisboa, Caparica; Instituto Superior Técnico[(h)], Universidade de Lisboa, Lisboa; Portugal
[139] Institute of Physics of the Czech Academy of Sciences, Prague; Czech Republic
[140] Czech Technical University in Prague, Prague; Czech Republic
[141] Charles University, Faculty of Mathematics and Physics, Prague; Czech Republic
[142] Particle Physics Department, Rutherford Appleton Laboratory, Didcot; United Kingdom
[143] IRFU, CEA, Université Paris-Saclay, Gif-sur-Yvette; France
[144] Santa Cruz Institute for Particle Physics, University of California Santa Cruz, Santa Cruz CA; U.S.A.
[145] Departamento de Física[(a)], Pontificia Universidad Católica de Chile, Santiago; Universidad Andres Bello[(b)], Department of Physics, Santiago; Instituto de Alta Investigación[(c)], Universidad de Tarapacá, Arica; Departamento de Física[(d)], Universidad Técnica Federico Santa María, Valparaíso; Chile
[146] Universidade Federal de São João del Rei (UFSJ), São João del Rei; Brazil
[147] Department of Physics, University of Washington, Seattle WA; U.S.A.
[148] Department of Physics and Astronomy, University of Sheffield, Sheffield; United Kingdom
[149] Department of Physics, Shinshu University, Nagano; Japan
[150] Department Physik, Universität Siegen, Siegen; Germany
[151] Department of Physics, Simon Fraser University, Burnaby BC; Canada
[152] SLAC National Accelerator Laboratory, Stanford CA; U.S.A.
[153] Department of Physics, Royal Institute of Technology, Stockholm; Sweden
[154] Departments of Physics and Astronomy, Stony Brook University, Stony Brook NY; U.S.A.
[155] Department of Physics and Astronomy, University of Sussex, Brighton; United Kingdom
[156] School of Physics, University of Sydney, Sydney; Australia
[157] Institute of Physics, Academia Sinica, Taipei; Taiwan
[158] E. Andronikashvili Institute of Physics[(a)], Iv. Javakhishvili Tbilisi State University, Tbilisi; High Energy Physics Institute[(b)], Tbilisi State University, Tbilisi; Georgia
[159] Department of Physics, Technion, Israel Institute of Technology, Haifa; Israel
[160] Raymond and Beverly Sackler School of Physics and Astronomy, Tel Aviv University, Tel Aviv; Israel
[161] Department of Physics, Aristotle University of Thessaloniki, Thessaloniki; Greece
[162] International Center for Elementary Particle Physics and Department of Physics, University of Tokyo, Tokyo; Japan
[163] Department of Physics, Tokyo Institute of Technology, Tokyo; Japan
[164] Tomsk State University, Tomsk; Russia
[165] Department of Physics, University of Toronto, Toronto ON; Canada
[166] TRIUMF[(a)], Vancouver BC; Department of Physics and Astronomy[(b)], York University, Toronto ON; Canada
[167] Division of Physics and Tomonaga Center for the History of the Universe, Faculty of Pure and Applied Sciences, University of Tsukuba, Tsukuba; Japan
[168] Department of Physics and Astronomy, Tufts University, Medford MA; U.S.A.

JHEP10(2021)013

[169] Department of Physics and Astronomy, University of California Irvine, Irvine CA; U.S.A.
[170] Department of Physics and Astronomy, University of Uppsala, Uppsala; Sweden
[171] Department of Physics, University of Illinois, Urbana IL; U.S.A.
[172] Instituto de Física Corpuscular (IFIC), Centro Mixto Universidad de Valencia — CSIC, Valencia; Spain
[173] Department of Physics, University of British Columbia, Vancouver BC; Canada
[174] Department of Physics and Astronomy, University of Victoria, Victoria BC; Canada
[175] Fakultät für Physik und Astronomie, Julius-Maximilians-Universität Würzburg, Würzburg; Germany
[176] Department of Physics, University of Warwick, Coventry; United Kingdom
[177] Waseda University, Tokyo; Japan
[178] Department of Particle Physics and Astrophysics, Weizmann Institute of Science, Rehovot; Israel
[179] Department of Physics, University of Wisconsin, Madison WI; U.S.A.
[180] Fakultät für Mathematik und Naturwissenschaften, Fachgruppe Physik, Bergische Universität Wuppertal, Wuppertal; Germany
[181] Department of Physics, Yale University, New Haven CT; U.S.A.

[a] Also at Borough of Manhattan Community College, City University of New York, New York NY; U.S.A.
[b] Also at Center for High Energy Physics, Peking University; China
[c] Also at Centro Studi e Ricerche Enrico Fermi; Italy
[d] Also at CERN, Geneva; Switzerland
[e] Also at CPPM, Aix-Marseille Université, CNRS/IN2P3, Marseille; France
[f] Also at Département de Physique Nucléaire et Corpusculaire, Université de Genève, Genève; Switzerland
[g] Also at Departament de Fisica de la Universitat Autonoma de Barcelona, Barcelona; Spain
[h] Also at Department of Financial and Management Engineering, University of the Aegean, Chios; Greece
[i] Also at Department of Physics and Astronomy, Michigan State University, East Lansing MI; U.S.A.
[j] Also at Department of Physics and Astronomy, University of Louisville, Louisville, KY; U.S.A.
[k] Also at Department of Physics, Ben Gurion University of the Negev, Beer Sheva; Israel
[l] Also at Department of Physics, California State University, East Bay; U.S.A.
[m] Also at Department of Physics, California State University, Fresno; U.S.A.
[n] Also at Department of Physics, California State University, Sacramento; U.S.A.
[o] Also at Department of Physics, King's College London, London; United Kingdom
[p] Also at Department of Physics, St. Petersburg State Polytechnical University, St. Petersburg; Russia
[q] Also at Department of Physics, University of Fribourg, Fribourg; Switzerland
[r] Also at Dipartimento di Matematica, Informatica e Fisica, Università di Udine, Udine; Italy
[s] Also at Faculty of Physics, M.V. Lomonosov Moscow State University, Moscow; Russia
[t] Also at Giresun University, Faculty of Engineering, Giresun; Turkey
[u] Also at Graduate School of Science, Osaka University, Osaka; Japan
[v] Also at Hellenic Open University, Patras; Greece
[w] Also at Institucio Catalana de Recerca i Estudis Avancats, ICREA, Barcelona; Spain
[x] Also at Institut für Experimentalphysik, Universität Hamburg, Hamburg; Germany
[y] Also at Institute for Nuclear Research and Nuclear Energy (INRNE) of the Bulgarian Academy of Sciences, Sofia; Bulgaria
[z] Also at Institute for Particle and Nuclear Physics, Wigner Research Centre for Physics, Budapest; Hungary
[aa] Also at Institute of Particle Physics (IPP); Canada
[ab] Also at Institute of Physics, Azerbaijan Academy of Sciences, Baku; Azerbaijan
[ac] Also at Instituto de Fisica Teorica, IFT-UAM/CSIC, Madrid; Spain
[ad] Also at Istanbul University, Dept. of Physics, Istanbul; Turkey

JHEP10(2021)013

[ae] Also at Joint Institute for Nuclear Research, Dubna; Russia
[af] Also at Moscow Institute of Physics and Technology State University, Dolgoprudny; Russia
[ag] Also at National Research Nuclear University MEPhI, Moscow; Russia
[ah] Also at Physics Department, An-Najah National University, Nablus; Palestine
[ai] Also at Physikalisches Institut, Albert-Ludwigs-Universität Freiburg, Freiburg; Germany
[aj] Also at The City College of New York, New York NY; U.S.A.
[ak] Also at TRIUMF, Vancouver BC; Canada
[al] Also at Universita di Napoli Parthenope, Napoli; Italy
[am] Also at University of Chinese Academy of Sciences (UCAS), Beijing; China
[*] Deceased

JHEP10(2021)013